

EFFECT OF PERCOLATION IN SOLID ELECTROLYTE COMPOSITES IN SODIUM BATTERY

Thesis Submitted for the Award of the Degree of

DOCTOR OF PHILOSOPHY

in

PHYSICS

By

Owais Amin

(Reg. No. 11919629)

Supervised By

Dr. Rupam Mukherjee (23644)

Assistant Professor



LOVELY PROFESSIONAL UNIVERSITY, PUNJAB

2024

*Dedicated to my Uncle
Late Ali Mohammed
Rather, My Family & My
loving parents (Mr.
Mohammad Amin Rather
& Mrs. Shakeela Akhter)*

DECLARATION

I hereby declare that the thesis entitles “**Effect of percolation in solid electrolyte composites in sodium battery**” submitted for the award of degree of Doctor of Philosophy in Physics, Lovely Professional University, Phagwara, is my own original work conducted under the supervision of **Dr. Rupam Mukherjee (Supervisor)**, Assistant Professor in Department of Physics at School of Chemical Engineering and Physical Science, Lovely Professional University, Phagwara, Punjab, India. I further declare that the thesis does not contain any part of any work which has been submitted for the award of any degree in this university or in any other University/Deemed University without proper citation.

A handwritten signature in black ink that reads "Owais Amin". The signature is written in a cursive style and is underlined with two parallel lines.

Author: **Owais Amin**

Reg. Number: 11919629

Department of Physics

School of Chemical Engineering and Physical

Sciences Lovely Professional University

Phagwara, Punjab-144411

CERTIFICATE

This is to certify that the work entitled “**Effect of percolation in solid electrolyte composites in sodium battery**” is a piece of research work done by **Mr. Owais Amin** under my guidance and supervision for the degree of Doctor of Philosophy in Department of Physics, School of Chemical Engineering and Physical Sciences, Lovely Professional University, Phagwara (Punjab) India.

To the best of my knowledge and belief, the thesis:

1. Embodies the work of the candidate herself.
2. Has duly been completed.
3. Fulfils the requirements of the ordinance related to the Ph.D. degree of the university.
4. Is up to the standard both in respect of contents and language for being referred to the examiner.



Supervisor: **Dr. Rupam Mukherjee**

(Assistant Professor)

Department of Physics

School of Chemical Engineering and Physical Sciences

Lovely Professional University

Phagwara-144411

Punjab, India

ACKNOWLEDGEMENT



I would like to pay my thanks to Almighty Allah (SWT) for giving me strength and patience to carry out my PhD research work. I pay my sincere gratitude to my supervisor **Dr. Rupam Mukherjee**, Assistant Professor, School of Chemical Engineering and Physical Sciences, Department of Physics, Lovely Professional University. With his assistance, Scientific support, and dedicated involvement throughout this process, to complete my PhD work. I am truly very fortunate to have the opportunity to work with him. I found this guidance to be remarkably valuable.

A big thanks to the entire staff of the Department of Physics, Lovely Professional University for giving me a word of encouragement. My acknowledgement also goes to my Head of School, Dr. K. C. Juglan for providing me such a wonderful opportunity to work under the guidance of Dr. Rupam Mukherjee that has brought the new beginning to a revolutionary change in my carrier. My sincere appreciation also goes to Dr Mukesh Kumar, Dr S. D. Pathak, Dr. Rajesh Kumar, Department of Physics, Lovely Professional University (LPU), Punjab, Dr. Subhojoyti Sinha, Department of Physics & Nanotechnology, SRM Institute of Science and Technology, Tamil Nadu for their wonderful support whenever I needed. I would also like to give special thanks to Nitin Kumar Yadav & Ramesh Kumar (Lab. Technician) Department of Physics, Manoj Kumar Department of Chemistry from School of Chemical Engineering and Physical Sciences and other faculty members of Lovely Professional University, Punjab for always being cooperative and helpful.

I would like to express my sincere and profound appreciation to my colleagues, Shahid Ahmad Shah, Anjori Sharma, Shakira, Simrandeep Kaur, Rikky Sharma, Azad Qayoom Malik, Hamnesh Mahajan, Indu bala, Ibrahim Mohammed, Irtiqa Ashraf, Ruhail Showkat and Bilal Ahmad for always being there for me and for making the journey memorable forever. A special thanks to my friend Tehmeena without whom it would have really been impossible to carry out this task.

Most importantly none of this could have happened without my loving family. My Parents has been a vital part of my life right from the moment I came into this world and has been very supportive throughout my entire PhD endeavor. I am always thankful to them. With the blessings of my Uncle Late Ali Mohammad Rather who has always motivated me to do hard work to achieve big in life. A special thanks to my brothers who have always been supportive and encouraged me, and my sisters have always supported and inspired me throughout my PhD.

Author: **Owais Amin**

Registration number: 11919629

Abstract

In this era of technology, researchers are interested in synthesizing such solid electrolytes that may resolve the major problems of high efficiency, energy storage, safety, and stability of solid electrolytes. The existing materials that are being used for solid electrolytes have low efficiency, high dielectric losses, high prone to leakage, low stability & safety. Many researchers have used and synthesized solid electrolyte materials with high ionic conductivity to tackle problems related to solid electrolytes. Most of the composites that have been used for solid electrolyte applications either showed very good results for dielectric properties or thermal stability. But for better efficiency and stability, both thermal as well as dielectric properties must be excellent. In this research we have synthesized and characterized solid electrolytes and their composites to study applications. We have also studied the different properties such as structural, dielectric, and thermal properties for solid electrolytes and composites. In the present research work, the sol-gel auto-combustion method is adopted to synthesize the solid electrolytes. The following mentioned samples of solid electrolytes and its composites have been synthesized and characterized:

- $\text{NaAl}_{11}\text{O}_{17}$
- $\text{NaIn}_x\text{Al}_{11-x}\text{O}_{17}$ ($x = 0, 0.1, 0.2, 0.3, 0.4$)
- $\text{NaZn}_x\text{Al}_{11-x}\text{O}_{17}$ ($x = 0, 0.1, 0.3$)
- $\text{NaZr}_x\text{Al}_{11-x}\text{O}_{17}$ ($x = 0, 0.2, 0.3$)
- $\beta\text{-Al: PVDF}$ ($x = 5\%, 10\%, 20\%, 30\%$)

All the prepared samples in the thesis have some specific results at different conditions. These prepared samples have their application for Solid electrolytes.

For the study thermal stability and dielectric property sodium beta alumina solid electrolyte is chosen and characterized. The research work explores the effect of indium doping on thermal and dielectric property of sodium beta-alumina solid electrolyte ($\text{NaIn}_x\text{Al}_{11-x}\text{O}_{17}$). Sol-gel auto combustion method was adopted to prepare ($\text{NaIn}_x\text{Al}_{11-x}\text{O}_{17}$) and sintered at 1100°C . X-ray diffraction (XRD) confirms the crystalline phase of produced samples and intense sharp peaks of indium doping concentrations demonstrates proportionate and uniform doping in pure alumina. Field Emission Scanning Electron Microscopy reveals that morphology changes from long

cylindrical particles to small and thin sized grains leading to formation of clusters. At an input frequency of 10^4 Hz, the dielectric measurement reveals a sharp decrease in the real part of the dielectric permittivity from 10^5 for $x=0$ to 10^2 for $x > 0$. The screening effect of the indium atom and cluster formation, which lessens the polarization impact, are primarily responsible for this decrease.

The hybrid nanocomposite system of PVDF-sodium β -Al with varying PVDF weight % was prepared by mechanical blending method to study the ionic conductivity, thermal, and dielectric properties. Thermal stability has substantially improved and is now found to be temperature independent across a wide range. From FESEM, morphology plays a crucial role in determining the dielectric properties which leads to large interparticle sodium beta alumina.

There are five chapters in this thesis. The first chapter provides an overview of the research, as well as an analysis of crystal structure, dielectric properties, thermal stability as well as the applications of solid electrolytes. The critical review of literature is presented in chapter two, while the research methodology is covered in chapter three. The experimental data for each of the compositions is discussed in detail in Chapter four. The fifth chapter contains the summary and conclusion.

Table of Content

Declaration	iii
Certificate	iv
Acknowledgement	v
Abstract	vi
List of figures	xii
Chapter 1: Introduction	1
1.1 Introduction	1
1.2 Theory of Percolation	4
1.2.1 The site-bond percolation Model	4
1.2.2 The continuum Percolation Model	6
1.2.3 Dielectric Properties of composites	7
1.3 Ionic Conductivity of solid electrolytes	7
1.3.1 Solid Electrolytes	8
1.3.2 Structure of Solid Electrolytes	10
1.3.3 Sodium beta alumina solid electrolyte (BASE)	12
1.3.4 Properties of Solid electrolytes	13
1.3.5 Application of Solid electrolytes	15
1.4 Solid state batteries	16
1.5 Sodium Ion battery	17
1.6 Polyvinylidene Fluoride (PVDF)	20
1.6.1 Properties of PVDF	21
1.6.2 Applications PVDF	22
Chapter 2: Literature review	25
2.1 Literature review	25
2.2 Motivation and research gap	39
2.3 Objective of the study	40
Chapter 3: Research methodology	41
3.1 Introduction	41

3.2 Synthesis method	41
3.2.1 Sol-gel auto-combustion	41
3.2.2 Synthesis of Sodium beta alumina solid electrolyte (NaAl ₁₁ O ₁₇)	43
3.2.3 In ³⁺ substituted in sodium beta alumina.	43
3.2.4 Zr ³⁺ substituted in sodium beta alumina.	44
3.2.5 Zn ³⁺ substituted in sodium beta alumina.	44
3.2.6 Synthesis of polymer based solid electrolyte (NaAl ₁₁ O ₁₇)	45
3.3 Characterization Technique	45
3.3.1 Introduction	45
3.3.2 X-ray Diffractometer (XRD)	46
3.3.3 Field Emission Scanning Electron Microscope (FESEM)	47
3.3.4 Scanning Electron Microscope (SEM)	49
3.3.5 Energy Dispersive Spectroscopy (EDS)	50
3.3.6 Electrochemical Impedance Spectroscopy (EIS)	51
3.3.7 Thermogravimetric Analysis (TGA)	53
3.3.8 FTIR	54
3.3.9 UV spectroscopy	56
3.4.0 Mortar & pestle	57
3.4.1 Cold press die set	58
3.4.2 KBr press instrument	59
Chapter 4: Synthesis of structural, thermal & dielectrical properties of indium doped sodium β-alumina.	60
Abstract	60
4.1 Introduction	60
4.2 Experimental	62
4.2.1 Materials and Method of Synthesis	62
4.2.2 Synthesis of Indium doped Sodium β-alumina.	62
4.2.3 Characterization Techniques	62
4.3 Results and Discussions	63
4.3.1 X-ray Diffraction (XRD) analysis	63
4.3.2 Energy Dispersive X-ray (EDX)	64
4.3.3 Thermal analysis (TGA)	66

4.3.4 Morphological analysis (SEM)	67
4.3.5 Staircase type DC resistivity	68
4.4 Dielectric Studies	69
4.4.1 Study of dielectric permittivity vs frequency	69
4.4.2 Dielectric tangent loss vs frequency	71
4.4.3 Cole-cole plot	72
4.4.4 Ionic conductivity	74
4.5 Conclusion	75
Chapter 5: Tuning of structural & dielectric properties of Zirconyl/Zinc doped sodium β-alumina.	76
Abstract	76
5.1 Introduction	76
5.2 Experimental	77
5.2.1 Materials and method of synthesis	77
5.2.2 Synthesis of Zr/Zn dope sodium β -alumina.	77
5.2.3 Characterization techniques	77
5.3 Results & Discussions	78
5.3.1 Dielectric Analysis	78
5.3.1.1 Study of real part of permittivity vs frequency	78
5.3.1.2 Dielectric tangent loss vs frequency	79
5.3.1.3 Cole-cole plot of Zirconyl doped sodium β -alumina.	80
5.3.1.4 AC conductivity of Zr doped sodium β -alumina.	81
5.3.6 XRD analysis of Zr doped sodium beta alumina	82
5.3.7 FESEM of Zr doped sodium beta alumina	83
5.3.1.5 Cole-cole plot of Zinc doped sodium β -alumina.	85
5.3.1.6 AC conductivity Zn doped sodium β -alumina.	86
5.3.10 XRD analysis of Zn doped sodium beta alumina	87
5.3.11 FESEM analysis of Zn doped sodium beta alumina	88
5.4 Conclusion	89
Chapter 6: Optimization of electrical and thermal properties of sodium β-alumina-PVDF composites.	90
Abstract	90

6.1 Introduction	90
6.2 Experimental Details	91
6.2.1 Materials and method of synthesis	91
6.2.2 Characterization technique	91
6.3 Results & Discussions	92
6.3.1 Dielectric analysis	92
6.3.1.1 Variation of real part of permittivity vs frequency	93
6.3.1.2 Dielectric tangent loss vs frequency	93
6.3.1.3 AC conductivity	94
6.3.1.4 Cole-cole plot	95
6.3.2 Thermal analysis	96
6.3.3 Morphological Analysis	97
6.3.4 EDX Analysis	98
6.3.5 Relation between weight% vs Conductivity	100
6.3.6 XRD analysis	101
6.4 Conclusion	102
Chapter 7: Summary & Scope for future work	103
Future work	106
Bibliography	107
Publications	129

List of Figures

Figure 1.1 Site and bond Percolation model in 2 dimensions.	6
Figure 1.2 Continuum Percolation Model	7
Figure 1.3 Solid-state electrolyte	10
Figure 1.4 Crystal structure of sodium β -Al ₂ O ₃ and Sodium β'' -Al ₂ O ₃	12
Figure 1.5 Sodium beta alumina	13
Figure 1.6 Composition of solid-state sodium batteries and the corresponding requirement of SSE	15
Figure 1.7 Representation of applications of solid electrolyte	16
Figure 1.8 Various components of sodium ion battery	18
Figure 1.9 working principle of the sodium ion battery	19
Figure 1.10 Molecular structure of PVDF	20
Figure 1.11 Alpha and beta phase structure of PVDF	22
Figure 1.12 Application of PVDF	24
Figure 1.13 Design of polymer based solid electrolyte	24
Figure 3.1 (a) Sol-gel auto combustion process (b) Steps of Preparation.	42
Figure 3.2 Instrument & analysis principle of XRD	47
Figure 3.3 FESEM Instrument & Working principle of FESEM technique	48
Figure 3.4 SEM instrument & Working principle of Scanning Electron Microscopy	50
Figure 3.5 Schematic representation of EDS	51
Figure 3.6 Instrument & Experimental EIS System	52
Figure 3.7 Instrument & Schematic representation of TGA	53
Figure 3.8 Principle of FTIR Technique	55
Figure 3.9 Working of FTIR Technique	55
Figure 3.10 All possible transitions after absorption of photons	57
Figure 3.11 The agate mortar pestle used for fine grinding powder	58
Figure 3.12 Cold Press Die set 12mm Diameter	58
Figure 3.13 KBr press instrument	59
Figure 4.1 XRD pattern of Sodium beta alumina (NaAl ₁₁ O ₁₇) with indium dopant	64
Figure 4.2 EDX spectra of Sodium beta alumina with indium dopant	65
Figure 4.3 TGA Curve of Sodium beta alumina (NaAl ₁₁ O ₁₇) with different amounts of indium doping. Inset: Derivative weight % of pure sodium beta alumina corresponding to the same temperature.	67
Figure 4.4 SEM images of sodium beta alumina and different indium dopants	68

Figure 4.5 Temperature dependent DC resistivity of undoped sodium beta alumina	69
Figure 4.6 Variation of real part of dielectric with frequency for pure sodium beta alumina with different indium doping	71
Figure 4.7 Dielectric tangent loss with frequency for sodium beta alumina with different indium doping	72
Figure 4.8 Cole-cole plot of sodium beta alumina with different indium doping inset: concentration vs frequency	72
Figure 4.9 Fitting of electrochemical data of cole-cole plot of sodium beta alumina with indium doping	74
Figure 4.10 Ionic conductivity of Sodium β - Al with different indium doping. Inset: Concentration vs ionic conductivity at 30 KHz	74
Figure 5.1 Variation of real of dielectric permittivity with frequency of pure sodium beta alumina with Zirconyl doping	79
Figure 5.2 Dielectric tangent loss of pure sodium beta alumina with zirconyl doping	80
Figure 5.3 Cole-cole plot of sodium beta alumina with zirconyl doping	80
Figure 5.4 Ionic conductivity of sodium β -Al with Zr doping	81
Figure 5.5 XRD pattern of zirconyl doped beta alumina	82
Figure 5.6 FESEM images of zirconyl doped beta alumina	83
Figure 5.7 Cole-cole plot of sodium beta alumina with different zinc concentration	85
Figure 5.8 Conductivity vs Frequency of sodium beta alumina with zinc dopant	86
Figure 5.9 XRD pattern of Zinc doped beta alumina	87
Figure 5.10 FESEM images of zinc doped beta alumina	88
Figure 6.1 Variation of real part of permittivity of sodium beta alumina ($\text{NaAl}_{11}\text{O}_{17}$) and PVDF composite	92
Figure 6.2 Tangent loss of sodium beta alumina with PVDF composite	93
Figure 6.3 Frequency vs Ionic conductivity of PVDF composites. Inset: sodium β -Al Ionic conductivity with same frequency	94
Figure 6.4 Cole-cole of PVDF composite. Inset: Cole-cole plot of Sodium beta alumina solid electrolyte	95
Figure 6.5 (a) TGA Curve of Sodium beta alumina ($\text{NaAl}_{11}\text{O}_{17}$) with PVDF Composite. (b) Derivative weight% of pure sodium beta alumina with PVDF Composite corresponding to the same temperature.	96
Figure 6.7 SEM images of sodium beta alumina with PVDF composites	97
Figure 6.8 EDX spectra of PVDF-Sodium β -Al solid electrolyte	99
Figure 6.0 Relationship between conductivity vs weight % of sodium beta alumina: PVDF	100
Figure 6.10 XRD pattern of PVDF: sodium beta alumina	101

Chapter 1

1.1 Introduction

Today we are living in the 21st century, a century full of technology where everyone is using high-tech gadgets. Since they are commonly used in electronic products like laptops, cameras, and smart phones and have low costs, extended life cycles, high capacities, and no memory effect, lithium-ion batteries have gained more focus [1]. Since the launch of LIBs into the market they have been more and more studied in recognition of their use of power energy sources similar to those used in BEVs and sustainable energy storage devices [2, 3]. Nevertheless, there are safety hurdles associated with their flammable organic liquid electrolytes, and these issues get worse when the size of batteries is increased for usage in electric vehicles and another high-temperature application [4, 5]. The necessity for effective rechargeable batteries has recently been of the utmost importance due to the rising demand when it comes to energy storage technologies, and research are concentrating on the complex technologies in the manufacture of the batteries for many applications [6]. Due to sodium's abundant supply and low cost, the surrounding temperature of sodium-based batteries that have ability to gather the comprehensive grid of energy storage needs. Additionally, because sodium (Na) is so inexpensive and widely available, sodium-based batteries may eventually be competitive with lithium-ion batteries in some markets. [7,8]. These days, the development of sustainable sources of energy has become essential on account of limited resources. LIBs as one of the typical rechargeable electrochemical batteries had influenced the markets of portable electronic devices, due to their high voltage, long life cycle, and high energy densities [9-12]. With performance comparable to that of LIBs, with resources of sodium are abundant, and low starting material costs since Na atoms are heavier than Li atoms, it is anticipated that the energy density of Na-ion batteries won't be higher than that of the Li analogue. One of the favorable substitutes for LIBs are sodium ion batteries. [13-15]. Solid-state batteries offer the potential to considerably improve battery innovation in names of good density, safety, energy, and quick charging capabilities, as is well known. Furthermore, they put forward reliability against

lithium to its extremely long-life cycle or better ionic conductivities than liquid electrolytes even at room temperature [16-18]. The growth of sustainable energy sources including wind energy, hydrothermal energy and solar energy depends heavily on smart materials. One such renewable resource that can store the chemical energy, and efficiently transform it into rechargeable batteries [19–22]. Due to its high energy density, lengthy lifespan, and high output voltage, lithium-ion batteries (LIBs) have until now dominated the market for portable electronic gadgets. [23]. Simultaneously, LIB has certain advantages over other chemistries as lithium has the lowest reduction potential among all elements which enable cells with high operational voltage and high energy density [24,25]. However, the high cost, high flammability, leakage of liquid electrolyte and inadequacy of lithium resources have undoubtedly hindered the applications of LIB in large-scale energy storage [26]. Solid-state sodium ion battery (SIB) on the other hand is another class of batteries which uses solid electrolyte rather than liquid organic electrolyte in LIBs [27-30]. SIB is recently found to be a good alternative of LIB because sodium is abundant, low cost, minimum leakage, greater thermal stability and does not support any dendrite formation [31,32]. Despite all the benefits of solid-state batteries, sodium ion batteries' ionic conductivity is still found to be significantly lower than that of (LIBs) lithium-ion batteries, which limits their use in commercial applications. Additionally, as the lithium (Li) atom grows larger relative to the sodium (Na) atom, the volumetric energy density of SIB decreases, making it less effective against LIBs [33-37]. Solid state SIB batteries are usually classified based on type of solid electrolytes as for example inorganic ceramic electrolytes (LATP), organic polymer electrolyte (PVA) and polymer ceramic composite electrolytes (PEO/LGPS). β -alumina ($\text{NaAl}_{11}\text{O}_{17}$) which comes in two distinct phases, hexagonal symmetry, and rhombohedral symmetry (β'' -alumina) is an oxide based inorganic ceramic electrolyte that exhibits high ionic conductivity $\sim 1 \text{ S cm}^{-1}$ especially in the rhombohedral phase at 573 K [38-42]. It is an anisotropic layered material with different layers of spinel block and loosely packed conduction planes where Na ion conduction takes place through hopping [43]. The demerit of this ceramic compound is that the compound with hexagonal symmetry yields σ (ionic conductivity) of around $10^{-3} \text{ S cm}^{-1}$ at 300 K whereas the

synthesis of rhombohedral phase is too expensive to grow at large scale for industrial application. Moreover, the presence of unwanted phases such as NaAlO_2 due to high temperature sintering makes $\text{NaAl}_{11}\text{O}_{17}$ inhomogeneous and susceptible to H_2O and CO_2 absorption from atmosphere [44-46]. As a result, the absorbents make the solid electrolyte less thermally stable and induce chemical instability too. Elemental doping is a well-known method used to expansion the mechanical & electrochemical properties of solid state $\text{NaAl}_{11}\text{O}_{17}$ electrolytes [47, 48]. It is found that addition of metal oxides increases the conductivity of sintered samples of β -alumina, but large concentration of metal oxides leads to formation of β'' -alumina phase [49-52]. In our research work, the main objective is to improve the ionic conductivity in polycrystalline form of β -alumina through new growth method, while still maintaining thermal and chemical stability at ambient condition [53,54]. Our work thus includes systematic analysis of electrical, chemical, and thermal properties of substitutional doping of indium at aluminum sites which might affect the lattice volume to weaken the ionic conduction due to the increased ionic radius. Till now, β - alumina on addition of only divalent impurities like Mg^{2+} , Cu^{2+} , Ni^{2+} , Zn^{2+} has shown better ionic conduction of Na^+ as reported by Imai *et.al* [55-57]. However very limited studies have been done with trivalent impurities in β -alumina. In sulfide, based solid state electrolyte, substituting phosphorous with indium (In^{3+}) in $\text{Li}_7\text{P}_{2.9}\text{S}_{10.9}\text{In}_{0.1}$ betrays the better ionic conductivity of $\sim 10^{-3} \text{ S cm}^{-1}$ and shows better interfacial similarity and better moisture stability [58-62]. Impurities with ionic radius $< 0.097 \text{ nm}$ are found to impaled into the spinel block successfully and equilibrate the β'' structure [63]. With the intensive development of various energy storage systems, sodium ion batteries have attracted tremendous recognition in the past decades to meet the urgent demands of commercial applications. SIBs with abundant sodium resources, low cost and suitable redox potential had been considered as a prospective alternative to LIBs [64-67]. Nowadays, demand for SIBs is high as tremendous work has been done on it as it one of the best alternatives for LIBs. Furthermore, electrochemical behaviour, thermal stability and fabrication of composite electrolytes based on Li- ion conducting for all SSBs are reported [68-72]. In the last few years, the growing demand for high energy storage batteries

has flourished with new technologies.

However, the LIBs energy density is restrained by low specific capacity and a real mass loading of the active material [73,74]. As we know that among the existing energy storage technologies LIBs have unmatched versatility and energy density but the growth in LIBs have been driven by portable devices. But in recent years however large-scale electric vehicles and stationary applications have emerged because LIB raw materials deposits are unevenly distributed and prone to price fluctuations as these are large scale applications have put unprecedented pressure on the LIB value chain that results in need for SIBs and SIBs are one of the most promising beyond lithium energy storage and has outstanding results in power, safety and cyclability is seen imminent. Moreover, in both composite electrode coating also looks similar because of same conductive carbon filler and binder materials and the only physical difference is the current collectors. In LIBs copper and aluminum foils are used as anode and cathode current collectors while as in SIBs aluminum foils are used as current collectors for both electrodes and it because of sodium does not alloy with aluminum current collectors at anode. Further, with the paucity of lithium metal and rising costs, as an alternative to LIBs, SIBs are showing potential due to higher atomic weight of Na which is somewhat restricted SIBs rate capacity and energy density but still has well application potential.

1.2 Theory of Percolation

When discussing the process of polymerization, Stockmayer (1943) and Flory (1941) were the first to mention the percolation phenomena. The basis for the percolation process is laid out in the polymerization process, in which small molecules join by chemical bonding to produce huge networks of single molecules. Broadbent and Hammersley created the first ever mathematical method for percolation theory (1957). In random medium they proved that percolation process arises from phase transition, and intriguingly, the alteration in the system's transport and physical properties complies with scaling laws and a universal power law. The two primary classifications for percolation processes are lattice (site bond) percolation models and continuous percolation models. A thorough explanation of each of them may be found below.

1.2.1 The Site- bond percolation model

Let's have a look at a standard 2-d lattice where each lattice site has the potential to be filled by an insulating particle with probability $1-P$ or a conducting particle with probability P . Each lattice site's occupation can occur regardless of the likelihood that other sites will also be occupied. In this system, an uninterrupted cluster of conducting sites must cover the entire lattice system for electric current to flow from one end to the other. Here, a cluster is defined as a collection of connected, insulating-site-bound conducting sites. There are isolated clusters of nearest neighbors conducting locations when P , the occupational probability, is low. The conducting isolated clusters do not communicate with one another, therefore the current through the lattice can't percolate. But the system continues to insulate. Alternatively, at high P , the quantity and sizes of the individual clusters increase until they combine to form a single infinite radiating cluster that facilitates the movement of electricity all over the system. The current percolates above a certain concentration with occupation probability P , and stays insulating below,

number (Z), of constituent particles are all directly dependent on the critical concentration PC . We have $PC = 0.5$ and 0.5927 , respectively, for square lattices with $Z=4$ and triangular lattices with $Z=6$. Additionally, we find $PC= 0.3116$ for the simple cubic lattice having an improvement in d but the same $Z=6$, which is less than the systems with $d=2$.

1.2.2 Model of Continuum percolation

Percolation in a continuous medium, have varied site to site to distribution of the coordination number, which makes the situation more intriguing. In this case, the component positions are not limited to the discrete locations of a typical lattice.

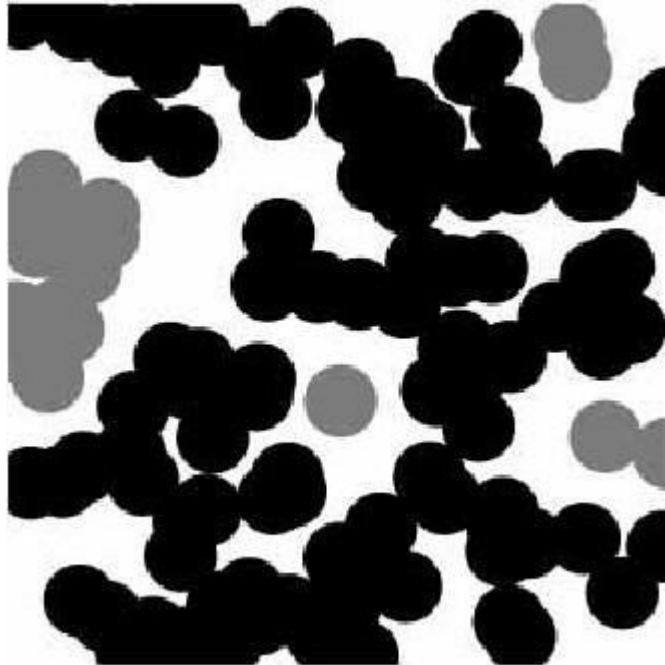


Figure 1.2 Model of Continuum percolation, distribution in continuous matrix

Let us use a conducting sheet as an example, in which round holes have been randomly punched. No matter whether the sites or bonds are occupied or not, the sheet becomes insulating beneath the critical number of holes (PC). It is called the Swiss cheese model because it resembles Swiss cheese. This model is suitable for describing the elastic or transport properties in porous material.

1.2.3 Dielectric properties of composite

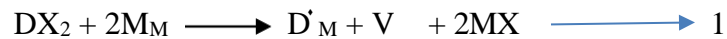
A growing number of environmentally friendly applications, including those for cellphones, digital cameras, chemical sensors, supercapacitors, biological equipment, and many more, call for innovative composites that may be made smaller and perform many functions. For high-tech applications in electrical devices, small loss & high permittivity is shown by the development of composites particularly promising. When high dielectric materials are utilized, memory and capacitance-based energy storage devices may increase energy and deliver it instantly. This motivated us to look for novel, promising materials or to develop techniques to enhance the dielectric response of appropriate materials.

1.3 Solid electrolytes (Ionic Conductivity)

Ionic conductivity of SSEs is a key consideration for modern battery applications. Which is determined by using the pellet's increased resistance, which is impacted by one or the other the physical parameters, such as a frequency, and the material's characteristics. This study demonstrates that the high-frequency point has a greater impact on the ionic conductivity than other factors. We think that with more studies on solid-state batteries, it is now necessary to create a standard method for determining the ionic conductivity of SSEs for Li-ion batteries. The high energy- density needs for future Li-ion batteries (LIB) are thought to be best met by solid state electrolytes (SSE). The fundamental difficulty with SSE is the low ionic conductivity since most SSE have good electrochemical stability and good dimensional stability to ensure the necessary energy density and safety.

Heterogeneous combinations of solid phases make up composite materials. Because of ferroelectric properties may be adjusted to some extent by mixing suitable phases, the development of composites offers a new level of freedom in the search for innovative functional materials There are two ways to improve solid ionic conductors: by looking for new substances and structures that can support

high levels of ionic conductivity, or by adding heterogeneous or homogeneous doping to already existing substances. In the latter, aliovalent dopant is homogeneously dissolved in the ionic conductor $M^+ X^-$ bulk to enhance the quantity of mobile charge carriers in accordance with bulk defect equilibrium. One instance is the so-called Kroger-Vink nomenclature, which describes the generation of additional vacancies by doping with cations of higher valence, such as D^{2+} in place of M^+ .

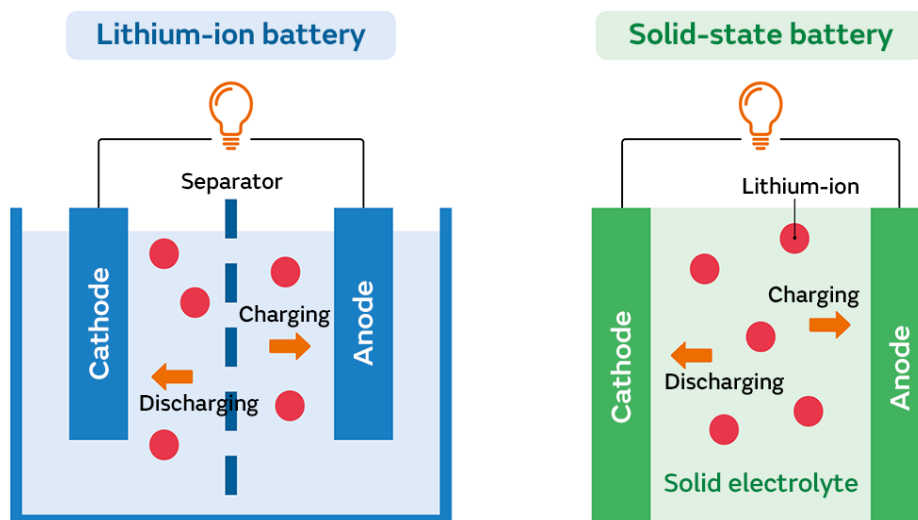


In addition to the advancement of electrical properties like high ionic transference number and high ionic conductivity, the creation of composite materials can also result in superior mechanical properties like better shock resistance or greater strength.

1.3.1 Solid-State Electrolytes

Since the nineteenth century, solid electrolytes and the more well-known superionic conductors have been known. The information about these items has been gathered in a very random manner, emphasizing various materials and elements at different times. Solid electrolyte theory and application have just recently started to coalesce into a single, coherent field. The techniques used to study solid electrolytes are rapidly diversifying, which goes hand in hand with this evolution. State solid in the last third of the century, the science of ions had been exceedingly productive. However, the first observation of conductivity in solid electrolytes was made more than 150 years ago. An SSE, which is an electrically non-conducting material and solid ionic conductor, is distinguishing components of SSBs. It can be utilized in electrical energy storage (EES) applications to swap out liquid electrolytes, such as those used in LIBs. The prime interest includes complete safety, no harmful organic solvent leakage issues, non-volatility, low flammability and is thermally stability, ease of processing, minimal self-discharging, attain higher power densities, and having a cyclability. The ability of

lithium to slow down dendrite growth in the existence of a solid-state electrolyte membrane enables, for instance, without the inherent restrictions of liquid electrolytes. The first step toward creating a lighter and less expensive rechargeable batteries is to use a small reduction potential of high-capacity anode, such as lithium, which has a 3860 mAh g⁻¹ specific capacity and a -3.04 V reduction potential vs Standard Hydrogen Electrode, in place of the conventional low-capacity graphite, which shows a (372 mAh g⁻¹) theoretical capacity in its extensively lithiated state LiC₆. Despite the promising benefits, there are still many obstacles preventing SSEs from being produced on a wide scale, most notably their weak ionic conductivity when resembles their liquid counterparts. Many different electrochemical devices and chemical sensors employ solid materials with extensively ionic conduction as their solid-state electrolytes. The corresponding charge carriers in these systems are ions like H⁺, Cu⁺, Ag⁺, Na⁺, Li⁺, F⁻, and O²⁻. The characteristics and accomplishment of the device are thus determined by the type of charge carriers because of the charged ion movement that results in electrolytes. In solid electrolytes, cations often migrate quickly and exhibit simple diffusion due to their short ionic radii.



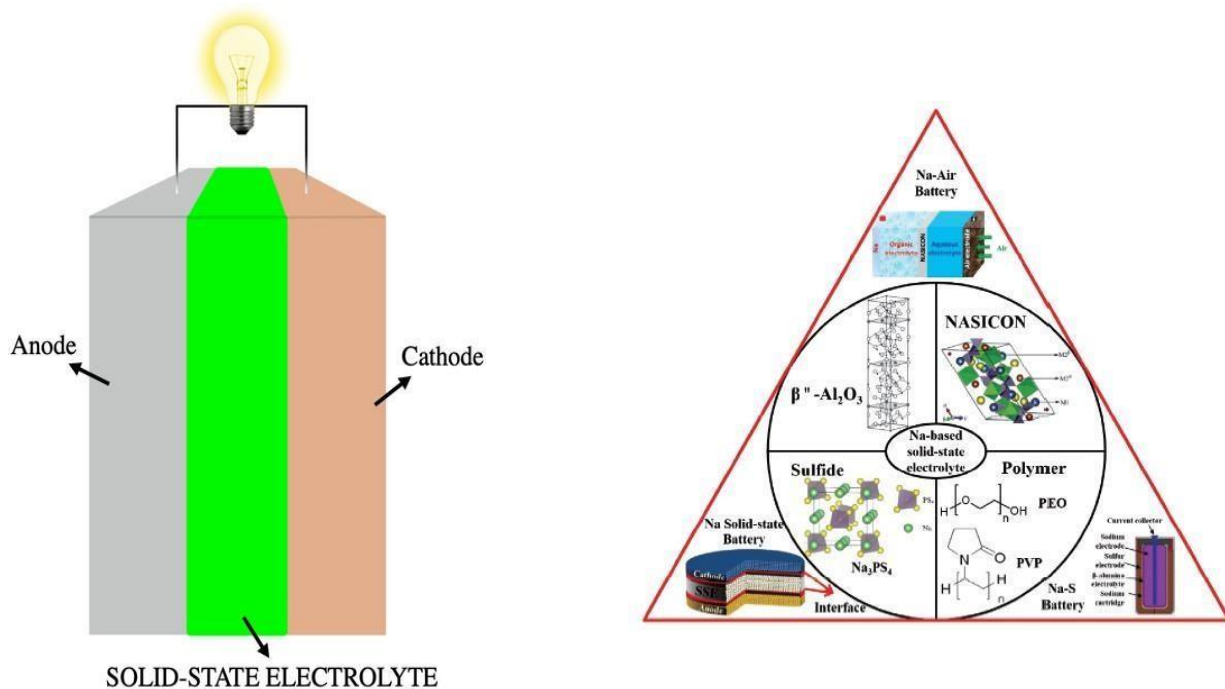


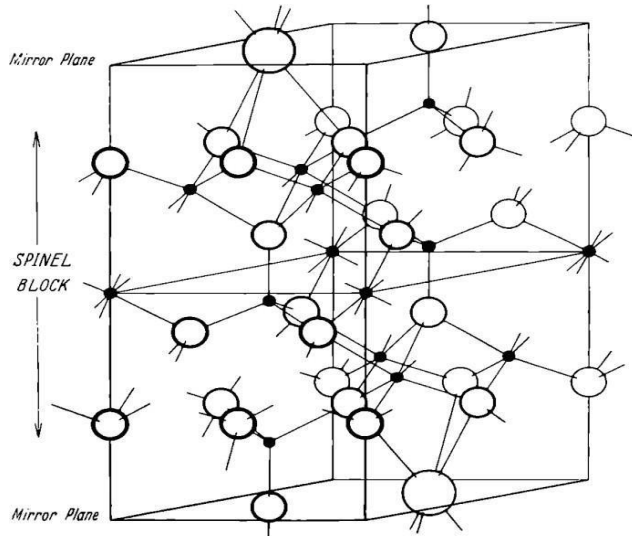
Figure 1.3 Solid State electrolyte

1.3.2 Structure of Solid Electrolytes

While the molten sublattice was proposed a necessary condition for obtaining this state was also recognized: Each of the mobile ions should have available more than the equivalent number sites. Thus, for one ion must have available 1.5, 2, or more sites. This leads to a fractional occupation of the sites when the closest fit between the calculated x-ray diffraction intensities and the observed values is obtained.

The early approach which has been applied till today must be used with the reservation when we want to interpret ionic conductivity. Furthermore, ions are balls albeit flexible. This means that at any time they are in a certain position they occupy space, vibrate, and move. It seems unreasonable to distinguish between different symmetric positions when they are located only a fraction of an angstrom away for vibrating ions of the size of an angstrom or more.

NaAl₁₁O₁₇ (Sodium β -Al)



- O₂ is packed like FCC.
- Na⁺ ions present as each fifth layer
3/4 of the O²⁻ ions missing,
- Spinel blocks are positioned in between layers.
- Having 2-dimensional ionic conductor.

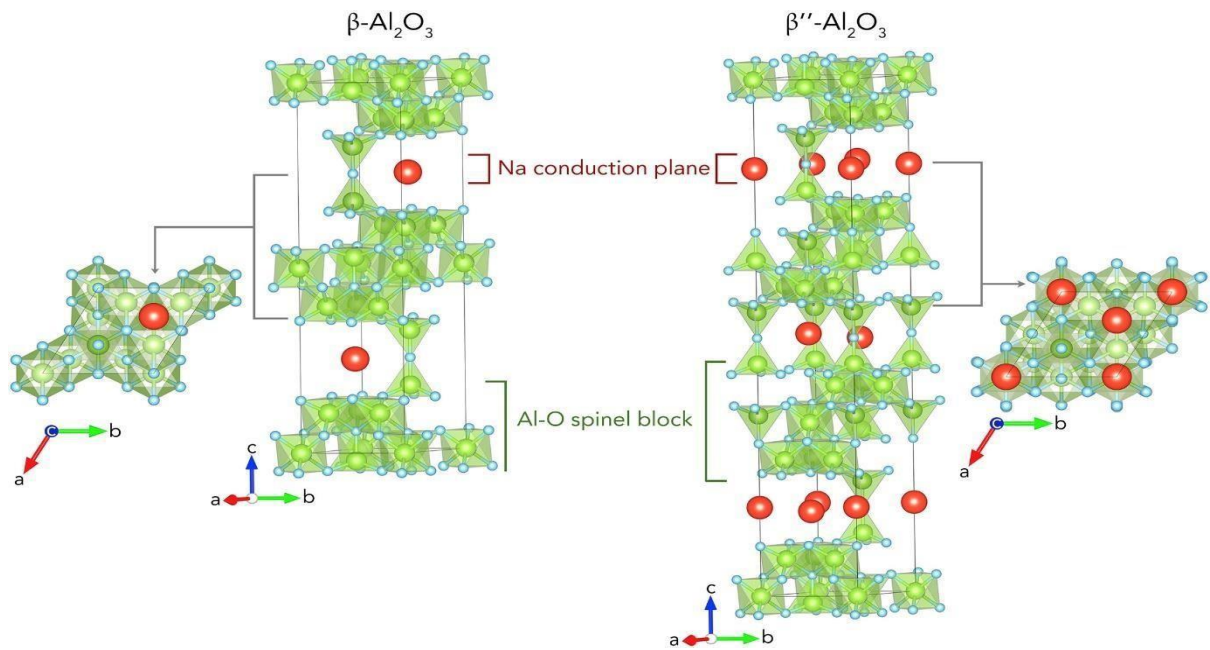


Figure 1.4 Crystal Structures of sodium β -Al₂O₃ and sodium β'' -Al₂O₃.

1.3.3 Sodium β Alumina Solid Electrolyte (BASE):

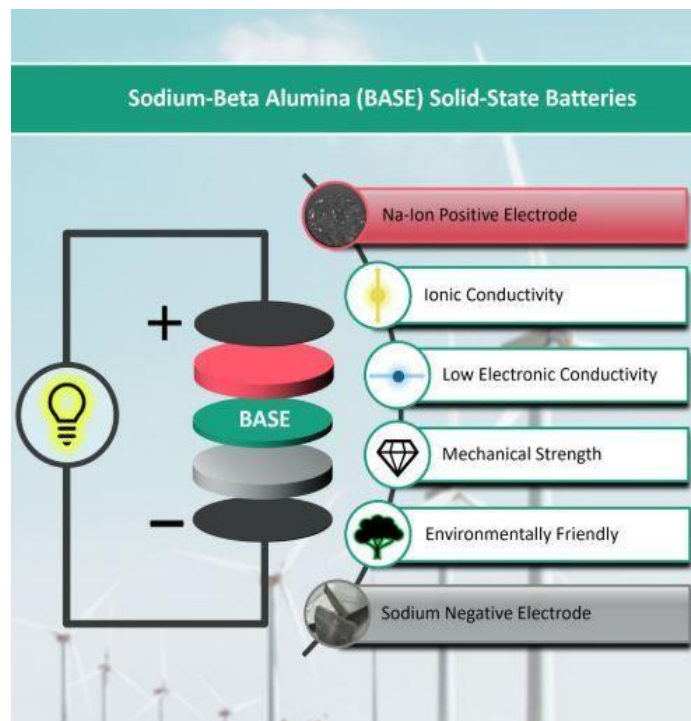


Figure 1.5 Sodium beta alumina (From high to low temperature. (Micha P et.al, 2022))

Sodium β -alumina meets important demands for SSBs in view of its small electronic conductivity, better ionic conductivity, chemically, mechanically, and thermally stable, non-toxicity, and environmental friendliness. At room temperature ionic conductivity is no longer a limiting factor because it now typically reaches levels of 5 mS cm^{-1} . To manufacture thin, however mechanically well-balanced ceramics with intense grain conductivity and small grain boundary resistance, low sintering temperature approaches in addition to standard solid-state synthesis are of interest. In most cell designs, BASE is between 0.5 and 1 mm thick. Overall, the resurgence of interest in sodium β -Al as a SE is due to the advancement of SSBs. The main benefit of sodium β -Al is its high mechanical qualities, which are based on available elements and are environmentally friendly.

1.3.4 Properties

To become a significant market competitor, Solid State Batteries (SSBs) and Solid Electrolytes (SEs) must meet a few important performance criteria. The primary requirements for SSB are:

Ionic Conductivity: Low ionic conductivities in SSBs have been a result of poor ion mobility and interfacial kinetics. Therefore, a SEs with a intense ionic conductivity is crucial. Electrochemical impedance spectroscopy (EIS) analysis can be used to assess very high ionic conductivity (at least higher than $10^{-4} \text{ S cm}^{-1}$).

Volumetric Energy Density: To provide very intense energy density to EV, the contender must also be able to be stacked inside of a single container. To enhance the driving range of EVs between charges, having an intense volumetric energy density is necessary.

Power Density: Which measures how quickly charging and discharging may occur, must be sufficient to make energy available when needed.

Thermal, Mechanical, and electrochemical stability: Experience of SSBs substantial volume changes and mechanically stressed during device or vehicle operation. Additionally, high working electrode potentials have electrochemical stability, which is advantageous for large energy densities. Therefore, it is crucial to consider their thermal, mechanical, and electrochemical stability. A conventional tensile test can be used to determine extreme mechanical strength. It is possible to detect broad ESW using cyclic or linear sweep voltammetry (CV).

Compatibility: Because there is previously significant risk of enhanced resistance in SSBs between electrode and electrolyte material due to the small contact area, the SE must be compatible with those materials. Additionally, when in contact with lithium metal, it must be stable. So that it may be utilized in portable electronic devices, it should be lighter. EIS examination carried out more than once over more consecutive days can measure intense compatibility with the material. A hybrid system of electrolyte, which incorporates the benefits of polymer and inorganic electrolytes, is one of the several additional strategies that can be utilized because it is tough for a single material to meet all the demands.

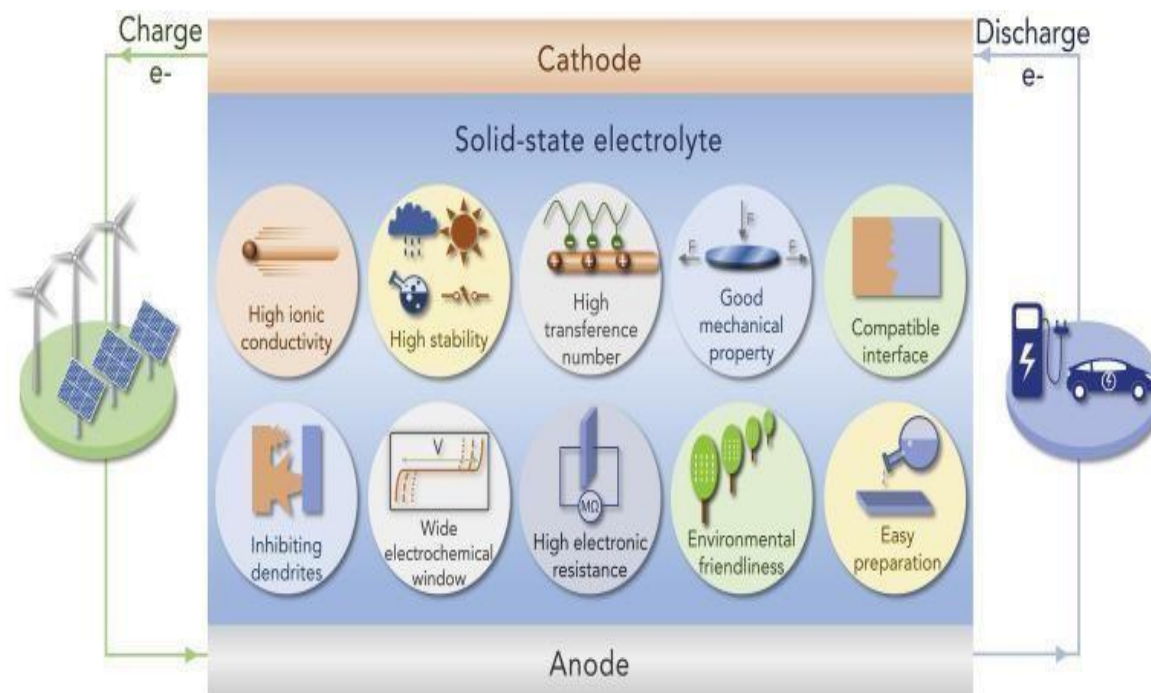


Figure 1.6 The Composition of Solid-State Sodium Batteries and the Corresponding Requirements of SSE.

1.3.5 Applications

Fast ion conductors (FICs), commonly referred to as solid electrolytes (SEs) and super-ionic conductors (SICs), are the substances that act as solid-state ion conductors in solid-state Ionics. They are used primarily in SSBs, Sensors and solid oxide fuel cells among other applications. Several types of devices, like sensors, batteries, thermal batteries, heart pacemakers, smart windows etc. are used because of their significant potential. solid electrolytes have garnered a lot of attention. This section will explore a few of the applications.



Figure 1.7 Applications of solid electrolytes.

1.4 Solid-State Batteries:

Two half-cells combine to form an electrochemical cell. An electrode and an electrolyte make up each half-cell. Either the same electrolyte or a separate electrolyte may be used by the two half-cells. The electrolyte, the electrodes, or an outside material are all involved in the chemical reactions within the cell (in fuel cells, which may utilize the H_2 gas as reactant). In a complete electrochemical cell, there is oxidation (loss of electrons) and reduction (gain of electrons) from electrode. In most liquid electrolyte cells to allocate ionic contact in between the two half-cells with separate the electrolytes to prevent the solutions from producing and mixing undesirable side effects as a use of salt bridge. A dissimilarity in charge is created as flow of electrons from one to the other half cell. This charge difference would stop further electron flow if no salt bridge were applied. A salt bridge keeps the contents of the oxidation and reduction vessels apart while allowing the of ions flow to maintain equilibrium in charge between

them. Gelled solutions and porous pots are additional tools for separating solutions. The Bunsen cell consists of a porous pot.

The voltage of each half-cell has different & having different material choices for each half-cell have several potential effects on variations. After reaching equilibrium, the cell is unable to produce more voltage. Every reaction goes through an equilibrium reaction involving several ion oxidation states. The more likely this reaction is, the closer the equilibrium is to the higher positive state of oxidation of the oxidizing ion/atom in the half-cell.

Electrode potentials can be used to forecast the cell potential. These half-cell potentials are obtained by giving the common hydrogen electrode a potential of 0 volts. The potential measured can be predicted from the dissimilarity in voltage between electrode potentials. One must adjust the half-cell reactions to create a balanced reduction-oxidation equation before calculating the voltage difference.

1. To establish an oxidation process and an overall positive cell potential, reverse the reduction reaction with the least potential.
2. To reach electron balance, half-reactions must be multiplied by integers.

1.5 Sodium ion Battery

One of the most interesting replacement to LIBs is SIBs, which have performance that is comparable to LIBs', abundant sodium resources, less cost, and sodium resources are naturally abundant. Since Na atoms are denser and larger than Li atoms, the gravimetric and volumetric energy density of a Na-ion battery is projected to be comparable to that of Li counterparts. Additionally, because sodium is abundant in nature and offers a superior alternative to lithium chemistry, SIBs may challenge with LIBs in the commercial sector.



Figure 1.8 Various components of a Na-ion battery system

For everyday applications, production of energy and storage technologies have garnered a lot of interest. Global living standards have increased because of developments in lithium-ion battery (LIB) technology in recent years. Both zero- emission electric vehicles and most mobile electronic devices employ LIBs. However, due to their limited supply and anticipated price growth, there are growing worries over the smart grid, load balancing of sustainable sources of energy, and the sustainability of lithium supplies. Therefore, it is yet unclear whether LIBs alone will be able to meet the growing requirements for small- or mid-to-large-format applications for storage energy. Current research has concentrated on different storage of energy technologies as a means of addressing these problems. Due to the availability of sodium and the fact that its chemistry is comparable to that of LIBs, SIBs are appreciated as the most potential next-generation power sources. Transition metal oxides, organic compounds and phosphates, with sodiated layers have recently been introduced as SIB cathode materials.

Despite these obvious drawbacks, the electronics and automotive industries have recently welcomed the technology of new SIBs as a cheaper alternative to pricey LIBs. Due to the wide range of applications and the safety concern surrounding energy storage devices, research communities are making significant efforts to solve the issues they are now experiencing. Finding long-term stable and

affordable materials is one of the most intriguing ways to increase safety as well as power and energy densities for SIBs.

Throughout charging, ions of sodium are drawn out from positive, and transferred into the negative electrode via an electrolyte. The battery discharges spontaneously when current flows through an external circuit; specifically, on the anode, an oxidation reaction takes place when sodium ions leave the negative electrode's structure and enter the layers of the cathode. The negative electrode and positive electrode are the two materials that can accept Na^+ ions in a rechargeable Na^+ ion cell. Electronically electrodes are isolated by electrolyte (pure ionic conductivity). The assembly's performance changes as the components' shape, condition, composition, and alignment are changed, converting the chemical energy stored into electrical energy. A description of SIBs is indicating in Fig 1.9.

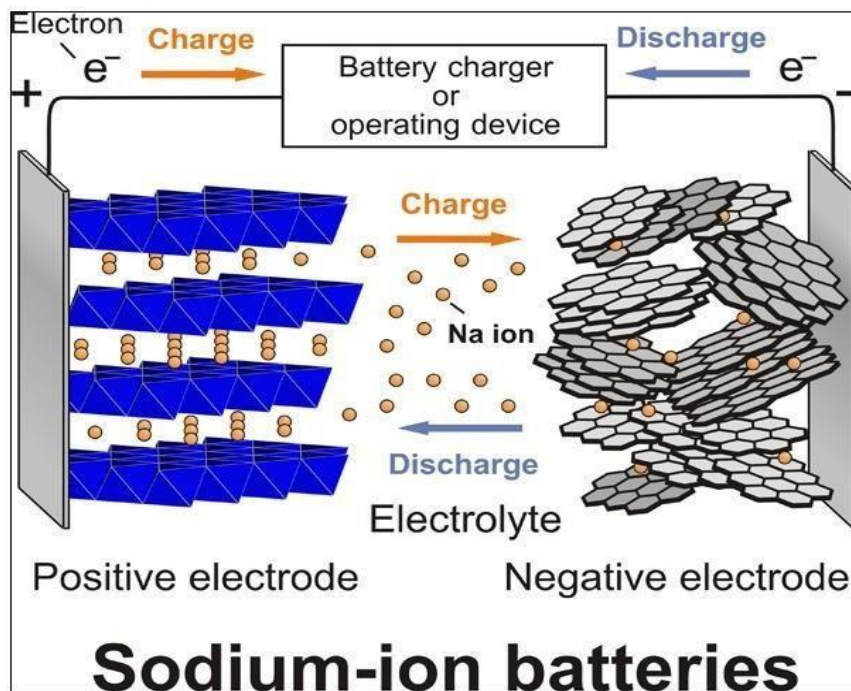


Figure 1.9 working principle of the SIB

1.6 Polyvinylidene Fluoride (PVDF)

PVDF (also known as Polyvinylidene Difluoride or PVDF) is a better purity thermoplastic fluoropolymer, semi-crystalline, composed of vinylidene fluoride. With a suitable temperature can reach 150°C, PVDF combines several properties, including as:

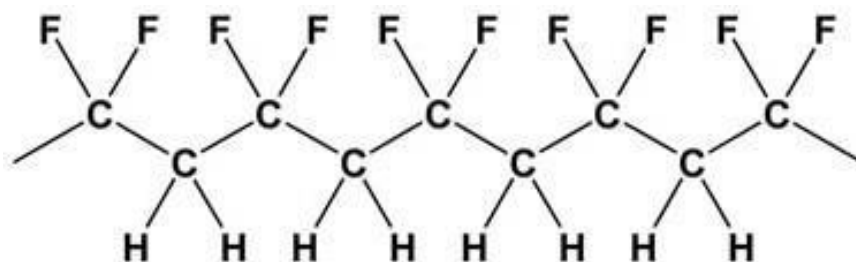
- Outstanding chemical resistance
- Strong mechanical strength
- Piezoelectric and pyroelectric properties
- In addition to having good processability

The highly desirable insolubility and electrical properties of the polymer are due to the polarity of the exchanging CH₂ and CF₂ groups on the polymer chain. PVDF is easily melt-processible, and injection and compression molding can be used to create parts from it. It is therefore frequently used in components for chemical processing machinery including pumps, actuators, valves, pipelines, tubes, and sensors, etc.

It can be used in a wide range of automated devices, particularly as a enrobing material for plenum-rated wire found in phones and video equipment's. The low flame spread, and smoke generation of Polyvinylidene Fluoride are a significant advantage in many applications.

PVDF is growing more popular both as battery separator and as a cathode and anode binder in lithium-ion batteries.

Membranes of fuel cell, inside the parts for airplane, and automation technology are some of the newer uses for PVDF.



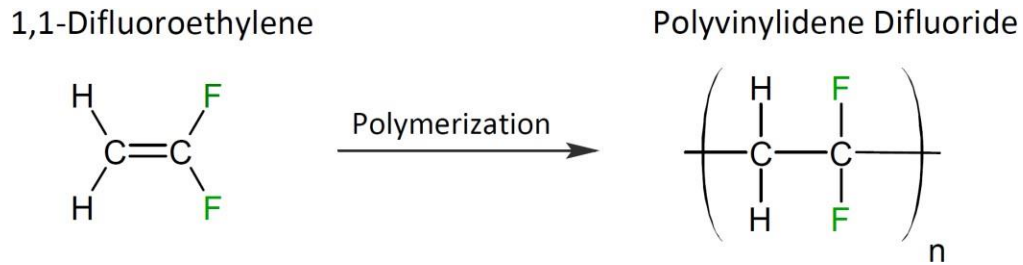


Figure 1.10 Molecular Structure of PVDF

1.6.1 Properties of Polyvinylidene Fluoride (PVDF)

Polyvinylidene fluoride has several properties like crystal structure, physical & mechanical properties, thermal stability, chemical resistance & electrical properties.

➤ Crystal Structure

Typically, it is semi-crystalline that contains around 50% amorphous material. Its structure is extremely regular, with very few monomer units connected head-to-head and the majority units of VDF connected as head-to-tail. The four potential conformations of this fluoroplastic are called phase, phase, phase, and phase.

- C-F bonds are polar, and PVDF's α -phase corresponds to the layout in the same direction for all polymer dipoles to provide the largest dipole moment. Due to the polymer's piezoelectric properties, the β -phase is the preferred phase.
- There is no net polarization since the moments of dipole α crystallites are oppositely orientated.

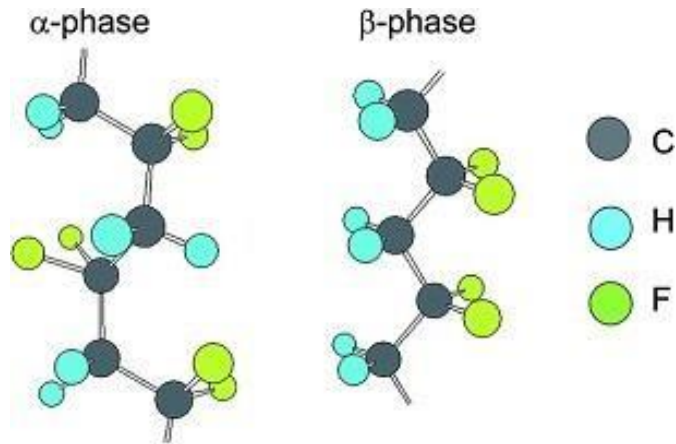


Figure 1.11 Alpha & Beta phase structure of PVDF

➤ **Electrical properties**

Due to its high dissipation factor and dielectric constant, PVDF is employed mainly in wire and cable isolation. However, PVDF sheets with pyroelectric and piezoelectric activity can be generated despite having weak electrical characteristics. Extruded films in B-phase conformation are used to make these films. The film is metalized, then both surfaces are exposed to high voltage, permanently polarizing it. When these films are heated (pyroelectricity), stretched or squeezed (piezoelectricity) to a temperature near their melting point, a voltage is produced. Ferroelectricity can also be seen in polymer films.

In recent years, the piezoelectric polymer sensor industry has experienced some of the fastest technological growth. Currently, they serve as adaptable tools for measuring a variety of processes.

1.6.2 Applications of Polyvinylidene Fluoride (PVDF)

PVDF and its copolymers, which exhibit qualities like flexibility and electroactive responses including piezoelectricity, pyroelectricity, and ferroelectricity, are important polymers. They have been used in a variety of applications during the last several years, including memory, transducers, actuators, and energy harvesting. Check out a few of the applications covered below:

- VDF-based seals, gaskets, lining, etc. are needed by energy-intensive industries, the automotive, military, and petrochemical sectors to resist corrosive elements.
- **Electronic and Electrical Devices:** for high temperature wiring, industrial power control systems, cable jacketing, wire insulation, and electronics sector wiring.
- **Equipment's of Chemical Processing:** Flexible tubing constructed of PVDF resin is frequently used in excessive purity water systems, chemical pipelines, and fuel lines for automobiles, among other applications. As a liner for valves and pipes, it is widely utilized.
- Very sensitive transducers with many uses are piezoelectric films. These films can be shaped into distinctive designs, are robust, light, and flexible, and can be attached with common adhesives.
- Polyvinylidene Fluoride is also used in filters, membranes, housings etc.
- In more complex applications, it could also be employed as a sensor of pyroelectric and a sensor of laser beam profile.
- Since PVDF membrane is chemical as well as thermal stability, it can be employed as separators in LIBs. These membranes feature suitable pore sizes, good mechanical strength, and shutdown characteristics.

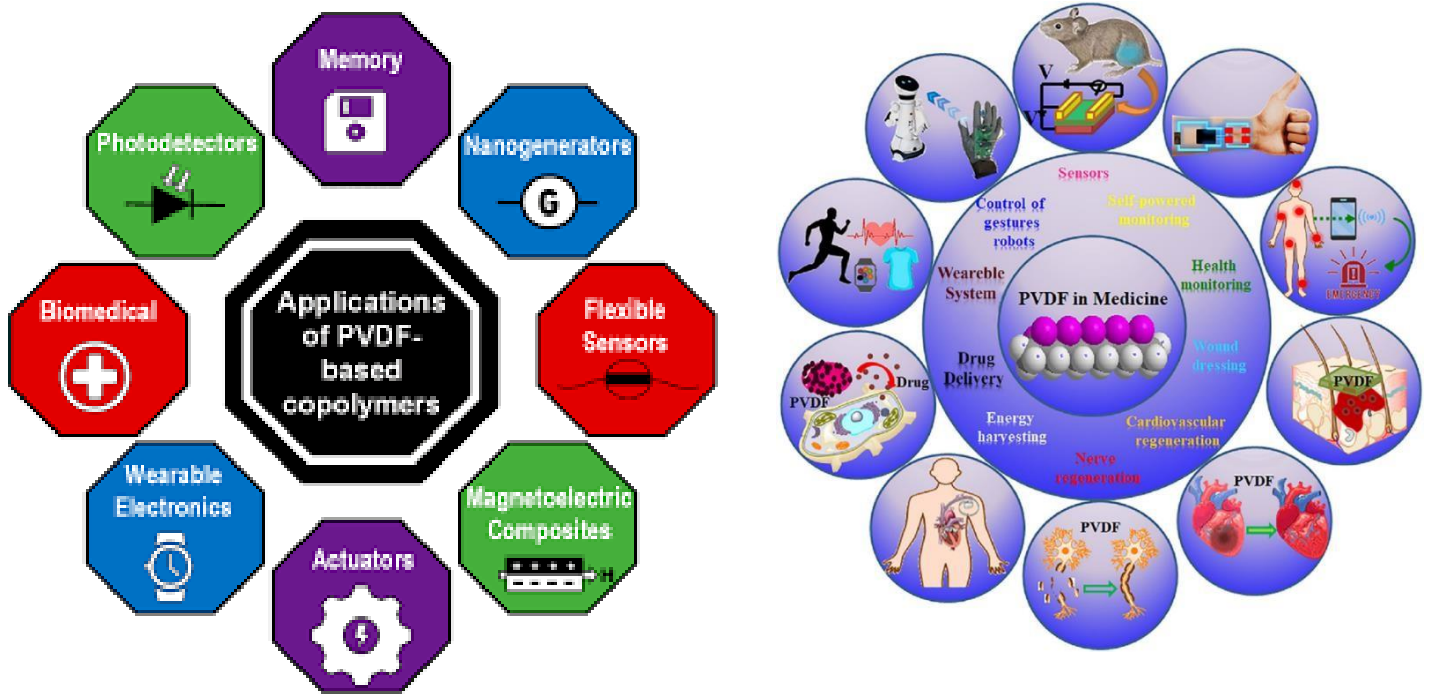


Figure 1.12 Applications of PVDF

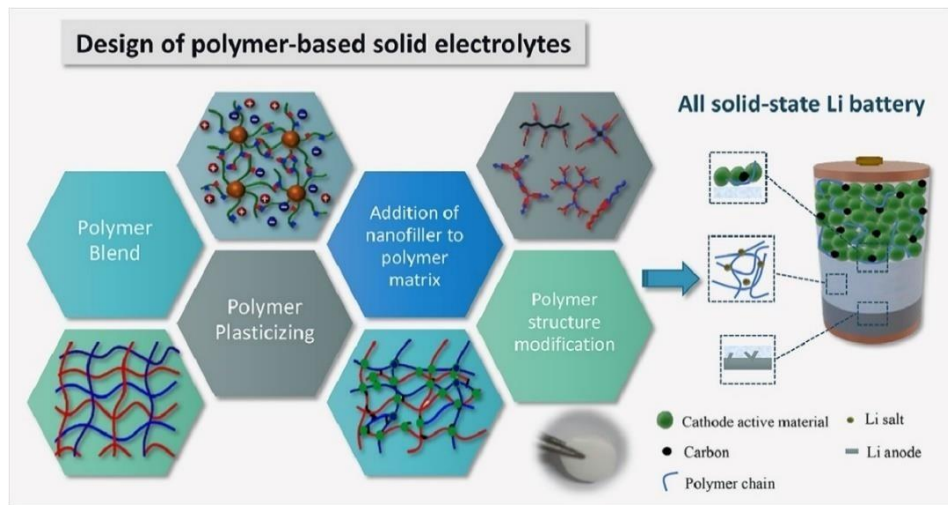


Figure 1.13 Design of Polymer based solid electrolyte.

Chapter 2

Review of Literature

2.1 Literature Review

M. Fertig et al., 2022, in this paper gave a broad review of the development of the innovative, Na-placed batteries with the positive sodium ion electrodes and the ceramic sodium β -Al solid electrolyte. Current research suggests that sodium-beta alumina may potentially be a good material for SSBs, in addition to its successful use in high-temperature batteries. Additionally, sodium-beta alumina satisfies key criteria for SSBs, including non-toxicity, intense ionic conductivity, mechanical, chemical & thermally stability. Furthermore, sodium offers good specific capacity and potential versus the common hydrogen electrode, making the batteries of sodium-based are promising to post LIBs technology. Because of its intense ionic conductivity, mechanical and chemical durability against sodium, and high ionic conductivity, the SE sodium β -Al ($\text{NaAl}_{11}\text{O}_{17}$) displays a special combination of features. In the review's final section, future research directions are predicted. This review's conclusion highlights the intriguing potential of employing $\text{NaAl}_{11}\text{O}_{17}$ in the creation of solid-state batteries [203]. Jieqiong Li et. al., 2021, had talked about how spray drying, and calcinations techniques may successfully create indium-doped solid electrolytes while improving their electrochemical stability and ionic conductivity. By using XRD, FESEM, and FTIR, various characterization results are confirmed. Additionally, they obtain the correct data showing that solid electrolytes function far better than others. Additionally, these findings present a successful Indium ion doping technique that may advance the creation of SEs for LIBs. [1].

Jing Chen et. al., 2021, had noted that the review's primary focus is the viability and safety of LIBs. Additionally, rather than just classifying and gathering fresh materials, they had addressed the tactics by illustrating them with some superb examples. They also explained the main issues with electrodes and electrolytes for Solid batteries. They primarily summarize the four types of practical SSEs (Poly {Ethylene Oxide} PEO-based, polymer gel and S-type electrolyte (Sulfide)), whose potential for improvement method, applications, and potential for mass manufacturing are all examined in this work [2].

Hongliang Li et. al., 2021, in this paper they discussed the electrochemical spectroscopy of

solid electrolytes for all solid-state lithium batteries. As we know, electrochemical spectroscopy is a widely used technique for analysis of interfacial properties related to battery system. In this work they had taken a solid electrolyte and initially the charge-discharge process of batteries at different potential were investigated by EIS and then Nyquist plot, charge transfer process of lithium-ion battery. From experimental results they were concluded that between solid electrolyte and electrode may give rise to all solid-state batteries experiencing capacity fading during charge-discharge [3].

Laurence A. Middlemiss et. al., 2020, had discussed the battery's characterization by electrochemical impedance spectroscopy that is nondestructive technique to investigate the battery system without disrupting the performance of the cells. Additionally, this method is rather simple to use, but in order to analyze the spectroscopic characteristics of battery components, we need very important data. Additionally, the research evaluates and contrasts the benefits of the three-electrode designs reported in the literature. [4].

Hanqing Dai et al., 2020, an investigation was conducted on solid-state sodium-ion batteries (SIBs), which are among the finest possibilities for developing systems which has storage energy in broad range due to their benefits of ample materials, low cost, and high security. Additionally, the CSEs of SIBs comprise outstanding temperature, σ (10^{-3} - 10^{-2} S cm⁻¹), having small activation energy (0.6 eV), and simple cold-press combination. Examined in this review are the CSEs' structure, electrochemical performance, modification tactics, and application technologies. [5].

Naoto Tanibata et al., 2020, discussed SEs with great extensibility in which the compacts of green that can stop the growth of lithium dendrites. Since Li dendrites are known to protect the Li metal electrode for use of high energy density, solid electrolytes are expected to reduce this phenomenon in all solid-state Li batteries. For result analysis, many forms of characterization, including XRD, SEM, NMR, and impedance spectroscopy, are carried out. First principles and conventional calculation of force field were used to thoroughly analyze the criterion for thermodynamic stability ionic conductivity, and formability [6].

Hee-Je Kim et al., 2020, in this review, their analysis focuses solely on current developments in cathode and anode materials for upcoming generation LIBs to meet their increased energy and power requirements for use in upcoming energy storage applications, where the choice of materials is crucial. In this review, they thoroughly illustrated the most recent advancements in anode and cathode materials based on the reactions they undergo. Different types of electrode materials, including metal oxides, semiconductors, nitride, sulfide, and phosphide oxides, influence important characteristics of Li-ion batteries, such as a low diffusion distance and better conductivity. Additionally, because of their drawbacks, such as greater hysteresis potential and poor capacity retention, other conversion materials, such as oxide, nitrides, and sulfides, need to be thoroughly researched. [7].

Archana Chandra et al., 2020, had discussed the preparation for synthesis & characterization of sodium ion conducting electrolyte and successfully explained this. Distinct theoretical and experimental tools have been used for preparation and ion conduction mechanism of solid electrolytes as well as working principle of some of the polymer electrolytes based on conductors had been described. Different characterization had been done like XRD, SEM, FTIR, & TGA to analyze the results. Furthermore, enhancement of conductivity of some sodium ions conducting solid polymer electrolytes has been explained [8].

Anisa I. Agustina 2019, In this study, the sol-gel Pechini process was successfully used to synthesize Li stabilized sodium alumina with a range of sodium contents and sintering temperatures. Characterization was carried out using XRD, SEM, and impedance spectroscopy, and the solvent stabilizer was citric acid with a small amount of ethylene glycol. Additionally, conductivity rises as the sintering temperature rises [9].

Penghui Yao et al., 2019, had talked about their work on lithium-ion solid electrolytes based on composite polymers. Polymer-based solid electrolytes stand out among other solid electrolytes for their superior flexibility, great thermal stability, high level of safety, and minimal flammability. The only promising solution to address or decrease those worries is solid electrolytes. This research also concentrated on ionic conductivities, architectures, electrochemical and chemical stabilities, and the production of solid polymer electrolytes. [10].

Wenjia Zhao et al., 2019, has previously provided a review based on the introduction of common lithium-ion conductors using these electrolytes, hybrid electrolytes (inorganic-organic), inorganic, and organic as well as the conduction mechanism and the relative parameters impacting the accomplishments. They also provide a thorough analysis of a new, enhanced characterization technique and provide a fundamental master plan to enhance ionic conduction as well as future advancement. [11].

Yumei Wang et al., 2019 had addressed the sodium ion battery, its benefits, and provided a differentiation of the ionic conductivity (σ) of several solid-state electrolyte materials as well as the most recent advancements in these technologies. They investigated a variety of electrolytes, but their main interest was in SSEs, which have different advantages over liquid organic electrolytes, including enhanced durability, decreased flammability, and design stability. [12].

Froboese et al., 2019, had discussed about the conductivity of SSEs was analyzed in relation to the influence of electrode structure, which is defined by structures using electrochemically inert glass particles. As they manufacture the electrode structure and this structure is decided by various properties like porosity, pore size distribution, particle size distribution contact area between the morphology of transport pathways or different material phases & the structure is controlled by production and formulation technologies like dispersing, drying calendaring, or mixing. With the help of Electrochemical impedance spectroscopy particular ionic conductivity of SE interior, the electrode is measured and is used to disconnect the electrochemical interaction between solid electrolyte and active material. Furthermore, experimentally manufactured electrode model consists of SE and AM (Model active Material). SE was made of PEO, conducting salt. Materials were granulated and mixed as dry powder, that is fully expressed in electrode and electrolyte manufacturing. SEM images are used to investigate the electrodes model cross section with the following active materials. At last, by combining the volume fraction and asymmetry it was forecast the specific ionic conductivity in the electrodes and possibly by reducing the complexity of model it was predicted the ionic conductivity of SE in all SSB electrodes. With the increase in power and energy density, overall porosity in all solid-state battery electrodes is minimized and porosity minimization is

vigorously dependent on the manufacturing technological processes [13].

Xingwen Yu 2019, In this paper, high performance PEO {poly (ethylene oxide)} composite electrolyte and SE composite approaches for all SSBs were presented. These approaches incorporate the flexibility of polymer electrolytes with the high ionic conductivity of ceramic electrolytes. Because of the plentiful resources and low cost, large-scale energy storage systems are, as we all know, receiving greater attention. In this, a solid electrolyte made of a ceramic/polymer composite was illustrated, which offers hope for the upcoming generation of all SSBs. For the analysis of various outcomes, many types of characteristics including XRD, SEM, CV, and EIS have been performed [14].

X.Chen & P. Vereecke 2019, had discussed the interactions and structural modifications related to polymer-SCE and ILE-SCE interface conduction as well as mechanism of ion conduction of polymer SCE, inorganic particle-based SCE, which presents that by engineering conduction interface we can increase the ionic conductivity of electrolytes which is good strategy for this. The performance of batteries today is limited by numerous key concerns, including the solid electrolyte's ionic conductivity, which are briefly reviewed in this paper along with the replacement of the liquid electrolyte in LIB. Additionally, they provided brief explanations of the ILE-SCE and their preparation as well as the Space Charge Layer Theory, Percolation Model, Conductivity Model, Resistor Network Model, and Effective Medium Model for Solid Composite Electrolyte. [15].

Famprakis et al., 2019, talked about the fundamentals of inorganic SSBs. As is well known, the benefits of solid-state batteries' potential for safety, energy density, and cycle life have drawn a lot of interest. As was already stated in the lines above, by addressing the critical matters in regions of multiscale mechanical properties, ion transport, and electrochemical properties and route of current processing, the authors of this review highlighted the recent progress in the basic understanding of inorganic solid electrolytes that is pertinent to solid-state battery applications [16].

Hasyim and Lanagan 2018, had investigated the dispersed ionic conductors (DICs), a type of composite solid electrolyte that combines insulator and conductor composites. They observed that certain previous models were deficient in some crucial areas, such as the explanation of the non-universal conductor-insulator transition, a solid theoretical basis for their physical theory, and the classification of DICs. Additionally, their work presents a percolation's bond

model for CSEs in the frequency domain using an effective medium approximation (EMA) that is wholly derived from equations of Maxwell's and includes fundamental microstructure factors. Last but not least, impedance spectroscopy of the majority of DICs is illustrated how relaxation modulus peaks and semicircle irregular arcs develop for distinct types of classes and provides information on the percolation behavior and degree of homogeneity of DICs. [17].

Anil Arya and A. L. Sharma 2018, in this paper they reported the electrical, dielectrical, micro structural and structural properties of sodium ion conducting polymer electrolyte prepared by solution caste method. XRD & FESEM is used for analysis of structural and morphological properties of the sample also FTIR analysis confirms the presence of interactions & complex phase formation. The improvement of ionic conductivity of prepared samples with maximum of 4 wt. additionally, they notice that a high value of the dielectric constant and an increase in frequency cause a drop in the dielectric permittivity and dielectric loss. [18].

A. M. Skundin 2018, had in-depth discussions about all aspects of sodium ion batteries in comparison to created lithium-ion analogs. We all know how popular sodium-ion batteries these days are. It had been demonstrated that it was possible to produce an electrode in concept that had a respectable specific capacity value and a relatively long lifetime. Additionally, economic factors are very significant. Because they had no raw material limitations and Therefore, won't face challenges when it continues to stationary plants, sodium ion batteries are significantly less energy dense than their lithium-ion analogs. Additionally, SIBs and LIBs will each have their own marketplaces in distinct application areas without ever going head-to-head [19].

Weimin Xia and Zhicheng Zhang 2018, had talked about the uses of dielectric polymers with a PVDF base in electronic materials. Since they have the highest electroactive response, including the piezoelectric, ferroelectric effect, and dielectric constant, attractive dielectric PVDF and its copolymers are well known to have a immense range of applications in energy generation, transfer, and storage. In this study, numerous physical and chemical fabrication techniques to generate diverse forms of Polyvinylidene fluoride samples, such as ferroelectrics, linear polymers, and others, were found and measured. This was done by identifying the credibility of dielectric performances on the phase crystal structure of distinct Polyvinylidene

Fluoride polymers. Additionally, numerous recent developments in PVDF-based polymer dielectrics are presented, along with some applications that have been created using these polymers, providing references for engineering and academic fields to choose an appropriate PVDF series [205].

Bing-Ang Mei et al., 2018, has discussed the physical interpretation of the Nyquist plot of the electric double layer capacitor. Devices were numerically reconstructed and using an improved “Poisson-Nernst Planck model” and closely matched experimental results because of complex impedance each individual EDLC electrode is represented by a plot exhibiting real versus imaginary sections. With no RC circuits used, the main aim of this study is to clearly explain the physical interpretations of the EIS results for EDCL devices and electrodes. The charge transfer mechanism in the electrode, the formation of the EDL at the interface of electrolyte or electrode, and ion electro diffusion in binary and symmetric electrolytes were all quantitatively simulated by the physiochemical transport model. [20].

Abud Kappel et al., 2017, In this, it was discussed how to use a stochastic method to fit an identical electrical circuit to an electrochemical impedance. As is well known, equivalent circuits are typically used to represent electrochemical impedance spectroscopy, and in order to enable the simulation of impedance data, these equivalent circuits contain characteristics that must be accurately determined. They were each utilizing a different approach to fitting impedance data, but in the end, equivalent circuit fitting was used to mimic fabricated experimental data and show how it worked. Additionally, they have indicated how the study of the suitability of the identical electrical circuit to the physical situation is aided by the frequency effect on impedance spectra [21].

W Liu et al., 2017, in this they had studied that to strengthening the achievements of lithium-ion batteries, the PVDF-HFP gel polymer electrolyte had been examined and was created using the solvent casting method. The conductivity, morphological structure, electrochemical and thermal stability of the electrolyte of polymer were examined using several characterization techniques such as SEM, TGA, EIS, and Linear Sweep. Additionally, it has been shown that the prepared PVDF-HFP gel polymer electrolyte is a useful gel-polymer for use with lithium-ion batteries [206].

S.B. Aziz 2015 had reported the electrical (pc) threshold percolation phenomenon in radiated chitosan-based polymer mixture that was analyzed by EIS. The electric modulus formalism

and dielectric constant to investigate the occurrence of electrical pc in radiated chitosan-based polymer composites is the prime purpose of this work. As far as a recent survey is concerned that there is much less work on chitosan-based polymer composites. Solution cast technique is used to prepare the solid polymer composite of Chitosan and Silver iodide powders for preparation 1 gram of CS is disintegrate in 60 ml solution of acetic acid and continuously stirred for several hours for completely dissolving of chitosan and acquired viscous liquid by adding powder of AgI [22].

A. Saberi 2015, this paper is all about the percolation recent advances & its applications on social, technological & variety of natural have been described & successfully by theory of percolation & also some of the important phenomena are characterized. They talked about the various applications of the theory of percolation to investigate the properties of artificial & natural landscape. Variant of percolation were also talked in which explosive percolation, achlioptas process, correlated & non-self-averaging percolation. Though all this about the advances in percolation & its application having a wide area of network sciences & particle physics, models of percolation are governed by the very simple rules yet fascinating fundamental features [23].

Anand B. Puthirath et al., 2015, analyzed the electrochemical characteristics of LIBs (lithium-ion batteries) constructed using lithium-substituted polyaniline (PANI) and their composites with LiMn_2O_4 and LiFePO_4 as the active cathode materials. Using n-butyllithium, a less expensive alternative to more expensive counterparts like LiPi_6 and LiBF_4 , to synthesize the Li replacement employed as an active cathode material in rechargeable lithium-ion cells, was highlighted in the present. To carry out the experimental results, a class of techniques were utilized to investigate the material, including XRD, SEM, XPS, FTIR, and cyclic voltammetry. [24].

Jialiang Tang 2015, in this paper they had discussed the progress in sodium-ion rechargeable batteries. As we see that day-by-day significance of high accomplishments and the increasingly portable energy storage. Due to the similarities in electrochemical the SIBs are best alternative to LIBs and had put forwards its great fungal & sustainability without sacrifices in electrochemical performances. Moreover, various methodologies are provided by several research groups in accelerating the optimal electrolyte formulation, but it needed more study to develop scalable anode, cathode & electrolyte materials. We had to investigate the

electrochemistry of these materials using whole cell designs in order to obtain long life cycle, good safety features, and adequate energy density [25].

Mukherjee et al., 2014, used the annihilation of matrix at high temperature and, they observe the comprehensive improvement in dielectric permittivity near pc in nanoparticle composites. Using the solid-state technique & process of sol-gel for understanding the dielectric responses they also show that the percolation effect & Maxwell-Wagner effect both have been accountable for the improvement of dielectric permittivity. The characterization was done by XRD, SEM & Energy Dispersive X-ray (EDX) [26].

S. Anwane 2014, had discussed the solid electrolyte's principles and their applications. Gives a detailed overview of solid electrolytes particularly the applications include sensors, batteries, thermal batteries, heart pacemakers, smart windows and explained some of them in this paper. A type of solid known as solid electrolytes possesses ionic conductivity that is analogous to that of liquid electrolytes. The application field is enhanced by the fascinating advantages provided by the electrolytes' solid form. Additionally, it creates a brand-new market for specially created desirable/suitable materials [27].

Mahak Chawla et al., 2014, had discussed about the cole-cole investigation and mechanism of electrical conduction of polycarbonates as cole-cole plot determining the relaxation time with frequency by elucidate static dielectric constant (ϵ_s) value, spreading factor (α), average relaxation time (τ_0), optical dielectric constant (ϵ_1), and molecular relaxation time (τ). In this paper they analyzed the dielectrics (tangent loss, conductivity, dielectric constant), nitrogen and pristine ion's electrical properties implanted polycarbonates. Frequency range of 100KHz to 100MHz were performed for dielectric measurement of samples also it had been noticed that conductivity and tangent loss enhances with enhancement in ion fluence and dielectric constant drops [28].

Mukherjee et al., 2014, this is about the multiple percolation tunneling near percolation threshold of metal-semiconductor nanoparticles composites. They also investigate the various types of percolation tunneling in staircase that are associated with more insulating & conductive complex particle microstructure. In addition to tunneling, they also talked about the classical percolation threshold which can be supplemented by transition tunneling. The characterization is done by TEM, SEM & EDS (Energy Dispersive Spectroscopy) for analyzing the structure, composition & morphology [29].

Vineet Tiwari and Geetika Srivastava 2014, presented their research on polyvinylidene fluoride and how the structural and dielectric properties of PVDF films are affected by the thermal processing conditions. They are primarily concerned with performing a thorough examination of the polyvinylidene fluoride phase and determining how annealing and quenching temperatures affect crystallinity. Different techniques are used for structural and dielectric analysis, such as XRD and FTIR, which indicate that heating effect plays an extraordinary contribution in the formation of the polyvinylidene fluoride's β phase [204].

J. W. Fergus 2012 presented their research on sodium ionic conductivities, compared the findings of various electrolyte materials described in the literature, and reviewed the ceramic and electrolyte properties. As we've seen, the interest in sodium-based batteries is increasing due to concerns over the availability of natural resources. Recently, SIB energy storage improvement has been built using chloride (rather than sulfur) & cathodes, which are known as ZEBRA cells and have varied requirements for different designs. Furthermore, extensively sodium ion conducting solid electrolyte is used frequently known as NASICON that has corner sharing ZrO_6 octahedral and PO_4-SiO_4 tetrahedral that creates a 3-D network channels by which transportation occurs. In addition to this the replacement of zirconium with titanium is improving the conductivity of NASICON at room temperature with high sodium content but another review reveals that at $300^\circ C$ conductivity of NASICON with sodium content ranges drops with titanium doping. Moreover, one more electrolyte is used, that is beta alumina electrolyte that has layered structure and comprise of dense block of Al_2O_3 (aluminum oxide) that is intersected by less heavy packed layered of sodium oxide. Polymer electrolytes have different advantages related to ceramic electrolytes and polyethylene gel as a plasticizer leads to improvement in the conductivity one of the differences between ceramic and polymer electrolytes is that in amorphous, comparatively than crystalline structure is impulsive for intense conductivity in polymer electrolytes [30].

Garagounis et al., 2011, This study provided an overview of the research done in SCERs. As is well known, SEs are used in a variety of products, such as solid oxide fuel cells, separators, sensors, and solid-state batteries. Additionally, solid electrolyte cell reactors had been built using solid state electrolytes. The fundamental operational concept, technologically significant reaction, and obstacles that must be surmounted to implement SCERs in industrial practice are explored. All this research has paid off, though; SCERs offer details on reaction

mechanisms that would not have been possible to learn any other way [31].

Xiaochuan Lu et al., 2010, the full outline of materials used as electrolytes and electrodes in sodium beta alumina batteries, as well as the problems that lie ahead for these materials, were covered in this study. As we the growing interest in Na β -Al ($\text{NaAl}_{11}\text{O}_{17}$) batteries via sodium ion transport stores electrical energy across a β "- Al_2O_3 SEs at typical temperatures. Different kinds of characterization (XRD, SEM & EIS) for analyzing the results [32].

N. F. Uvarov 2008 had presented their research on the physical characteristics of solid electrolytes, emphasizing the significance of component-to-component interaction and the influence of transport parameters and thermodynamic parameters on their interfaces. Additionally, attention is given on the genuine measurement outcomes caused by changes in the ionic salts' vast properties in the nanocomposites, and adhesion energy is merely the primary driving force behind their thermodynamic creation, γ a. Further, experimental data was analyzed and shows that non-autonomous interface phase, amorphous and crystalline, is present in several composites. Adsorption of oxides to ions with the generation of charge layer, deformation of lattice along the interface, and the arrival of interdomain borders caused by misfit dislocation is the main result of enhancement in conductivity. Additionally, a method of theoretical calculation based on an estimating model for a particular morphologically simplified Maxwell-Garnett equation had also been developed. Focus on the size effect also included changes in ionic salt nanocomposites' bulk properties brought on by the impact of energy and the development of the phase interfaces. [33].

R Agrawal and G Pandey 2008, in this a brief discussion of applications of electro-chemical devices (ECD) for fundamentals of perfect electrolyte polymer was made in this review, along with an overview of the development of electrolyte (polymer) materials, their vast group, and recent developments in this area of material science. Additionally, they had talked about use of SSBs and the usual benefits of using electrolyte membranes. Commercial batteries serve as the primary foundation for Li-ion conducting polymer electrolyte, but green and clean electrochemical power sources are increasingly required. [34].

P. Kumar & S. Yashonath 2006, had described the solid state's ionic conductivity, and the NASICON structure is also covered. It seems that ionic conductors of the solid-state ionic are preferable to electrolytes of liquids in several aspects since they have thorough computational,

theoretical, and experimental investigations on them. But rapid ion conductors, also known as superionic conductors, are another name for good ionic conductors and provide a quick summary of superionic conductors. Moreover, NASICON (Na Superionic Conductor) was first discovered by Hong and Goodenough that has progress in the direction of tailored make fast covalent ion with the body structure and because of its some interesting properties that it attributes has unique structural features and properties like high ionic conductivity, low thermal expansion, high thermal and chemical stability & chemical substitution that makes it technologically important material. NASICON is prepared by method of ceramic comprising of solid-state procedure, Process of sol-gel. Because of mixing of components at molecular level most of casessol-gel is found to be superior. Experimentally superionic solid had been studied by using various techniques like X- ray and diffraction of neutrons are used for structural features of superionic solids, DSC & Differential thermal analysis (DTA) are used for thermodynamical properties of solids, Infrared (IR), Raman or far-infrared (FIR) that are useful for recording the vibrational spectra of solids, QENS is important in superionic solid for depicting the ionic motion and NMR that is very useful for confirm in gaining insight to the microscopic ion dynamic in the research of to locate the normal superionic transition in superionic solids[35].

Bluma G. Soares 2006, in this they used various methods to successfully synthesis polyaniline. The equivalent emeraldine base's electric properties, including its complex dielectric modulus, dielectric constant, and losses, have been examined by a DETA in range of temperature of 130 °C to 200 °C and in the frequency range of 0.03 Hz to 10⁵ Hz. Additionally, it was shown that these various methods had a sizable impact on Pani's dielectric characteristics as well as produced polyanilines with various electric relaxation process distributions [36].

F. C. Fonseca & R. Muccillo 2004, had reported that study of percolation in nonconducting SE ceramic composites using the General Effective Model and Impedance Spectroscopy Technique. They prepare a ceramic composite (Ytria Stabilized Zirconia) YSZ varying the small concentration of yttria from 0 to 70 mol% that was prepared with the evaporation of elimination of Zirconia dioxide (ZrO₂:8) mol% Yttrium Oxide, and Yttrium oxide in ethanol followed by pressing and sintering. Furthermore, they are investigating the system both theoretically and experimentally and one of the great things is that in both the investigations there is increase in conductivity (σ) of SEs, with the inclusion of minutely dispersed in

insulating second phase and physical properties, such as dielectric constant, magnetic susceptibility, thermal conductivity & resistivity (ρ) of composite media can be predicting with the percolation theories and general media. Simply experimental techniques by which metallic contamination of Yttrium Stabilized Zirconia powder were decided by spectrographic investigation and samples of composite which they vary from 0 to 70 mol% are make-ready by evaporation of Zirconia dioxide ($Zr_2O_2:8$) mol% yttrium oxide and yttrium oxide in ethanol. Pellets were prepared by pressing at 100 and 200 MPa respectively with thickness of about 2mm. Later, sintering was carried out to avoid the growth of grain and solubilization of YSZ. X-ray diffraction (specimens were analyzed at room temperature with the range $10 \leq 2\theta \leq 90$ having step size of 2θ and 2s counting time, scanning electron microscope (For morphological evaluation of polished and thermal surfaces) and impedance spectroscopy (determination of electrical properties from 300° to 500° in 5 Hz to 13 MHz frequency range) were used for characterization of specimens [37].

Tongwen et al., 2001, discussed the ionic conductivity in SPPO membrane using three-phase model and theory of percolation. They had reported the experimental data of conductivity membranes with distinct degrees of sulfonation that are transit from insulator to conductor and showed the slight change in threshold from 0.14 to 0.19 having concentration range from 0.01 to 0.01. The idea of theory of percolation becomes a strong device for description processes that are like transport properties in disordered medium. Mostly in this research article they plan to explain the transport characteristic of ions through SPPO membranes, and it is widely used in many industrial processes as it has extraordinary mechanical and electrochemical properties. To identify the ionic conductivity transition in such a sulfonated poly (phenylene oxide) membrane they use modern percolation theory as well. Moreover, they used the theory of percolation and three phase model for the theoretical development of various things in SPPO membranes and have been extensively explaining the transport characteristics of the membrane. Experimentally, PPO and DMF are used as analytical reagents, stirring of PPO to form 8% solution at 0.5-1.0 room temperature for with solvent of chloroform [38].

Kumar et al., 2001, discussed ionic conductivity of ceramic composite electrolyte systems PEO: $LiBF_4$ -MgO/BaTiO₃. They are observing in composite system that ceramic phase presents dual effect and suppresses crystallization and interacts with the polymer phase. The main goal of their work is to investigate the relative importance of variables in PEO: $LiBF_4$ -

MgO/BaTiO₃ system and extend the observations in the general class of polymer ceramic composite materials and discussed the effects of dielectric constant and particle size of ceramic additives MgO (10 wt. %) and BaTiO₃ (20 wt. %). These enhance the low temperature conductivity of electrolyte composite either in micro or nanosized. Further, the electrolyte composite LiBF₄-MgO/BaTiO₃ was prepared using reagent of carbide union grade by melt-casting method. The technique involves the mixing of three constituent's elements in solid particle form, melting at 200°C for 15 min. EG & G IS model 398 with frequency range 0.1 Hz -100 kHz on composite electrolyte cells are using for ac impedance measurement [39].

O. G. Gromov et al., 1996, In this the ionic conductivity of SE found on LTP was covered in this study. They were successful in creating a solid electrolyte based on lithium titanium, and they looked at the absorptive of the pellets and electrical conductivity. By substituting the titanium ion and phosphate ion in LiTi₂(PO₄)₃, they were witnessing an increment in conductivity and a decline in porosity. The enhanced sintered pellet density and higher concentration of lithium at grain boundaries appear to be the causes of the increased conductivity in these solid electrolytes. Additionally, the increase in the amount of lithium at grain boundaries as well as the substitution or addition of binder are both effective ways to boost conductivity [40].

Chayambuka et al.,(2020) In this paper they had discussed that challenges and opportunities of LIBs and SIBs as we see that SIBs can replace LIBs and become economically competitive and SIBs have in short period of time demonstrated matching performance metric with LIBs and potential to replace them in large-scale stationary applications. LIB raw materials deposits are unevenly distributed and prone to price fluctuations, these large scale applications have put unprecedented pressure on the LIB value chain resulting in alternative need. SIBs have evolved with the guiding mindset of earth abundant elements and have achieved a high performance/cost ratio as well as SIBs have great recyclability, power, cyclability and safety and the path towards SIBs commercialization is seen imminent.

XU et al., (2023) had discussed the anode materials for lithium ion and sodium ion batteries as we see that characteristic of not being constrained by the lattice structure and cation size, electrochemical conversion reaction is becoming an increasingly prominent type of electrochemical reaction. LIBs can achieve superior performance by utilizing conversion reaction, moreover, SIBs are expected to become alternatives to LIB because of plentiful

sodium resources as well as significant application potential.

Dong Xu et al., (2014) in this paper they had studied the characterization of sodium beta alumina widely known as solid electrolyte exhibiting unusual sodium ionic conductivity properties. As they synthesize the Y_2O_3 doped beta alumina by double zeta process. They synthesis the sample through zeta double process and solid-state reaction and for different analysis they are performing the XRD, SEM, EDS. It has been seen that Y_2O_3 plays a vital role in improving the ionic conductivity and mechanical properties.

2.2 Motivation and Research gap

The literature survey on various papers on solid state electrolytes and sodium batteries has been done. From literature survey it has been found that till now the focus of research is oriented mostly of liquid electrolytes and LIBs. In literature it had been found that mostly electrolytes are got ready by solid-state method and sol-gel auto combustion method. Also, very less literature is found on solid electrolyte in sodium battery. In literature, the ionic conductivities of solid-state electrolytes were also focused, and a lot of discussion had been done on ionic conductivities of SSEs of different electrolytes in various papers. Further, as we see in most of the paper's ionic conductivities of different SSEs where focused the structures of solid-state electrode on the ionic conductivity of SE within a solid-state battery electrode were also demonstrated. Nearly the entire scientific and industrial sectors had turned their attention to solid-state electrolyte because of its exceptional safety and energy density despite of these outlooks solid- state electrolytes face different kinds of formidable barriers due to which the commercialization including surge transfer impedance and insufficient lithium-ion conduction at the interface between solid-state electrolytes and electrodes. Now as far as topic is concerned it is all about the solid-state battery electrolyte and with the help of percolation or percolation based solid- state electrolytes it can helps us to understand the electrical properties of SSEs, effect of percolation in these battery electrolytes.

2.3 Objectives of the study

1. Investigate the effect of percolation in composite electrolytes for Na ion battery.
2. To increase the ionic conductivity of solid electrolytes in Na ion battery.
3. To synthesize polymer-based Na electrolytes and to study the percolative response in polymer composite system.

Chapter 3

Research Methodology

3.1 Introduction

In our research work, we have adopted the process of sol-gel auto combustion to synthesize solid electrolyte sodium beta alumina. Structural, and dielectric properties of solid electrolyte sodium beta alumina ($\text{NaAl}_{11}\text{O}_{17}$) & its composites with composition and different concentration have been investigated. Pure sodium beta alumina and doped composites have been synthesized and characterized to study the ionic conductivity and percolative response.

3.2 Synthesis Method

3.2.1 Sol-gel auto-combustion Method

Sol-gel auto combustion is used to prepare sodium beta alumina, a solid electrolyte. An exothermic reaction between fuels and oxidized occurs throughout the preparation process; this is a wet chemical technique. Nitrates are used as an oxidant and citric acid as a fuel in the current work. Over other synthesis methods, this is the one that is most suitable for creating solid electrolyte sodium beta alumina. The cheapest approach is sol-gel auto combustion method because the precursors are nitrates and there is no need for expensive machinery. It also offers controlled morphology, homogeneity in the samples, time savings, required low temperature, and controlled morphology. The first step in this process is to transform monomers or starting materials into colloidal solution (sol), which serves as a precursor for the subsequent gel formation. The raw material, such as metal nitrates or alkoxides, is usually dispersed in a particular solvent, such as ethylene glycol water, or suitable acid, to form a “sol”, which is then aged and heated to form “gel”, which is then dried or heated at higher temperatures to evaporates the liquid medium and transform the gel into a “precursor”. A sol is a colloid suspension in liquid, whereas gel is a suspension that maintains its shape, hence the name “sol-gel”.

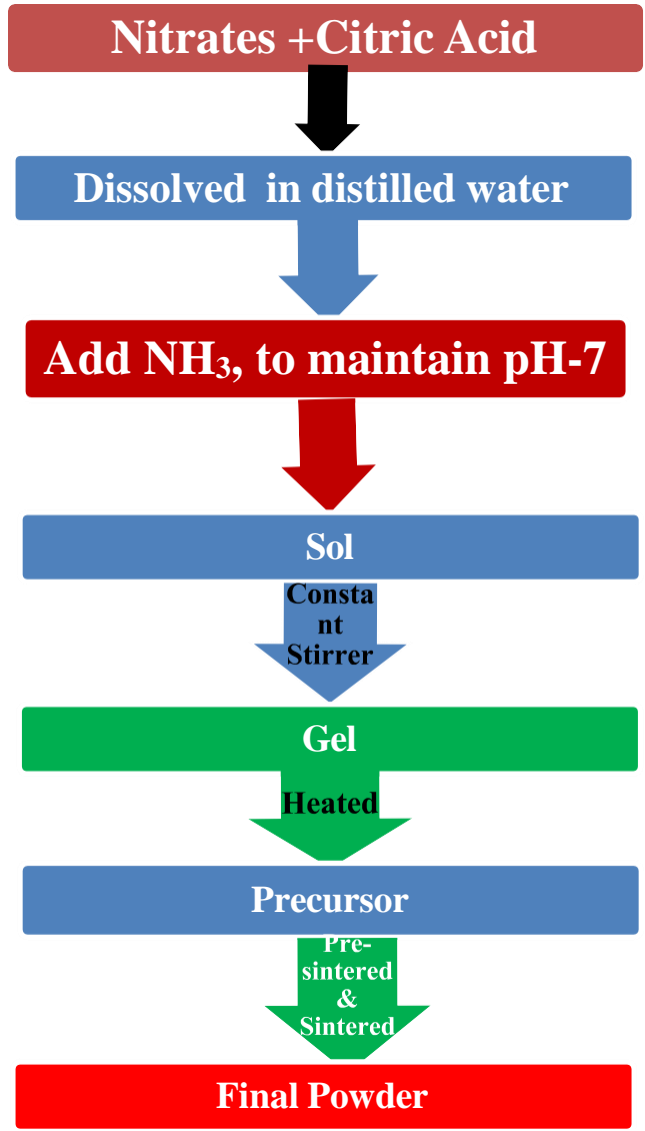
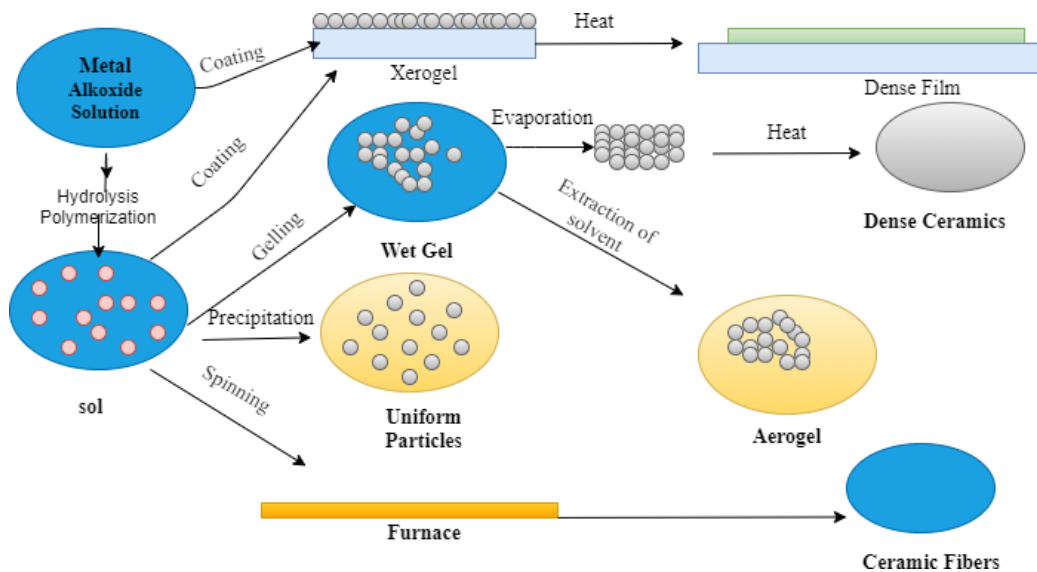


Figure 3.1 a) Process of Sol-gel. (b) Steps of preparation.

In the beginning of the process of sol-gel, gel is formed because of the hydrolysis, condensation, and polymerization of monomers to produce particle and particle agglomeration, followed by the development of a network that spreads over the liquid media. Hydrolysis is the reaction of a material with water, while condensation is the change of a gas or vapor into a liquid.

3.2.2 Synthesis of Sodium Beta alumina (NaAl₁₁O₁₇)

The method adopted to prepare for sodium beta alumina (NaAl₁₁O₁₇) is the sol-gel auto combustion process. The Sodium nitrate, aluminum (III) nitrate [Al₃(NO₃)₃.6H₂O], and Citric Acid (C₆H₈O₇.H₂O) of precursors of grade AR were used to make sample. Weighing the nitrates indicated above in accordance with the stoichiometric ratio was the first step in the formation of sodium beta alumina.

The nitrates along with citric acid were combined in 100ml of purified water with the 1:1 ratio and then remain on magnetic stirrer for half an hour to continuously stirred for clear solution was obtained. Stirring for half an hour, pH of 7 of the solution was stabilized by adding ammonium solution drop by drop into solution. Following that, the solution was heated to about 70 °C while being stirred to generate gel. The gel was heated at 200-250°C for an hour to get black powder. The powder was then finely ground using a mortar pastel. The sample was then sintered in a muffle furnace for 5 hours at 1100 °C.

3.2.3 Synthesis of In³⁺ doping into Sodium beta alumina (NaAl₁₁O₁₇)

Sol-gel auto combustion method is adopted for preparation of In³⁺ doped NaIn_xAl_{11-x}O₁₇ (x=0,0.1,0.2,0.3,0.4). The Sodium nitrate, Indium (III) nitrate, aluminum (III) nitrate [Al₃(NO₃)₃.6H₂O], and Citric Acid (C₆H₈O₇.H₂O) precursors of grade AR were used to make sample. Substituted indium doped beta alumina samples (x=0,0.1,0.2,0.3,0.4) were obtained by weighing these nitrates in accordance with a stoichiometric ratio and placing them into various beakers with 100 ml of distilled water. To obtain a clear solution, these various composition solutions were then maintained on a magnetic stirrer for 30 minutes. Then, to achieve a pH of 7, ammonia solution was gradually added to each solution while stirring continuously. Once a gel had formed, these solutions were kept on a magnetic stirrer for continuous stirring and heating at 70 °C. Then the obtain gel for three samples as kept for heating at 200-250°C for an

hour. When exposed to air, this gel swells, dries up, and burns. The samples' obtained powder dried entirely. The obtained powder for sample $x=0,0.1,0.2,0.3$ and 0.4 is firstly grounded finely and as well as it is sintered at 1100°C in a furnace for 5 hours.

3.2.4 Synthesis of Zr substituted into Sodium beta alumina ($\text{NaAl}_{11}\text{O}_{17}$)

Sol-gel auto combustion method was used to prepare Zr doped beta alumina ($\text{NaZr}_x\text{Al}_{11-x}\text{O}_{17}$) [$x=0,0.1,0.3$]. The Sodium Nitrate, Zirconyl Nitrate, aluminum (III) nitrate [$\text{Al}_3(\text{NO}_3)_3 \cdot 6\text{H}_2\text{O}$], and Citric Acid ($\text{C}_6\text{H}_8\text{O}_7 \cdot \text{H}_2\text{O}$) precursors of grade AR were used to make sample. Substituted Zirconyl nitrate samples were made by weighing the various nitrates in accordance with their stoichiometric ratios and adding them to several beakers containing 100ml of distilled water. To obtain a clear solution, these various composition solutions were then maintained on a magnetic stirrer for at least 30 minutes. Following that, ammonia solution was gradually added while the mixture was continuously stirred to achieve a pH of 7. Then, to provide constant stirring and heating at 70°C until gel is produced, these solutions were held on a magnetic stirrer. The obtained gel was then heated for an hour at $200\text{--}250^{\circ}\text{C}$ for these samples. In the presence of air, this gel swells, burns, and turns into powdered samples after being completely dried. Samples' obtained powder is first finely milled and as well as it is sintered at 1100°C in a furnace for 5 hours.

3.2.5 Synthesis of Zn substituted into sodium beta alumina.

Sol-gel auto combustion method was used to prepare Zinc doped beta alumina ($\text{NaZn}_x\text{Al}_{11-x}\text{O}_{17}$) [$x=0,0.1,0.3$]. The Sodium Nitrate, Zinc Nitrate, aluminum (III) nitrate [$\text{Al}_3(\text{NO}_3)_3 \cdot 6\text{H}_2\text{O}$], and Citric Acid ($\text{C}_6\text{H}_8\text{O}_7 \cdot \text{H}_2\text{O}$) precursors of AR grade was used to form sample. By weighing these nitrates in accordance with their stoichiometric ratio and adding them into several beakers with 100ml of distilled water, substituted zinc nitrate samples were created. To get a clear solution, these various composition solutions were then maintained on a magnetic stirrer for at least 30 minutes. Following that, ammonia solution was gradually added while the mixture was continuously stirred to achieve a pH of 7. Then, to provide constant stirring and heating at 70°C until gel is produced, these solutions were held on a magnetic stirrer. The obtained gel was then heated for an hour at $200\text{--}250^{\circ}\text{C}$ for these samples. In the presence of air, this gel swells, burns, and turns into powdered samples after being completely dried. The obtained sample powder is first finely milled before being sintered for five hours at 1100°C in a muffle furnace.

3.2.6 Synthesis of Polymer based solid electrolyte (Sodium beta alumina)

To intensify the ionic conductivity of the solid electrolyte, we consolidated a hybrid nanocomposite SSE system made of sodium β -Al ($\text{NaAl}_{11}\text{O}_{17}$) and polymer PVDF with different PVDF weight percentages. The hybrid nanocomposite system is prepared by mechanical blending method as per the weight percentage of polyvinylidene Fluoride (PVDF). At room temperature use of 20 -Ton KBR pellet press machine after adding composites. The final pellet was cross-examined by FESEM, Electrochemical Impedance Spectroscopy (EIS), Thermogravimetric Analyzer (Perkin Elmer), and FTIR (Perkin Elmer).

3.3 Characterization Techniques:

3.3.1 Introduction

Different characterizations of sodium beta alumina (substituted or pure) and its composites have been carried out to research and study the variance in structural, morphological, and dielectric properties. Tools for the contribution of new research, such as characterization approaches, are particularly helpful. For the investigation of the various characteristics of the synthesized materials, XRD (Bruker D8 Advance), FESEM Coupled with EDS detector, AU Sputter Coater (JEOL JSM-7610F Plus EDS: OXFORD EDS LN2 free, Au coater: JEOL smart coater), Energy dispersed Spectroscopy (EDS), Thermogravimetric Analyzer (Perkin Elmer TGA 4000) and Impedance spectroscopy (Metrohm: Multi-channel Autolab AUT.MAC.204) were employed.

3.3.2 XRD

XRD is a technique that is frequently operated to characterize the material. The study of crystallographic variations in a material, such as phase identification, is often done using an X-ray diffractogram. The fundamental idea behind the characterization method is based on the constructive interference that happens in cathode ray tubes and results in the monochromatic X-ray beam coming from the crystalline sample. The non-destructive XRD method examines how matter interacts with X-rays. When a monochromatic X-ray beam interacts with the object and scatters in erratic directions with the same energy as the input photons, the result is elastic diffusion, also referred to as Rayleigh diffusion. Only crystalline or semi-crystalline substances can be characterized using this method. Therefore, if the material under investigation has a regular arrangement of atoms, dispersed light is orientated in specific directions that are dictated by the X-ray wavelength, size, and orientation of the crystal lattice.

X-rays are a collection of electromagnetic radiation that is produced by atoms' electron clouds. A fast electron from the cathode collides with an atom from the anode to produce X-rays. A vacancy is produced when an electron from the cathode is expelled during bombardment. To fill the vacancy, the electron must go from its higher shell to its lower shell, and when it does so, an X-ray photon with a specific amount of energy is released. The atoms in the sample scatter the X-ray when it is attacked with it. arrays of spherical waves are created while interacting with the normal array of electrons in the atom. A significant number of waves were cancelled in many directions because of destructive interference. On the other side in some directions some waves added up constructively as explained by Bragg's law mentioned as follow:

$$2d\sin\theta = n\lambda \longrightarrow 3.1$$

d is spacing between diffraction planes, λ is the X-ray wavelength and θ is angle of incidence. All the attainable diffraction direction of the lattice are scanned by angles 2θ . Hence the XRD spectra is recorded in the form of diffraction peaks representing the definite

milller indices values (hkl). The sample identification is done with the help of diffraction peaks that are transformed to d-spacing, and every material has its unique d-spacing.

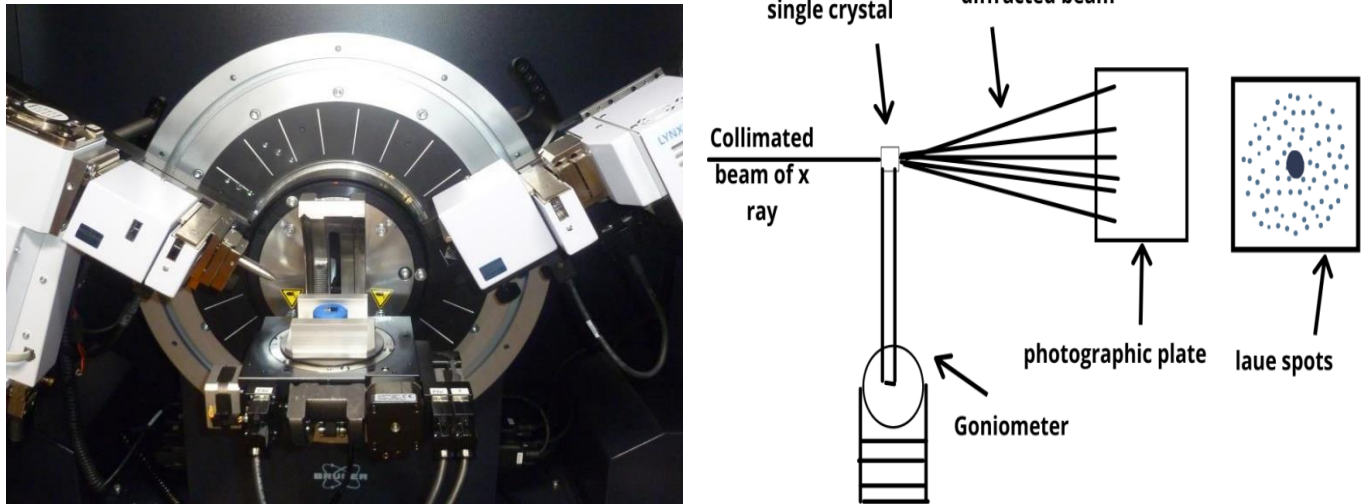


Figure 3.2 XRD Image and analysis principle

3.3.3 FE-SEM

FE-SEM is a helpful electron microscopic method for investigating the structural details of micro-structured materials in high resolution specimens at depths of between 10 and 300,000 times. FESEM has a high resolution that is three to six times better than scanning electron microscopes (SEM) resolution. Additionally, by adjusting the electron accelerating voltages with EDX, smaller contamination patches can be examined (EDX). X-rays and other types of radiation are produced when electron beams interact with a target. The distinctive X-rays of various elements are separated using an EDX detector to create an energy spectrum, which is then analyzed by software to determine how many distinct elements are present in the sample.

The beam is focused by passing through electromagnetically weaker material before it is allowed to fall on the samples. This concentration causes various types of electrons to be released from the material. The secondary electrons are collected by a detector and sample surface images are produced by contrasting their strength with the primary beam of electron used for scanning. The image is finally seen on a computer screen. In fact, the electrons that an X-ray tube emits are used to assess the size and form of objects. When incident electrons hit a material's surface, they cause a variety of effects, including backscattered and secondary electrons, X-rays, heat, and even transmission electrons. However, much of the information regarding the sample's surface structure is provided by secondary and backscattered electrons (topological contrast). To avoid the accumulation of spatial charge, which could destroy FESEM micrographs, the test specimen is first earthed. The specimen's surface is scanned by the electron beam, which subsequently reacts to reveal the particles inside.

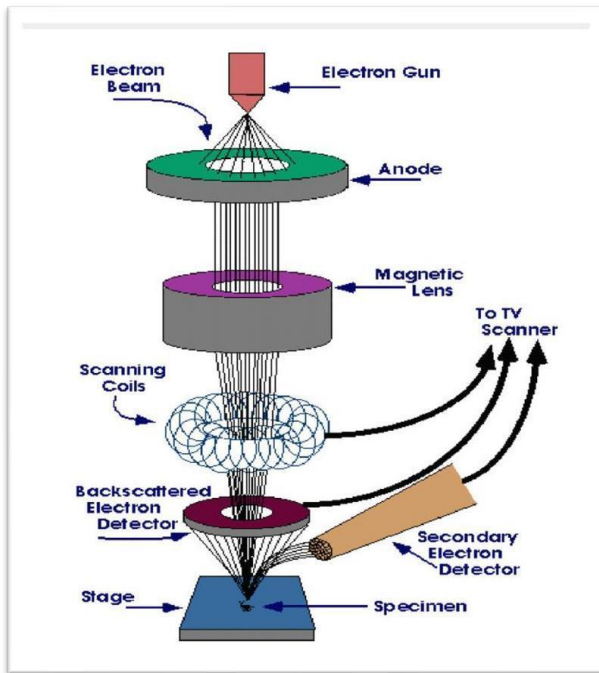


Figure 3.3 FESEM image and Working Principle of FESEM Technique

3.3.4 SEM (Scanning Electron Microscope)

One of the most prominent techniques for surface characterization methods utilized nowadays is scanning electron microscope (SEM). The extensive depth of field offered by SEM is one of its main benefits. Additionally, energy dispersive spectroscopy (EDS) and X-ray diffraction are frequently used in conjunction with SEM equipment to enable high magnification surface characterization as well as elemental composition investigation.

Instead of using light to create images, the scanning electron microscope does it use electrons. As a result, a great portion of the sample can be in focus at once and the depth of field can be increased. Additionally, the SEM generates high resolution images. Most SEMs merely require the material to be conductive, therefore sample preparation is generally simple. The SEM is one of the most popular tools for experimental materials characterization because of its intense magnification, deeper well focused, higher resolution, and simplicity of sample observation. A cathode filament emits electrons in a standard SEM configuration in the direction of an anode. Condenser lenses focus the beam of electron into a beam with a very small size of spot (of 5 nm), typically with an energy of a few keV to 50 keV. The scanning coil and objective lens are then used to focus the electron beam on the sample surface in the desired pattern. Atoms in the sample inelastically scatter the main electrons as they approach the surface. These scattering occurrences enable primary beams of electrons to spread, producing X-rays & electrons that are later picked up and utilized to create an image of surface.

Detecting the (BSEs) backscattered electrons, which are important earliest electrons that have been elastically dispersed, is another way to use a SEM. Although backscattered electrons' significantly higher energy (about equal to the main beam) makes them more likely to be dispersed from deep within the sample, they can still be employed to identify topological and compositional information. This leads to topologically less contrast than in case of SE in this result. In contrast, there might be some distinction between regions with diverse chemical compositions since the backscattering is only a fragile function of atomic number, particularly when the number of atoms is average of the various regions is significantly varied. The size of beams of electron spot and the size of the substance that the electron beam interacts with determine the SEM's spatial resolution. The interaction distance prevents imaging of atomic

scale images because these are larger.

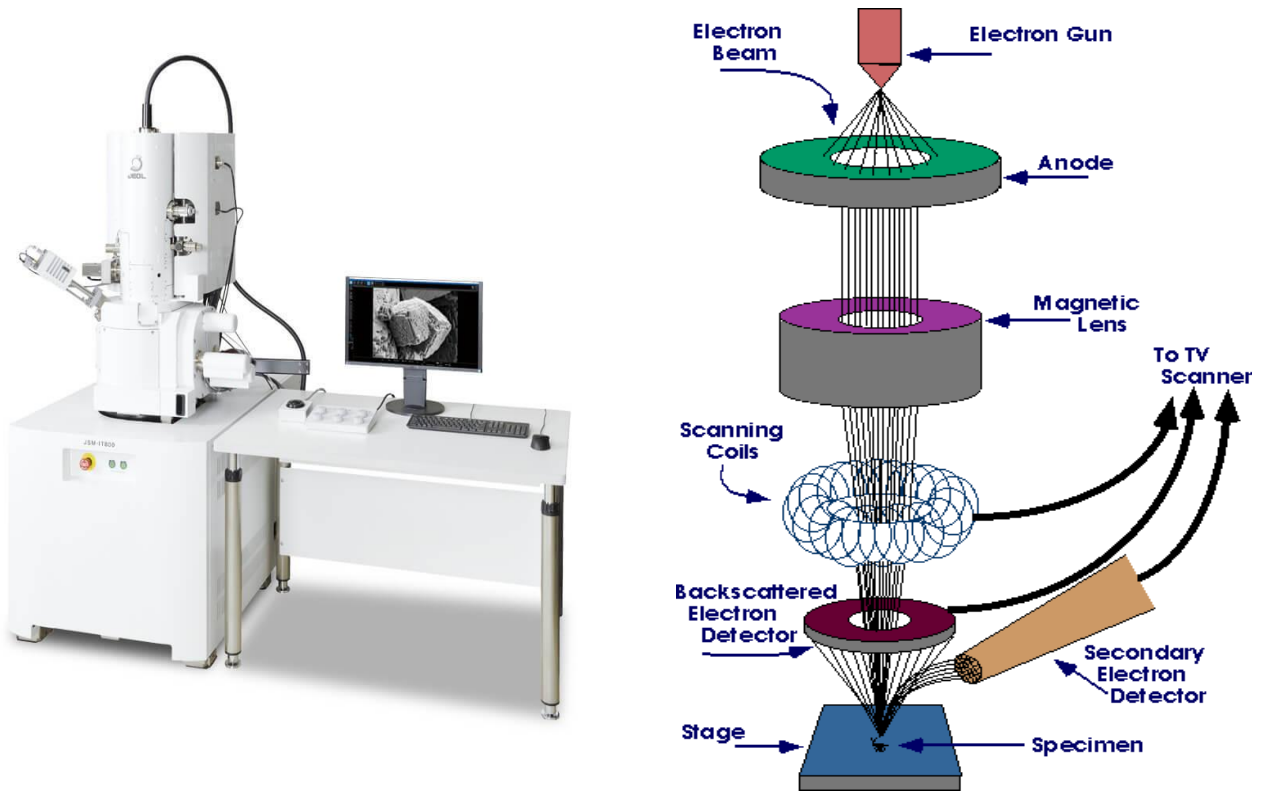


Figure 3.4 SEM image and Working Principle of Scanning Electron Microscopy (SEM)

3.3.5 Energy Dispersive Spectroscopy

An SEM is frequently used in conjunction with the chemical microanalysis method called as EDS. The EDS method uses X-rays produced to make the sample during beam of electron irradiation to identify the composition of elements that are examined by volume on a microscale.

Atoms in the beam of electron's path in a SEM's scan across the sample surface, emitting X-ray fluorescence. X-ray photons energies are suggestive of element that is generated by them. The X-rays that are released are counted and weighed by the Energy Dispersive Spectroscopy X-ray detector. The energy of the X-ray can be used to determine the chemical element that produced it.

The elements contained in the sample identified by measuring energy of the X-rays that are emitted when an electron beam excites a certain area. Qualitative analysis is used to identify the elements of samples. It is also possible to gauge the concentrations of the various elements by counting how often these distinctive X-rays are detected. Analyzing data quantitatively is this mode. The systems may obtain the X-ray maps indicating spatial difference of elements in sample if the beam of electron is swept across a portion of sample.

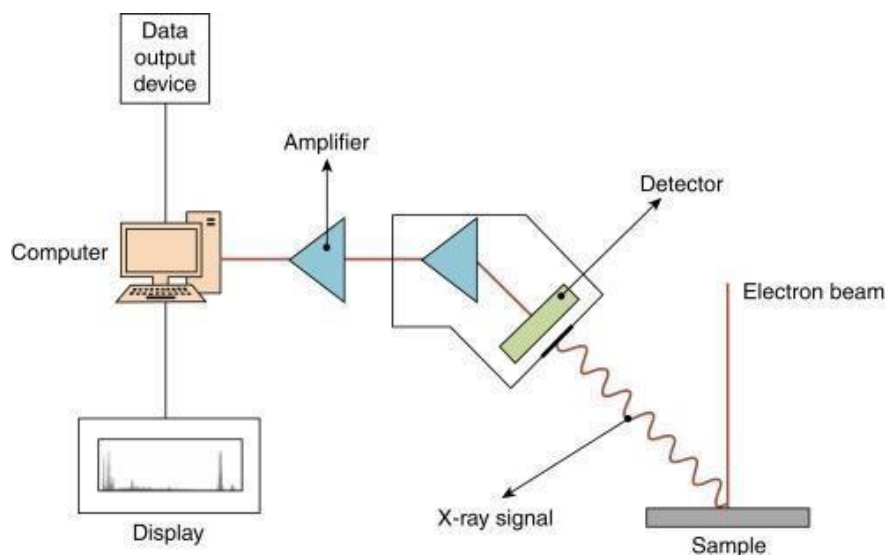


Figure 3.5 Schematic description of EDS

3.3.6 Electrochemical Impedance Spectroscopy (EIS)

Electronic Impedance The electrical response of chemical systems may be ascertained without causing damage using the highly sensitive characterization method known as spectroscopy. To characterize the material behavior of chemical methods, EIS systems employ low amplitude AC voltages dispersed over a broad area of frequencies. The working, reference, and counter electrodes are used in an electrode setup to transfer a known voltage via an electrolyte solution from the Counter electrode to working electrode. At the electrode contact and within the electrolytic solution EIS generates quantitative measurement by evaluation of microscale chemical mechanisms. EIS is useful in determining a various kind of electrical and dielectric properties of components.

To measure the electrical response of an electrolytic solution, an electrochemical spectrometer is electrically coupled to an electrochemical cell that houses the chemical reaction. Computer

programs created especially for EIS testing are used to operate EIS systems. Therefore, it is imperative that all system components are in place before conducting an EIS experiment. The typical electrode configuration for EIS studies consists of a working electrode, a counter electrode, and a reference electrode. The general experimental setup having the steps listed below, even though geometries of electrode may change.

On an electrode stage, the three electrodes are fixed in place. The sample container receives the electrolytic solution that has been prepared. If the sample container were composed of metal, electrons would have more locations to go during the experiment than the reference electrodes, reducing the EIS current response. As a result, the container of sample should be constructed of a nonconducting material, such as plastic or glass, that won't block the electron's flow throughout testing. The mount of electrode is placed on the containers of sample and in electrolytic solution each piece of electrode is immersed. Three electrodes are connected to the frequency analyzer of EIS via four connections. While the reference and working leads are used to recognize voltage, working lead and counter lead are used to carry current. The working electrode's exposed end is connected to the Electrochemical impedance spectroscopy by the working lead and recognized working leads. The counter lead is connected to the counter electrode, while leads of reference is tied to reference electrode. It is proposed that system is grounded in the time of testing using the fourth lead. The EIS system is configured and prepared for testing once all leads are connected.

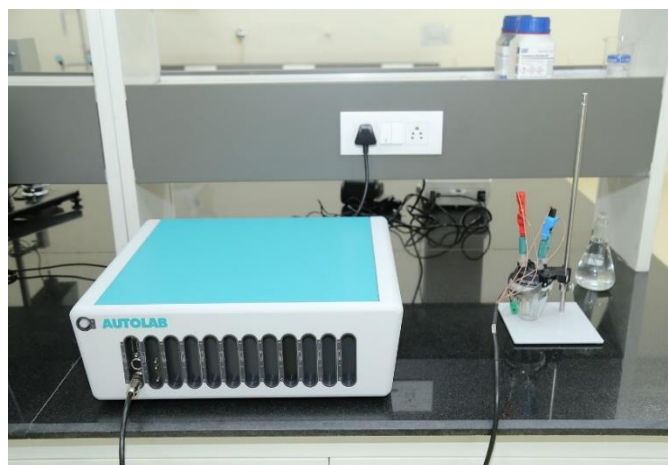
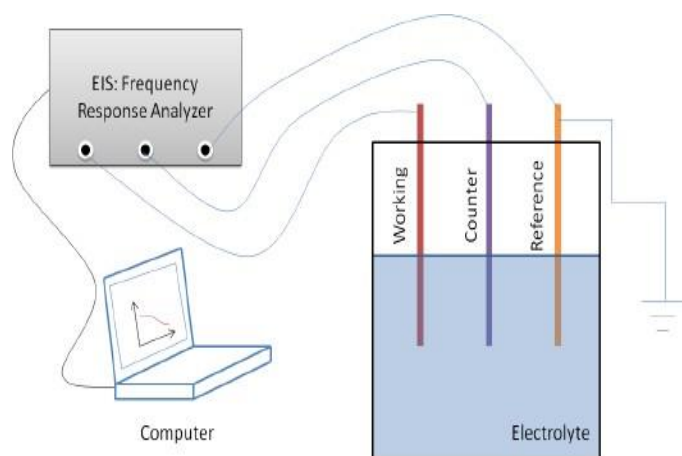


Figure 3.6 Image of EIS & Experimental system

3.3.7 TGA

Thermogravimetry is a branch of thermal analysis that focuses on how a substance's weight changes over time or space. After the sample has gone through a regulated heating or cooling process, the weight change profile is documented. The term "isothermal mode" is used when we are calculating the weight varies as time function. Weight fluctuation is quantified in scanning mode as a function of temperature. The primary idea behind thermogravimetric analysis (TGA) is that the sample's mass change can be seen when particular circumstances are met. Therefore, TGA is largely utilized to comprehend a wide range of thermal processes, including absorption, sublimation, breakdown, adsorption, oxidation, reduction, desorption and vaporization, on samples like fibers, paints, coatings, nanomaterials, polymers and polymer nanocomposites, and films, TGA can also be used to evaluate volatile or gaseous compounds lost through such chemical processes. TGA can be used to forecast the thermal stability of materials as well as to investigate the kinetics of chemical reactions under diverse situations. Optimizing the variables or conditions that affect the samples' mass change over the course of the experiment is crucial for studying kinetics. Weight and volume of the sample used for investigation, physical form of sample, shape & type of sample holder, nature of the atmosphere under which the investigation is conducted, pressure of the atmosphere maintained in the sample chamber throughout the analysis, rate of heating or cooling, and other factors have been found to affect mass change. It is common knowledge that sample mass changes with the effect of temperature. Not all kinds of thermal changes can influence how much weight of sample is changed which is crucial to realize. During melting and crystallization TGA, for instance, cannot be used to investigate the behavior of materials.

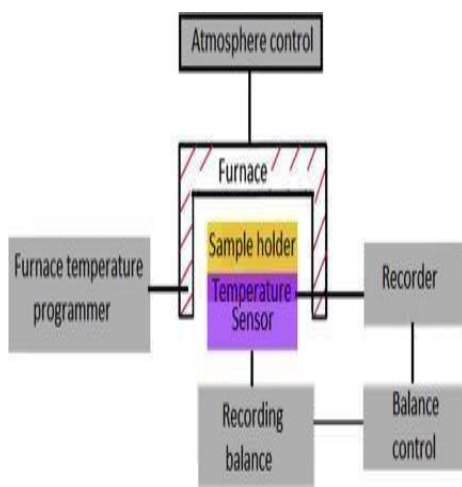


Figure 3.7 Image and Schematic representation of TGA

3.3.8 Fourier Transform Infrared Spectroscopy (FTIR)

The technology of FTIR spectroscopy was used to investigate the interactions between infrared and sample. It is preferred over the others since it is the most recently created type of spectrometer. Its success is largely due to its exceptional precision, enhanced sensitivity, accuracy, speed, simplicity of use, and sample non-destructiveness. Technology for infrared spectroscopy is based on the vibrations of atoms of a molecule, which only absorbs infrared radiation at certain frequencies and energies. Due to diverse infrared spectra of different chemicals, FTIR could be used to verify and categorize them. Its task is to investigate the vibrational characteristics of matter's molecules. The numerous functional groups and residues contained in a sample can be identified using this technique. The IR region, which extends from (0.7-1) to (200-350) μm and can be categorized into three ranges that are as follow: Near IR 13000 -4000 cm^{-1} 400-10 cm^{-1} , Mid IR between 4000-400 cm^{-1} Far infrared between 400-10 cm^{-1} . The far-infrared has low energy, so it is used to study the fundamental and rotational vibrations. Mid infra-red having moderate energy is used to study coupled rotational – vibrational structure. Far infra-red has high energy, so it is used to for the excitement of overtone vibrations. For the characterization purpose mid-infrared spectrum is used. Infrared radiation is passed through the material to be absorbed by the molecules it contains in FTIR spectroscopy. The vibration frequencies of the molecules must be equal to those of radiation so that matter can absorb energy. When light strikes a sample, one part of it is reflected, another is absorbed, and the third is transmitted. The exact frequencies of energy absorbed by the specimen match to the vibrational energy of the functional group in the sample. A detector collects the transmitted light that carries the sample's molecular information.

Figure: represents the basic principle of FTIR technique. The mid-infrared frequencies in FTIR are measured by the interferometer within a few seconds. The interferometer is used to analysis the energy that is transmitted through the material. The interferometer contains a beam splitter, stable mirror and moving mirror. that split the falling IR radiation in two parts. One beam is set so that it can retain fixed path length and create a path difference for the other beam that is varying according to moving mirror. These two beams interfere constructively, and a beam is emitted out from the interferometer which is known as interferogram. The emitted beam

consists of all the information about the sample. With the help of mathematical technique software named Fourier transformation, all the information is decoded from the individual frequencies. Nicolet FTIR interferometer IR prestige-21 with model-8400S was used for FTIR spectrometer

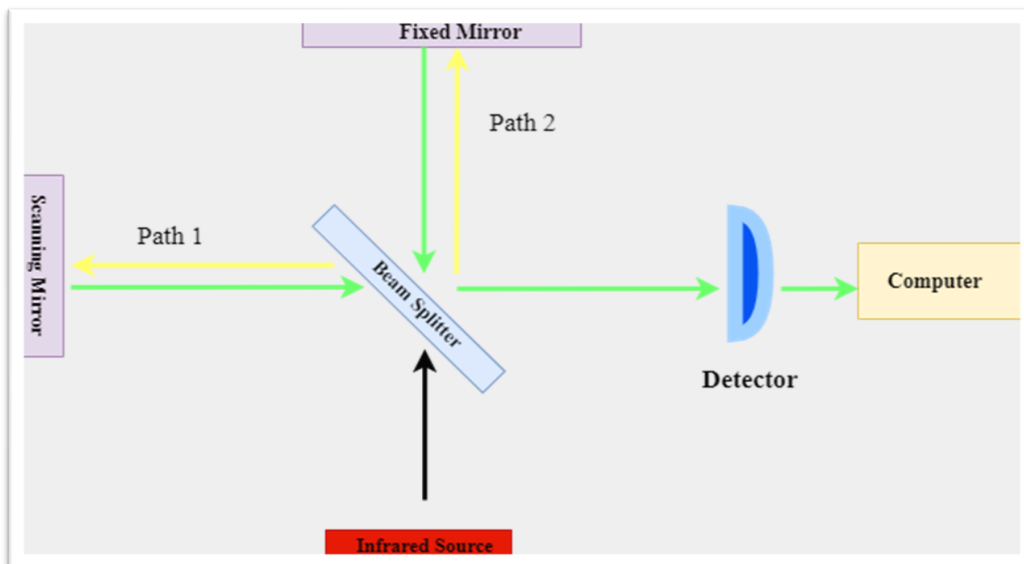


Figure 3.8 Principle of FTIR technique

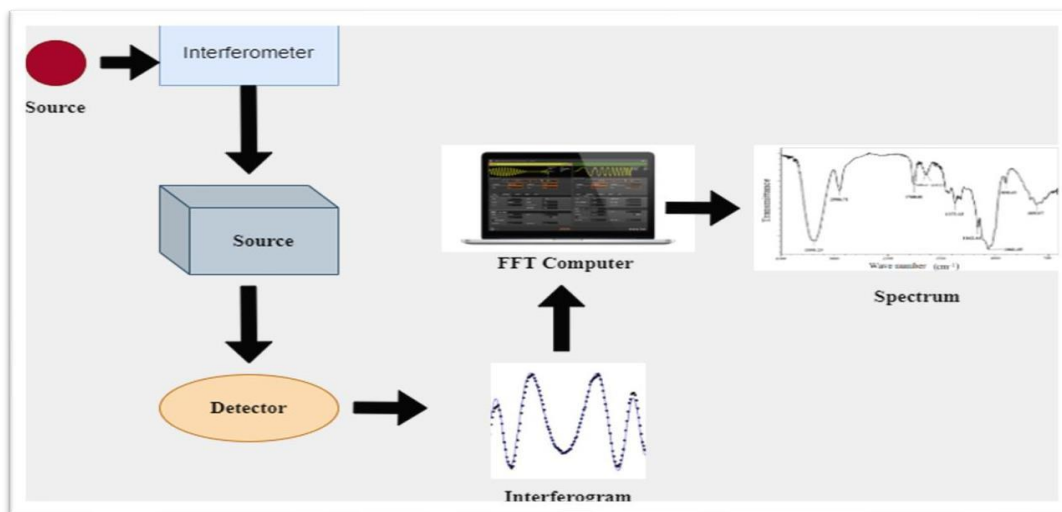


Figure 3.9 Working of FTIR Technique

3.3.9 Ultraviolet-visible (UV-vis) Spectroscopy

This method is mostly used to identify chemical species in a sample. This approach is unique in that it studies atoms' electronic transitions. Generally, excitation of electrons from lesser energy state to top energy state is typically observed when the atoms or molecules absorb the ultraviolet (UV) and visible radiation. The quantum energy levels of atoms imply that only that radiation is absorbed that have specific amount of energy and is capability to make transition from one state to another. The basic principle of spectroscopy is in accordance with Beer-Lambert's law. According to this law (**Equation 3.1**) the absorbance (α) is directly proportional to the path length of the absorbing medium (b) and quantity of the sample (c).

$$\alpha = \log_{10}(I_0/I) = \epsilon bc \quad (3.1)$$

Herein I_0 represents intensity of reference beam, I represent the beam of intensity of sample and ϵ is proportionality constant. The UV radiation have energy between 200 to 400 nm which is more enough capable of electronic excitations within molecular orbitals (ΔE). ΔE is the distinct of energy between the HOMO and LUMO. Which means if the value of ΔE is small than the energy requires for the excitation of an electron will also be small. The incident photon must have ΔE equal to or larger than the energy of the excited electron only than it can get absorb and able to excite the electron.

This method makes use of monochromatic radiation, which can be UV, visible, or near infrared. When radiation strikes a sample, it can cause the molecule to undergo an electronic transition. The color of a material is linked with its electronic structure. This spectroscopy allows for the evaluation of all electronic transitions as well as the determination of certain sample properties such as band gap energy, which allows for the classification of the sample as an insulator, semiconductor, or conductor. When light (energy) falls on a sample, it is usually absorbed. The absorbed energy encourages electrons to move from the lower state to top orbital state or to anti-bonding orbitals. Figure represents the all-possible transitions, when photon get absorbed ($\sigma\text{-}\sigma^*$, $\pi\text{-}\pi^*$, $\sigma\text{-}\pi^*$, $\pi\text{-}\sigma^*$, $n\text{-}\sigma^*$, $n\text{-}\pi^*$). But in UV- vis spectroscopy $\sigma\text{-}\sigma^*$, $\pi\text{-}\pi^*$, $\sigma\text{-}\pi^*$, $n\text{-}\sigma^*$, $n\text{-}\pi^*$

transitions are possible, whereas $\sigma\text{-}\sigma^*$ and $n\text{-}\sigma^*$ transition requires high energy and $\pi\text{-}\pi^*$ and $n\text{-}\pi^*$ require less energy.

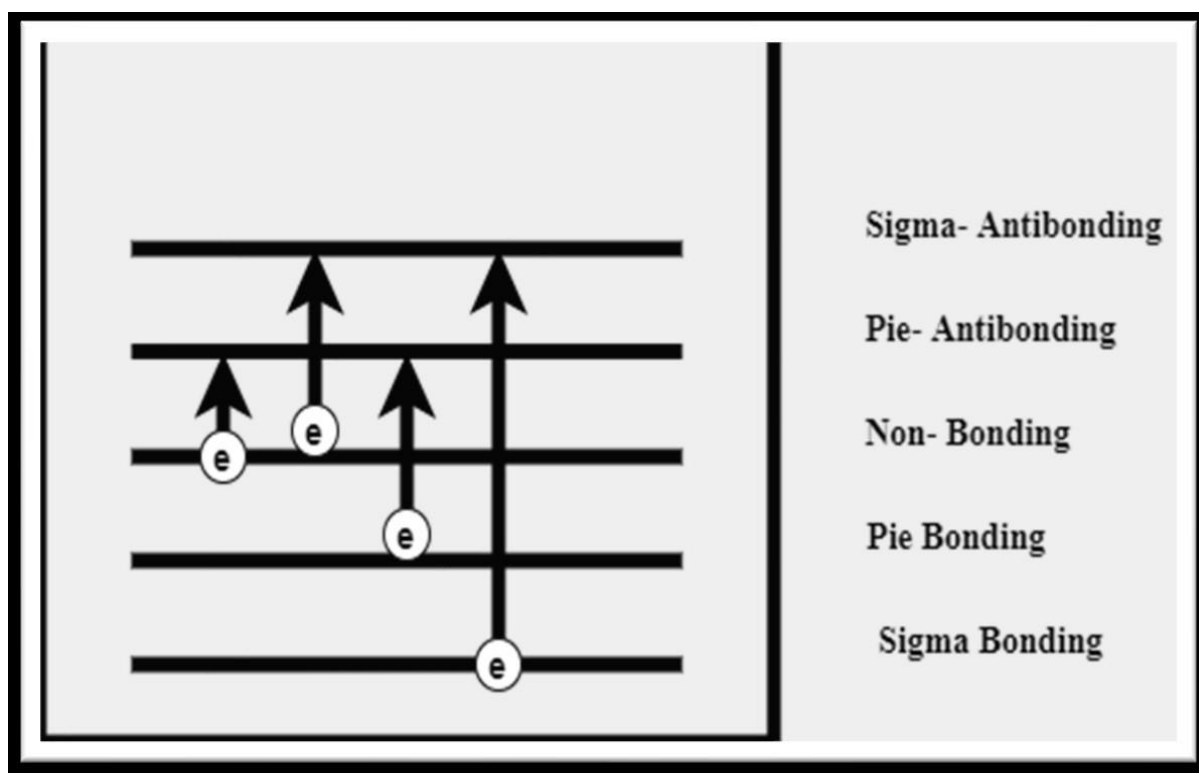


Figure 3.10 All possible transitions after absorption of photon.

3.3.10 Mortar and Pestle

Laboratory mortar and pestle are a pair of tools used to finely crush and grind substances into a powder or paste. A porcelain mortar and pestle set are sufficient for most laboratory applications, as unglazed porcelain is hard enough to crush most materials while being resistant to high temperatures. For labs concerned with contamination, an agate mortar and pestle set is preferred, as polished agate is an economical material with low porosity.



Figure 3.11: The agate mortar and pestle used for fine grinding of powders.

3.3.11 Cold Press Die-Set

The powder is compressed into the desired number of pellets using pressure in the dry pellet pressing die-set. A cold press die-set with a 12 mm diameter has been employed in our project. Moreover, to grind the desired materials into the correct granularity of powder (From millimeters to microns), the use of methods such as powder processing, ball milling, sol-gel process, etc, in combination with agate mortar and pestle sets are preferred. Figure represents the used Cold Press Die-set (diameter of 12 mm) in the laboratory.



Figure 3.12: Cold Press Die-set of 12 mm diameter.

3.3.12 KBr Press

It is a small hydraulic press that is efficient at producing pressure in the range of Tons. It has a variety of ranges that can make pellets of specimens for characterizations.



Figure 3.13: KBr Press Instruments

Chapter 4

Synthesis of structural, thermal and dielectrical properties of indium doped sodium Beta-alumina

Abstract

We report the effect of indium doping on thermal stability and ionic conductivity of beta alumina $\text{NaIn}_x\text{Al}_{11-x}\text{O}_{17}$ solid electrolyte which is synthesized by sol-gel auto combustion method on varying dopant concentration as $x = 0, 0.1, 0.2, 0.3, 0.4$. X-ray diffraction (XRD) pattern and microstructure are investigated on the doped samples calcined at 1100°C for 5 hours. XRD confirms the change in unit cell volume on increasing the dopant concentration. Field Emission scanning microscope (FESEM) reveals the conversion of cylindrical morphology to small spherical particles at dopant concentration $x \geq 0.5$. Thermal stability is found to improve drastically over a broad temperature range even at small dopant concentrations in β -alumina as found from thermo-gravimetric analysis (TGA). Electrochemical impedance spectroscopy (EIS) shows a considerable reduction in frequency-dependent dielectric permittivity for doped beta alumina. At frequency 1 kHz, the permittivity of around $\sim 10^5$ in as-prepared shows non-monotonous dependence and decreases to 10^3 for $x \geq 0.1$. This steep variation is mainly attributed to the change in morphology caused by steric effect and formation of random clusters which reduces the net polarization.

4.1 Introduction

Smart materials play an important role in the development of renewable energy sources such as solar energy, wind energy, and hydrothermal energy. Rechargeable batteries are one such renewable resource that can store chemical energy and convert it into electrical energy with high efficiency [44]. To date, the lithium-ion battery (LIB) has dominated the market of portable electronic devices due to its high energy densities, long life cycle & high output voltage [45]. Simultaneously, LIB has certain advantages over other chemistries as lithium has the lowest reduction potential among all elements which enable cells with high operational voltage and high energy density. However, the high cost, high flammability, leakage of liquid electrolyte and shortage of lithium resources have undoubtedly hindered the application of LIB in large-scale energy storage [46]. Solid state sodium ion battery (SIB) on the other hand is another class

of batteries which uses solid electrolyte rather than liquid organic electrolyte in LIBs [47]. SIB is recently found to be a good alternative of LIB as because sodium is abundant, low cost, minimum leakage, greater thermal stability and does not support any dendrite formation [31]. Despite all the advantages in solid state batteries, the ionic conductivity in sodium ion battery is still found to be much lower as compared to lithium-ion battery, thus restricting their use in commercial application. Moreover, as the sodium (Na) atom being larger in size with respect to lithium atom, the volumetric energy density in SIB remains low and makes it less competent against LIB [49-53]. Solid state SIB batteries are usually classified based on type of solid electrolytes as for example inorganic ceramic electrolytes (LATP), organic polymer electrolyte (PVA) and polymer ceramic composite electrolytes (PEO/LGPS). β -alumina ($\text{NaAl}_{11}\text{O}_{17}$) which comes in two distinct phases, hexagonal symmetry, and rhombohedral symmetry (β'' -alumina) is an oxide based inorganic ceramic electrolyte that exhibits high ionic conductivity $\sim 1\text{ S cm}^{-1}$ especially in the rhombohedral phase at 573 K. It is an anisotropic layered material with alternating layers of spinel block and loosely packed conduction planes where Na ion conduction takes place through hopping [54]. The demerit of this ceramic compound is that the compound with hexagonal symmetry yields ionic conductivity of around 10^{-3} S cm^{-1} at 300 K whereas the synthesis of rhombohedral phase is too expensive to grow at large scale for industrial application. Moreover, the presence of unwanted phases such as NaAlO_2 due to high temperature sintering makes $\text{NaAl}_{11}\text{O}_{17}$ inhomogeneous and susceptible to H_2O and CO_2 absorption from atmosphere [56]. As a result, the absorbents make the solid electrolyte less thermally stable and induce chemical instability too. Elemental doping is a well-known method used to improve the electrochemical and mechanical properties of solid state $\text{NaAl}_{11}\text{O}_{17}$ electrolytes [57,58]. It is found that addition of metal oxides increases the conductivity of sintered samples of β -alumina, but large concentration of metal oxides leads to formation of β'' -alumina phase. In our research work, the main goal is to improve the ionic conductivity in polycrystalline form of β -alumina through new growth methods, while still maintaining thermal and chemical stability at ambient condition [59]. Our work thus includes systematic analysis of electrical, chemical, and thermal properties of substitutional doping of indium at aluminum sites which might affect the lattice volume to tweak the ionic conduction due to the increased ionic radius. Till now, β -alumina on addition of only divalent impurities like Mg^{2+} , Cu^{2+} , Ni^{2+} , Zn^{2+} has shown better ionic conduction of Na^+ as reported by Imai *et.al*. However very limited studies have been carried out with trivalent impurities in β -alumina. In sulfide based solid state

electrolyte, substituting phosphorous with indium (In^{3+}) in $\text{Li}_7\text{P}_{2.9}\text{S}_{10.9}\text{In}_{0.1}$ exhibits high ionic conductivity of $\sim 10^{-3} \text{ S cm}^{-1}$ and shows enhanced interfacial compatibility and better moisture stability [60-63]. Impurities with ionic radius $< 0.097 \text{ nm}$ is found to enter the spinel block successfully and stabilize the β'' structure [64]. Hence, we investigate the influence of In^{3+} with ionic radius $\approx 0.080 \text{ nm}$ in the structural, thermal, and electrical stability of β -alumina.

4.2 Experimental

4.2.1 Materials and Method of synthesis

The Sodium nitrate, aluminium (III) nitrate [$\text{Al}_3(\text{NO}_3)_3 \cdot 6\text{H}_2\text{O}$], Indium nitrate [$\text{In}(\text{NO}_3)_3$] and Citric Acid ($\text{C}_6\text{H}_8\text{O}_7 \cdot \text{H}_2\text{O}$) of precursors of Sigma- Aldrich and LOBA Company with AR grade were used to make sample. Weighing the nitrates indicated above in accordance with the stoichiometric ratio was the first step in the formation of sodium beta alumina.

4.2.2 Synthesis of Indium doped Sodium Beta Alumina ($\text{NaAl}_{11}\text{O}_{17}$)

Sol-gel auto combustion method is adopted for preparation of In^{3+} doped $\text{NaIn}_x\text{Al}_{11}\text{O}_{17}$ ($x=0,0.1,0.2,0.3,0.4$). The Sodium nitrate, Indium (III) nitrate, aluminium (III) nitrate [$\text{Al}_3(\text{NO}_3)_3 \cdot 6\text{H}_2\text{O}$], and Citric Acid ($\text{C}_6\text{H}_8\text{O}_7 \cdot \text{H}_2\text{O}$) precursors of grade AR were used to make sample. Substituted indium doped beta alumina samples ($x=0,0.1,0.2,0.3,0.4$) were obtained by weighing these nitrates in accordance with a stoichiometric ratio and placing them into various beakers with 100 ml of distilled water. To obtain a clear solution, these various composition solutions were then maintained on a magnetic stirrer for 30 minutes. Then, to achieve a pH of 7, ammonia solution was gradually added to each solution while stirring continuously. Once a gel had formed, these solutions were kept on a magnetic stirrer for continuous stirring and heating at 70°C . Then the obtain gel for three samples as kept for heating at $200\text{-}250^\circ\text{C}$ for an hour. When exposed to air, this gel swells, dries up, and burns. The samples' obtained powder dried entirely. The obtained powder for sample $x=0,0.1,0.2,0.3$ and 0.4 is firstly grounded finely and as well as it is sintered at 1100°C in a furnace for 5 hours.

4.2.3 Characterization Techniques

The X-ray diffraction measurements are done with a (Bruker D8 Advance) Powder X-ray diffractometer with Cu-K ($= 1.5406 \text{ \AA}$) radiation to ensure the structure of the prepared

samples with diffraction angles from 10° to 90°, considering step size of 0.02°. (FE-SEM:JEOL JSM-7610F, Au coater: JEOL Smart Coater) to examine the morphology of the samples, a Field emission scanning electron microscope is employed. TGA measurement reveals that improvement in thermal stability over broad range of temperature. Electrochemical Impedance Spectroscopy (EIS) shows that reduction in frequency dependent dielectric permittivity.

4.3 Results and Discussions

4.3.1 X-ray Diffraction (XRD) Analysis

Fig 4.1 shows the XRD pattern of doped $\text{NaIn}_x\text{Al}_{11-x}\text{O}_{17}$ with $x=0.4$ which were calcinated at 1100 °C for 5 hours prior to XRD analysis. The crystalline phase is confirmed by the XRD pattern of the produced samples, and the intense sharp peaks of the indium doping concentrations demonstrate proportionate and uniform doping in pure alumina. Additionally, it is noted that doping causes a contraction in the unit cell's volume, which can be used to calibrate our materials' optical and electrical characteristics. The formation of secondary phases has been found to be influenced by the high annealing temperature. Furthermore, we discovered that some extra peaks are present in doped concentrated samples, which could be associated with phases such as In_2O_3 . Furthermore, it has been observed that the crystal structure of beta alumina is orthorhombic, and its space group is pbc_a with unit cell $a=10.38 \text{ \AA}$, $b=14.19 \text{ \AA}$ & $c=5.19 \text{ \AA}$. However, it has been found that there is a considerable rise in sodium beta alumina crystallinity when the indium concentration is raised, proving that the lattice strain is the cause of the monotonous increase in crystallite size. This is further supported by the Scherrer formula ($d=K\lambda/\beta\text{Cos } \Theta$) calculation of crystallite size on as-prepared and doped samples.

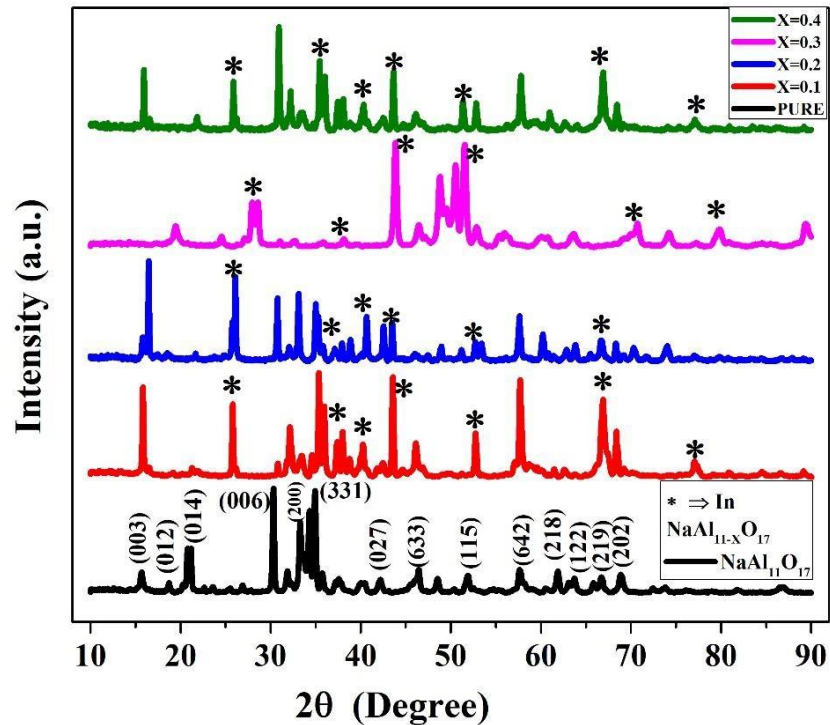


Figure 4.1 XRD pattern of $(\text{NaAl}_{11}\text{O}_{17})$ Sodium beta alumina and $\text{NaIn}_x\text{Al}_{11-x}\text{O}_{17}$.

4.3.2 Energy Dispersive X-ray (EDX)

To verify the presence of all elements in the prepared nanocomposites, EDX has been carried out. The EDX pattern of indium doped sodium beta alumina ($\text{NaInAl}_{11}\text{O}_{17}$) is shown in fig the EDX analysis which had been conducted out to ascertain the distribution of elements of specimen at the surface. The area scans in Fig.4.2 reveal the uniform distribution of elemental components and homogenous chemical composition over the whole specimen. The absence of any other elements confirms the purity of our synthesized $\text{NaIn}_x\text{Al}_{11-x}\text{O}_{17}$. From this spectrum, it has been observed that the presence of desired elements without any other undesirable elements. This confirms the successful synthesis of the phase pure nanocomposites.

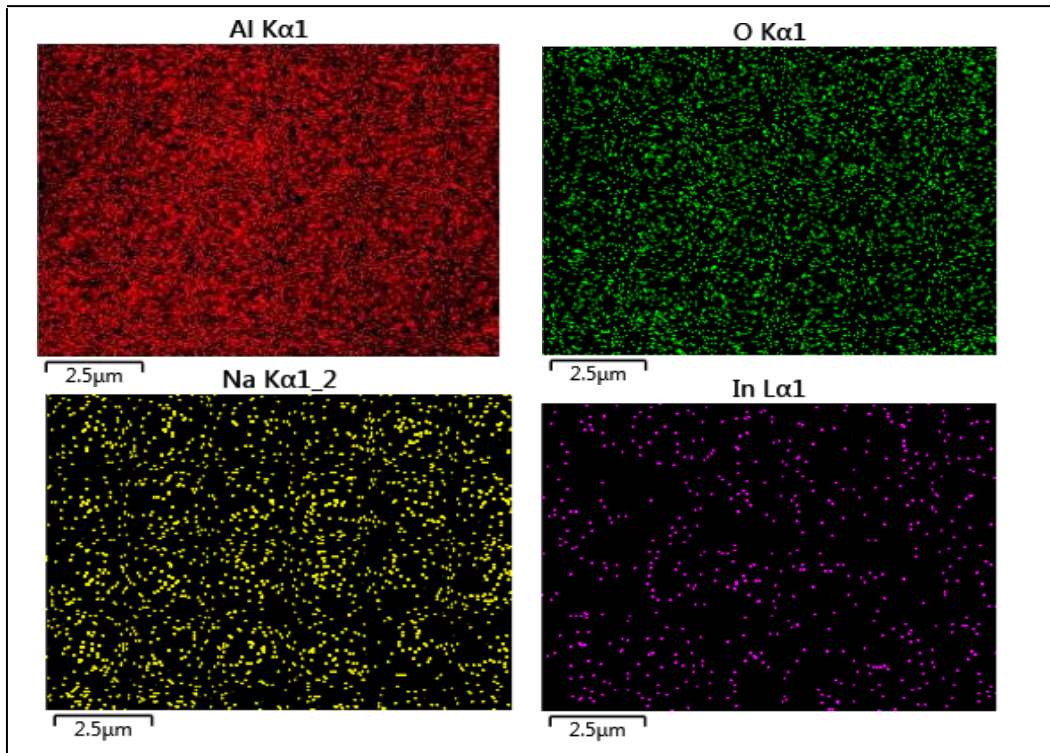
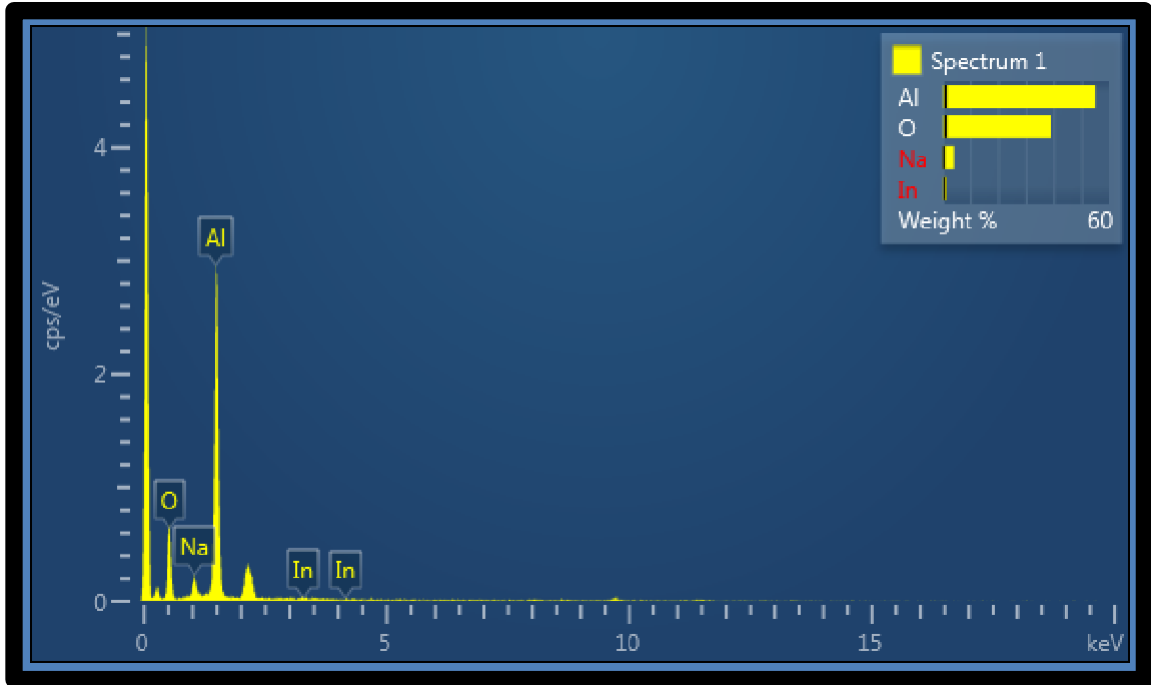


Figure 4.2 EDX spectra of sodium beta alumina with indium dopants.

4.3.3 Thermogravimetric Analysis (TGA)

From fig 4.3 shows the TGA curves of as-prepared sodium beta alumina along with different concentrations of indium dopant after calcination at 1100°C for 5 hours. On quantifying the material's thermal strength, it is noticed that the weight of as-prepared sodium β -Al has decreased by ~ 46% when heated in the range of temperature range from 30 - 600°C under the atmospheric air. From the temperature derivative of TGA curve (shown in the inset), sharp peaks of weight loss are observed at temperatures 177, 195 and 285°C which may be ascribed to temperature dependent structural changes in the crystal structure. Temperature dependent XRD data might give a better insight of structural dynamics which will be reported in our upcoming work. Interestingly, the TGA curve of the doping concentration of indium shows weak temperature dependence behavior and the weight loss of just 0.2% is noticed in the same temperature scale. This indicates that the indium doped β -alumina samples facilitate better thermal stability compared to as-prepared ones. The increase in thermal stability is a direct consequence of increase in densification of doped samples as it has previously been confirmed that as-prepared β -alumina inherits aluminum vacancies due to the high temperature calcination process. This quantification also confirms that indium has indeed diffused into the crystal structure of β -alumina successfully.

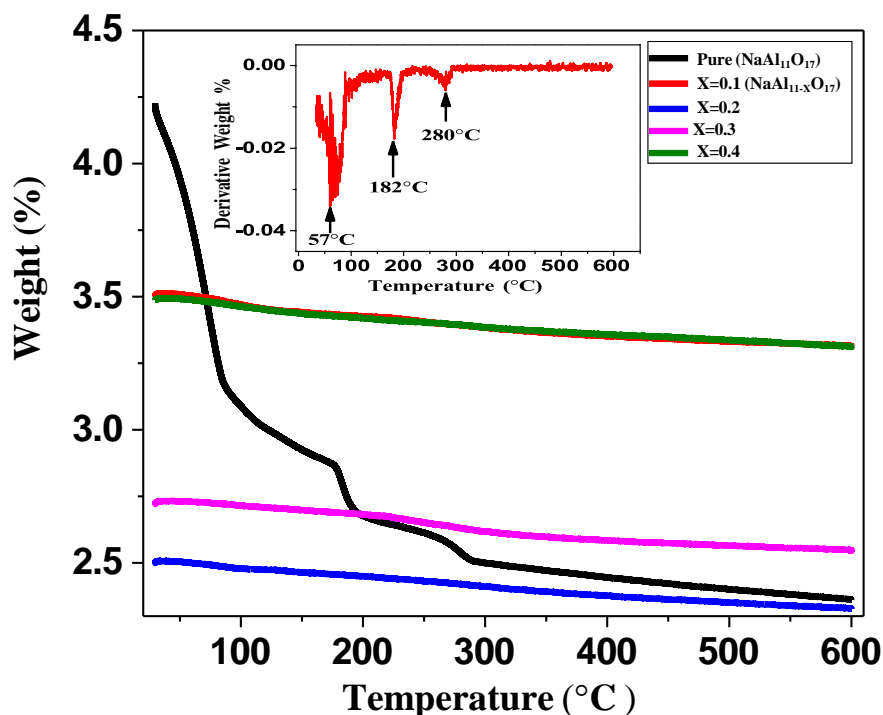


Figure 4.3 TGA Curve of Sodium beta alumina ($\text{NaAl}_{11}\text{O}_{17}$) with different amounts of indium doping. Inset: Derivative weight % of pure sodium beta alumina corresponding to the same temperature.

4.3.4 Scanning Electron Microscope (SEM) Analysis

In fig. 4.4 shows the images of as-prepared sodium β -alumina and indium doped samples of varying concentrations. The morphology of as-prepared sample shows thin cylindrical type elongated structure of length around 100 - 200 nm and diameter of 10 - 20 nm. Moreover, the undoped sample shows narrow distribution of its size and shape, which further conveys uniform reduction in stress among the particles during high temperature. Upon indium doping, the particles of the samples tend to disintegrate into smaller thin grains. The effect of Indium doping in our sample is to slow down the growth of grains which is exactly an opposite behavior observed in TiO_2 doped in sodium β -alumina [11]. On further increasing the indium concentration, small crystals are formed from an under cooled melt via nucleation and successive growth as shown in fig. It is also found that nucleation leads to the generation of

a new crystalline cluster phase which in turn makes it more difficult to determine the crystal structure accurately.

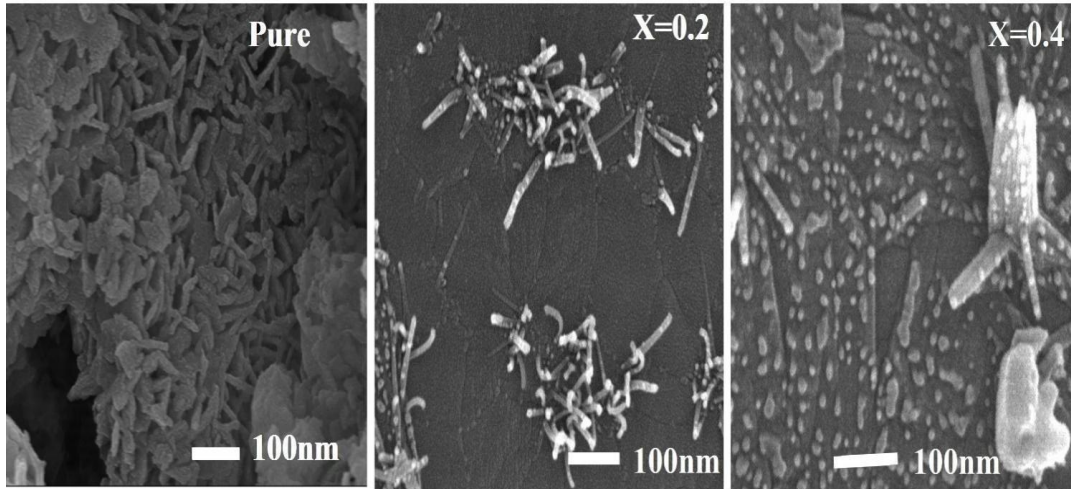


Figure 4.4 SEM images of Sodium Beta alumina ($\text{NaAl}_{11}\text{O}_{17}$) & different amount of Indium doping ($\text{NaIn}_x\text{Al}_{11-x}\text{O}_{17}$).

4.3.5 Staircase type DC Resistivity

Figure 4.5 shows the temperature dependent DC resistivity of the undoped β -alumina measured by Four probe method as shown in the inset. For practical applications, DC resistivity of solid electrolyte is very important as it signifies the stable electrochemical behavior in a cell. From the figure it is seen that with the improvement in temperature, the resistivity increases, thus implies phonon assisted scattering that reduces the mean free path of charge carriers. On addition, the change in resistivity resembles a staircase type phenomenon in the temperature range 300 - 420 K. This behavior may be attributed to the existence of different phases in undoped β -alumina at distinct temperature ranges. Above 420 K, the measurement of resistance was beyond the limit of our source meters. For the doped sample, it was not possible to measure the resistivity at any temperature range, implies indium acts more as a scattering center owing to high resistivity. To shed more-light on the electrical property of the material, dielectric spectroscopy was performed at room temperature for both as-prepared and undoped samples. As units of permittivity is $\text{C}^2\text{N}^{-1}\text{m}^{-2}$ Since dielectric permittivity is the ratio of permittivity's so it will be dimensionless. From frequency dependent conductivity data low frequency shows electronic conductivity and high frequency region shows ionic conductivity as only Al ions flow.

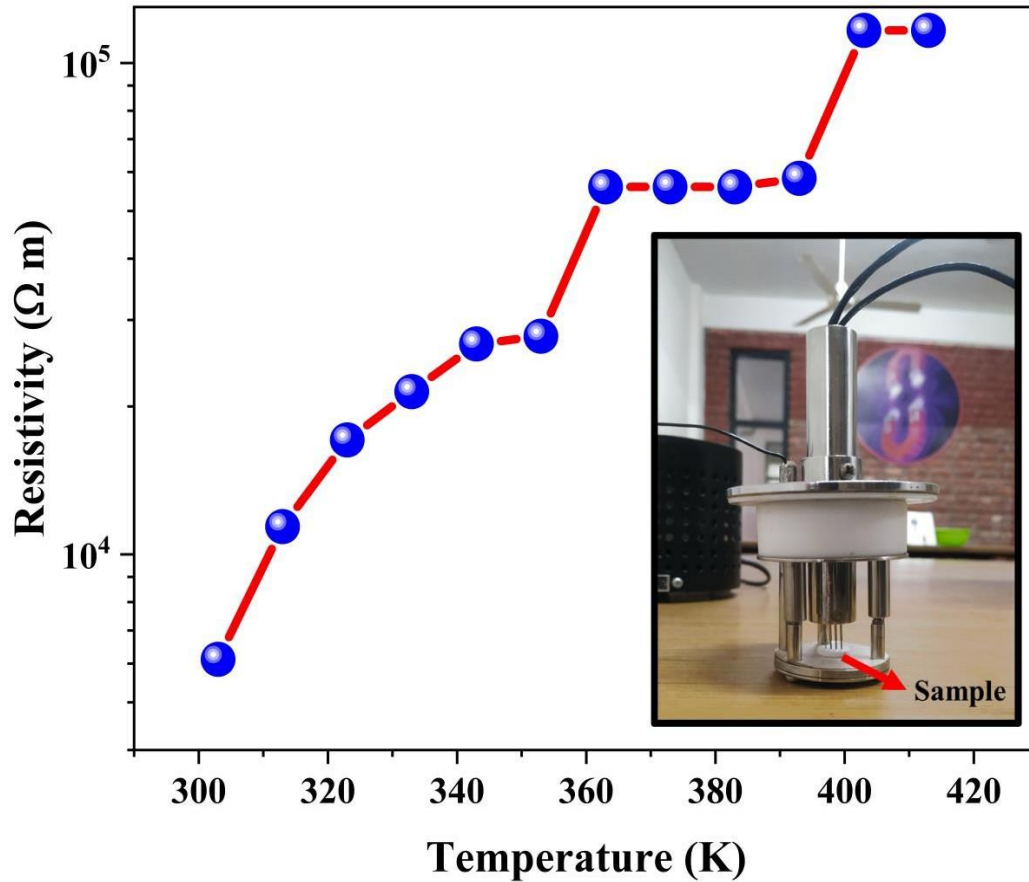


Figure 4.5 Temperature dependent DC resistivity of the undoped β -alumina.

4.4 Dielectric Studies

4.4.1 Study of dielectric permittivity vs frequency

Fig. 4.6 shows the variation of complex dielectric permittivity with frequency for as-prepared solid electrolyte and indium doped β -alumina electrolyte with increasing concentration. For the as-prepared undoped $\text{NaAl}_{11}\text{O}_{17}$ sample, it exhibits a large real part of dielectric permittivity of 10^5 at 1 KHz and low dielectric loss of around 10^{-2} as shown in the inset. The large value of

dielectric permittivity is leading because of presence of Al^{3+} vacancies which were influenced during sintering process high temperature. The crystal structure of β -alumina has alternate layers of $[\text{NaO}]$ and spinel like blocks of $[\text{Al}_{11}\text{O}_{16}]$ stacked alternately. The presence of Al^{3+} vacancies break the inversion symmetry due to which strong polarizing field yields large permittivity. Moreover, the distinct part of dielectric permittivity (ϵ') is found to decline linearly with constant slope (in fig black dotted line), thus verifies very limited interfacial electrode effect in our sample. The steady decline in permittivity with improving frequency is also ascribed to the decline the polarization because of displacement of Na^+ ions. Fascinatingly, when indium is doped with concentrations $x = 0.1$ and 0.2 , there is subsequent drop-in dielectric permittivity by two orders magnitude at 1 KHz which confirms that indium atom couples strongly with the β -alumina structure and held responsible for the decreases of electrical polarization. Moreover, upon doping, the Al^{3+} vacancies are occupied by indium atom which further tends to screen the electric field and reduces the net dipole moment which on turn reduces the dielectric constant of the system. At frequency close to 10^6 Hz, a small hump is observed in the real part of dielectric permittivity which implies strong movement of Na^+ ions at high frequency. For $x = 0.3$ and 0.4 , there is a little improvement in the magnitude of dielectric permittivity but the dielectric response with frequency remains unchanged. The small enhancement in permittivity is mainly due to the reduced morphology of the particles as observed from the SEM. With the reduction in particle size, the grain boundary resistance also tends to decrease which can lead to Maxwell-Wagner effect. When the size of the particles decreases, there is reduction in inter particle distance as a result the capacitance decreases which is in complete accord with the parallel plate geometry configuration.

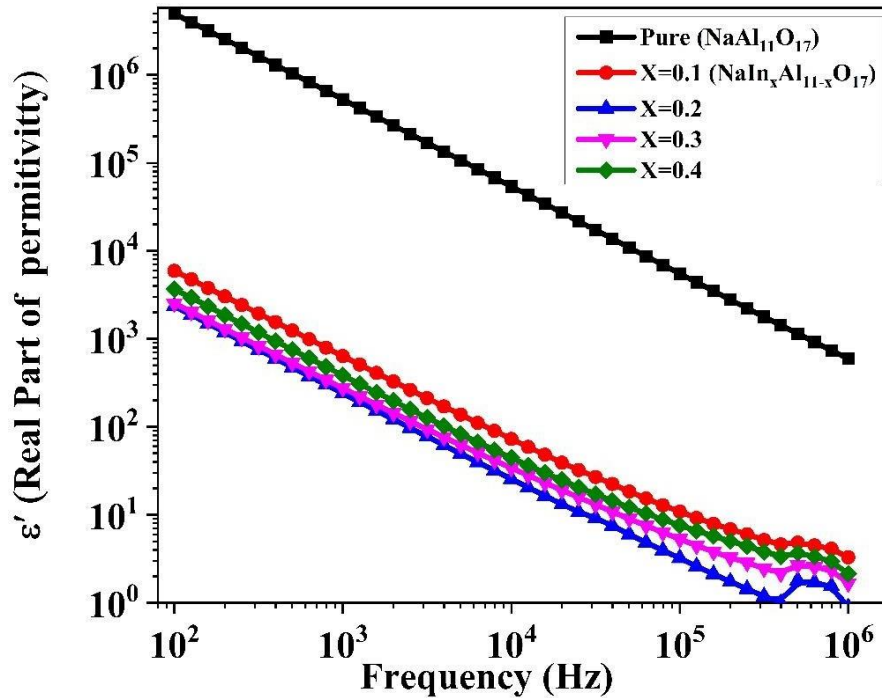


Figure 4.6 Variation of the real part of dielectric permittivity with frequency for pure Sodium Beta alumina ($\text{NaAl}_{11}\text{O}_{17}$) with different Indium doping.

4.4.2 Dielectric Loss vs Frequency

From fig 4.7, The function frequency represents the samples' dielectric loss. Loss is found to be virtually frequency independent for the $\text{NaAl}_{11}\text{O}_{17}$ sample as prepared, however for all values of $x > 0$, the peak in the dielectric loss is generally outside of our frequency range, indicating a short relaxation period for the dielectric dipoles. At 1 KHz, dielectric loss in doped samples is 10^{-2} which has enhanced to 10^{-1} at 10^4 Hz but stayed intense than as-prepared undoped sample. To shed more-light on the dielectric behavior, the dependence of a.c conductivity on frequency is also investigated.

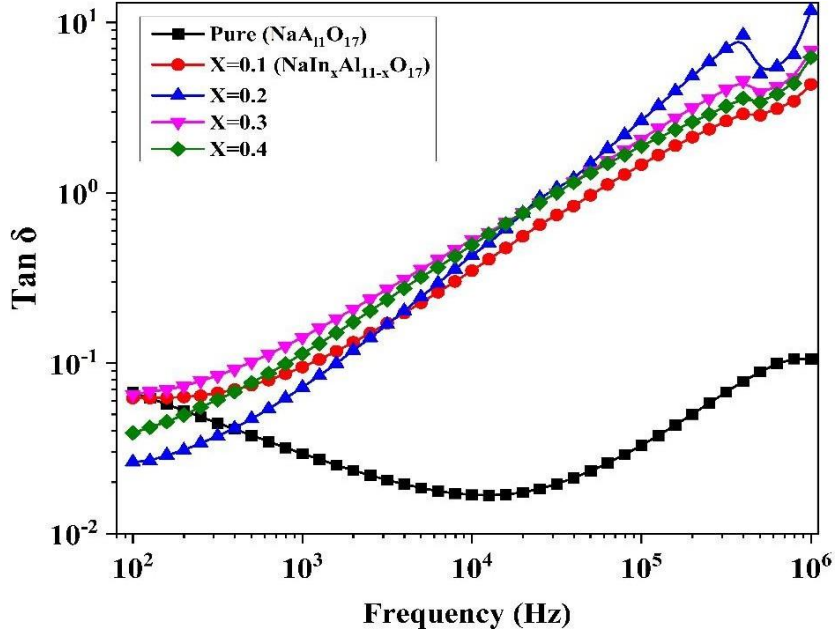


Figure 4.7 Dielectric Tangent Loss with frequency for pure Sodium Beta alumina ($\text{NaAl}_{11}\text{O}_{17}$) with different Indium doping.

4.4.3 Cole-Cole plot vs Frequency

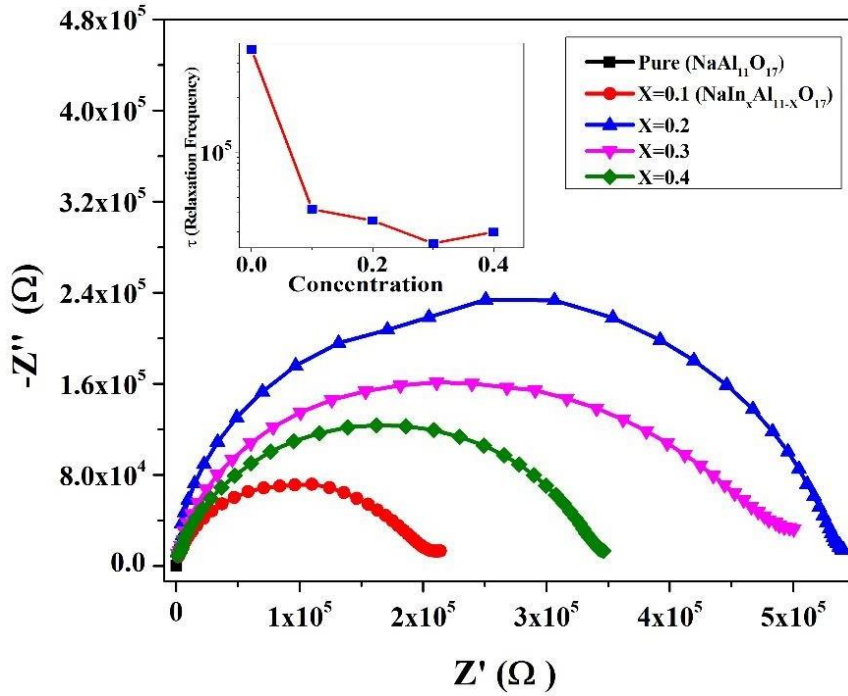


Figure 4.8 Cole-Cole Plot of Sodium beta alumina with different amounts of indium doping.

Inset: Concentration Vs Relaxation frequency (τ).

To determine the actual contribution from the grain and grain boundary, Cole-Cole plot of sodium β -alumina and its dopant is shown in Fig. 4.8. It is a graphical representation of electrical impedance's imaginary part and the real part. From the graph it is found that in the higher frequency regime, the impedance is of order $10^5 \Omega$ which increases with decrease in a.c frequency. According to the graphical observation, semicircle in eminent frequency area is ascribed to the interfacial resistance between SE and electrode, the portion in the medium frequency area ascribed to transfer of charge process and inclined line in small frequency area is allocated to solid-state dispersal of Indium-ion in the solid electrolyte. Based on the above investigation we provide the equivalent circuit to fit Cole-Cole plot from our experimental data as shown in Fig. 4.8 and the fitting parameters are mentioned in table 1.

Table 1 Fitting of data with generic battery model

$C_{ph}(F)$	capacitance corresponding to charge storage in new phase, serial to R_p
$R_{ser}(\Omega)$	resistance of separator and current collectors
$R_l(\Omega)$	resistance of passivating layer on particles
$C_l(F)$	capacitance of passivating layer on particles (parallel to R_l)
$R_{ct}(\Omega)$	charge transfer resistance
$C_{dl}(F)$	double layer capacitance (parallel to R_{ct})
$C_{ps}(F)$	pseudocapacitance related to finite length diffusion inside particles
$R_d(\Omega)$	resistance related to finite length diffusion inside particles
$R_m(\Omega)$	distributed resistance of transmission line representing electronic and ionic conduction inside the layer of active material
$R_p(\Omega)$	resistance of new phase growth inside particles

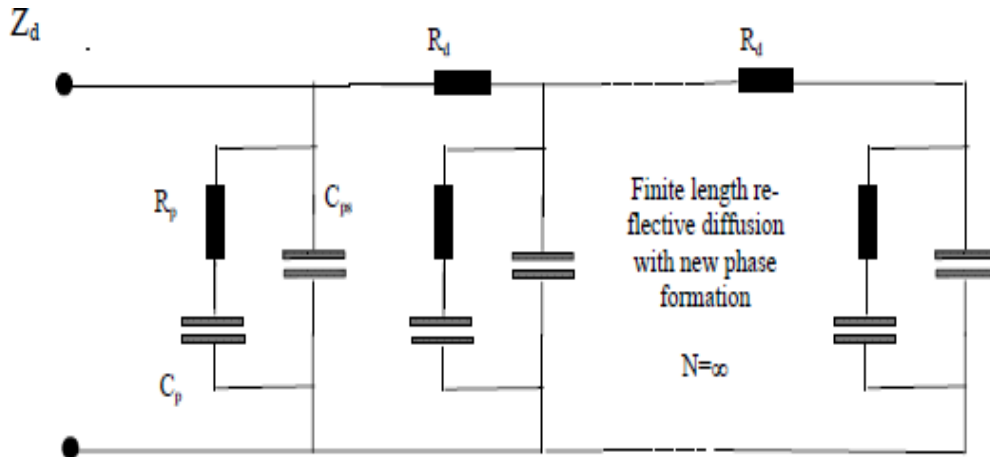


Figure 4.9 Fitting of Electrochemical data of Cole-Cole Plot of Sodium β - alumina with different amounts of indium doping.

4.4.4 Ionic Conductivity

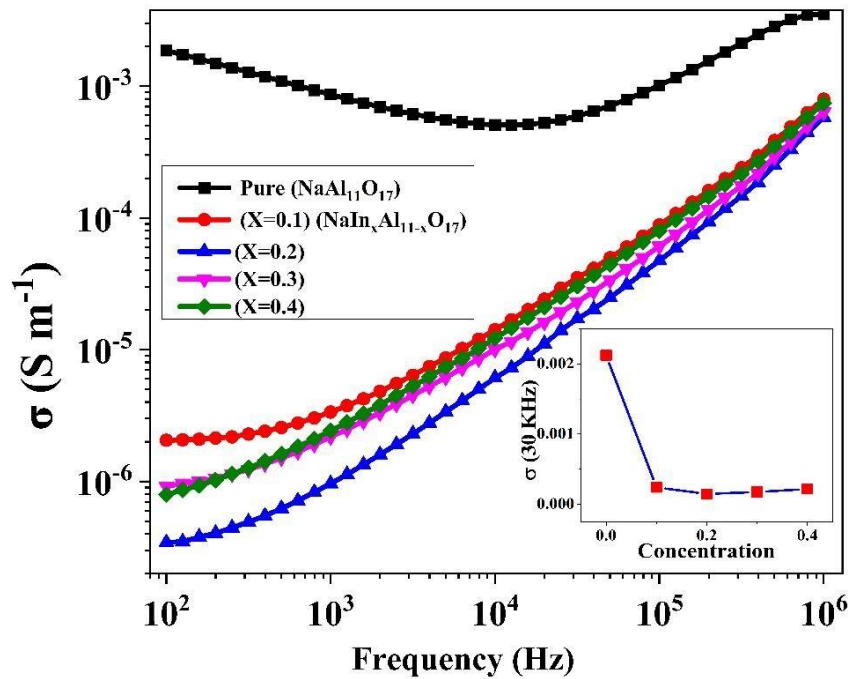


Figure 4.10 Ionic Conductivity of Sodium β - Al with different amounts of indium doping.

Inset: Concentration vs Ionic Conductivity at 30 KHz.

Fig 4.10 shows the modification as a function of the conductivity (a.c), then the input frequency for as- prepared sodium β -Al and indium doped samples of varying concentration at 300 K. Large conductivity of 10^{-3} S.m^{-1} is noticed for as-prepared sodium β -alumina and at room temperature it shows weak frequency dependent a.c conductivity. For $x= 0.1$ and 0.2 , a.c conductivity decreases to 10^{-5} S.m^{-1} at 10^4 Hz and is found to increase with rise in frequency. At a better frequency of 10^6 Hz , the a.c conductivity is found to be comparable to that of as-prepared sample. At low frequency ($< 1 \text{ KHz}$), the d.c part of the a.c conductivity is found to be negligible, which again confirms no contribution from the free charge carrier at the electrode-sample interface. For $x= 0.3$ and 0.4 , a little increase in a.c conductivity is noticed although it retains the same frequency dependent behavior at room temperature. With the increasing dopant concentration, the sample becomes denser which has further reduced grain boundary resistance. As a result, ionic conductivity for higher dopant concentration has increased by a small magnitude. Overall, it is found that the indium dopant has suppressed the ionic conductivity of sodium on account of the coulombic repulsion between In^{3+} and Na^+ , as a result the mobility of the Na^+ ion has decreased by significant factor at room temperature.

4.5 Conclusion

Successfully synthesized indium doped $\text{NaIn}_x\text{Al}_{11-x}\text{O}_{17}$ by the sol-gel auto combustion method. The results as obtained imply that with the addition of indium, the morphology changes from long regular cylindrical particles to small and thin sized grains leading to formation of clusters. Upon indium doping, the thermal stability is found to be temperature independent in wide range and has improved significantly with respect to undoped one. DC resistivity measurement confirms large electrical resistivity with the staircase type variation with increasing temperature. The dielectric measurement shows drastic drop in real part of dielectric permittivity from 10^5 for $x= 0$ to 10^2 for $x > 0$ at input frequency 10^4 Hz . This drop is mainly attributed to the screening effect by the indium atom and the cluster formation which reduces the polarization effect. With the increase in indium concentration ($x > 0$), the dielectric loss increases, and the relaxation frequency decreases. Further, the indium has suppressed the ionic conductivity to 10^{-5} S m^{-1} around 10^4 Hz in $\text{NaAl}_{11}\text{O}_{17}$ which is mainly due to the indium occupied vacancies which led to reduced mobility of Na^+ ion. This collective behavior suggests that indium is not a good candidate for improving the ionic conductivity of $\text{NaAl}_{11}\text{O}_{17}$. Further, morphology seems to play a vital role in determining the electrical property of the solid electrolyte.

Chapter 5

Tuning of Structural and dielectric properties of Zirconyl / Zinc doped sodium β -alumina

Abstract

We report the effect of Zirconyl /Zinc doping on ionic conductivity and structural property of beta alumina $\text{NaIn}_x\text{Al}_{11-x}\text{O}_{17}$ solid electrolyte which is synthesized by sol-gel auto combustion method on varying dopant concentration as $x = 0, 0.1, 0.3$. Electrochemical impedance spectroscopy (EIS) shows a considerable reduction in frequency-dependent dielectric permittivity for doped beta alumina. At frequency 1 kHz, the permittivity of around $\sim 10^5$ in as-prepared shows non-monotonous dependence and decreases to 10^3 for $x \geq 0.1$. This steep variation is mainly attributed to the change in morphology caused by steric effect and formation of random clusters which reduces the net polarization. As Indium doped sodium beta alumina is discussed in separate chapter 4.

5.1 Introduction

To date, the lithium-ion battery (LIB) has dominated the market of portable electronic devices due to its high energy densities, long life cycle & high output voltage. Simultaneously, LIB has certain advantages over other chemistries as lithium has the lowest reduction potential among all elements which enable cells with high operational voltage and high energy density [65]. However, the high cost, high flammability, leakage of liquid electrolyte and shortage of lithium resources have undoubtedly hindered the application of LIB in large-scale energy storage. Solid state sodium ion battery (SIB) on the other hand is another class of batteries which uses solid electrolyte rather than liquid organic electrolyte in LIBs [66]. According to reports, zirconyl and zinc doping could speed up the sintering of alumina by enhancing the Al^{3+} diffusion due to the rising concentration of Al^{3+} vacancies in conventional ceramics. These properties include densification, structural properties, and electrical properties [67]. Additionally, because sodium does not alloy with aluminum, it enables the use of aluminum current collectors rather than copper, potentially resulting in cost savings. However, sodium-ion batteries (SIBs) continue to use flammable, organic electrolytes, which poses similar safety risks as LIBs. The issues can be resolved by solid-state batteries (SSBs), which are based on

solid electrolytes (SEs). They are regarded as the next generation of batteries since they provide great thermal stability, minimal flammability, high safety, high specific energy, and extended cycle life. Research and development are still being done on commercially available cell systems that use sodium as the negative electrode and sodium-beta alumina as the solid electrolyte [203-206].

5.2 Experimental

5.2.1 Materials and Method of Synthesis

The Sodium nitrate, aluminium (III) nitrate [$\text{Al}_3(\text{NO}_3)_3 \cdot 6\text{H}_2\text{O}$], Zirconyl nitrate [$\text{Zr}(\text{NO}_3)_4$] or Zinc nitrate [$\text{Zn}(\text{NO}_3)_2$] and Citric Acid ($\text{C}_6\text{H}_8\text{O}_7 \cdot \text{H}_2\text{O}$) of precursors of Sigma- Aldrich and LOBA Company with AR grade were used to make sample. Weighing the nitrates indicated above in accordance with the stoichiometric ratio was the first step in the formation of sodium beta alumina.

5.2.2 Synthesis of Zirconyl/ Zinc doped Sodium beta alumina

Sol-gel auto combustion method is adopted for preparation of Zr/Zn doped sodium beta alumina $\text{NaZr}_x\text{Al}_{11-x}\text{O}_{17}$ / $\text{NaZn}_x\text{Al}_{11-x}\text{O}_{17}$ ($x=0,0.1,0.3$). The Sodium nitrate, Zirconyl nitrate [$\text{Zr}(\text{NO}_3)_4$] or Zinc nitrate [$\text{Zn}(\text{NO}_3)_2$], aluminum (III) nitrate [$\text{Al}_3(\text{NO}_3)_3 \cdot 6\text{H}_2\text{O}$], and Citric Acid ($\text{C}_6\text{H}_8\text{O}_7 \cdot \text{H}_2\text{O}$) precursors of grade AR were used to make sample. Substituted Zr/Zn doped beta alumina samples ($x=0,0.1,0.3$) were obtained by weighing these nitrates in accordance with a stoichiometric ratio and placing them into various beakers with 100 ml of distilled water. To obtain a clear solution, these various composition solutions were then maintained on a magnetic stirrer for 30 minutes. Then, to achieve a pH of 7, ammonia solution was gradually added to each solution while stirring continuously. Once a gel had formed, these solutions were kept on a magnetic stirrer for continuous stirring and heating at 70 °C. Then the obtain gel for three samples as kept for heating at 200-250°C for an hour. When exposed to air, this gel swells, dries up, and burns. The samples' obtained powder dried entirely. The obtained powder for sample $x=0,0.1 \& 0.3$ is firstly grounded finely and as well as it is sintered at 1100°C in a furnace for 5 hours.

5.2.3 Characterization technique

The dielectric and AC measurements have been performed using an Electrochemical impedance analyzer (FRA32M) in the 100 Hz to 1 MHz range (Potentiostat Galvanostat, by NOVA software), XRD and FESEM. The characteristics via. Impedance spectroscopy provides powerful techniques for understanding energy conversion and storage studies.

5.3 Results and Discussions

5.3.1 Dielectric Studies

5.3.2 Study of real part of permittivity vs frequency

Fig. 5.1 shows the modification of complex dielectric permittivity with frequency for as-prepared solid electrolyte and Zirconyl Nitrate doped β -alumina electrolyte with increasing concentration. For the as-prepared undoped $\text{NaAl}_{11}\text{O}_{17}$ sample, it exhibits a large real part of dielectric permittivity of 10^5 at 1 KHz and low dielectric loss of around 10^{-2} as shown in the inset. The large value of dielectric permittivity is mainly due to presence of Al^{3+} vacancies which were induced during high temperature sintering process. The crystal structure of β -alumina has alternate layers of $[\text{NaO}]$ and spinel like blocks of $[\text{Al}_{11}\text{O}_{16}]$ stacked alternately. The presence of Al^{3+} vacancies break the inversion symmetry due to which strong polarizing field yields large permittivity. Furthermore, the distinct portion of dielectric permittivity (ϵ') is found to decrease linearly with constant slope (shown in black dots), thus confirms very limited electrode interfacial effect in our sample. The steady decrease in permittivity with increasing frequency is also attributed to the decrease of polarization due to displacement of Na^+ ions. Interestingly, when Zirconyl nitrate is doped with concentrations $x = 0.1$ and 0.3 , there is subsequent drop-in dielectric permittivity by two orders magnitude at 1 KHz which confirms that Zirconyl atom couples strongly with the β -alumina structure and held responsible for the decreases of electrical polarization. Moreover, upon doping, the Al^{3+} vacancies are occupied by Zirconyl atom which further tends to screen the electric field and reduces the net dipole moment which in turn reduces the dielectric constant of the system. At frequency close to 10^6 Hz, a small hump is observed in the real part of dielectric permittivity which implies strong movement of Na^+ ions at high frequency. With the reduction in particle size, the grain boundary resistance also tends to decrease which can lead to Maxwell-Wagner effect. When the size of the particles decreases, there is reduction in inter particle distance as a result the capacitance decreases which is in complete accord with the parallel plate geometry configuration.

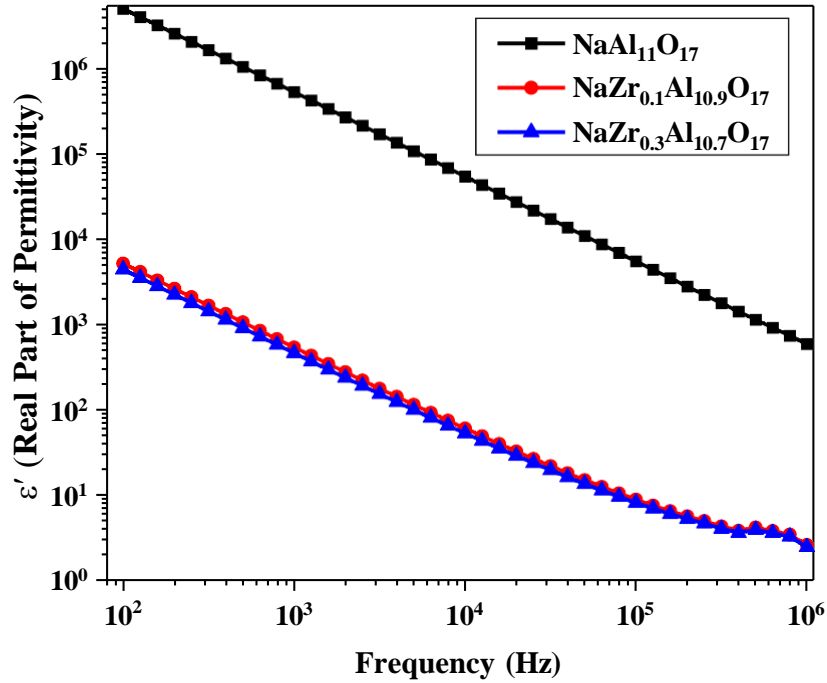


Figure 5.1 Variation of the real part of dielectric permittivity with frequency for pure Sodium Beta alumina ($\text{NaAl}_{11}\text{O}_{17}$) with different Zirconyl nitrate doping.

5.3.3 Tangent loss vs Frequency

In another *fig.5.2* The samples' dielectric loss is displayed as a function of frequency. The loss is found to be practically frequency independent for the $\text{NaAl}_{11}\text{O}_{17}$ sample as prepared, however for all values of $x > 0$, the peak in the dielectric loss is primarily outside of our frequency range, indicating a short relaxation time for the dielectric dipoles. At 1 KHz, dielectric loss in doped samples is 10^{-2} which has increased to 10^{-1} at 10^4 Hz but remains higher than as-prepared undoped sample. To shed more-light on the dielectric behavior, the dependence of a.c conductivity on frequency is also investigated.

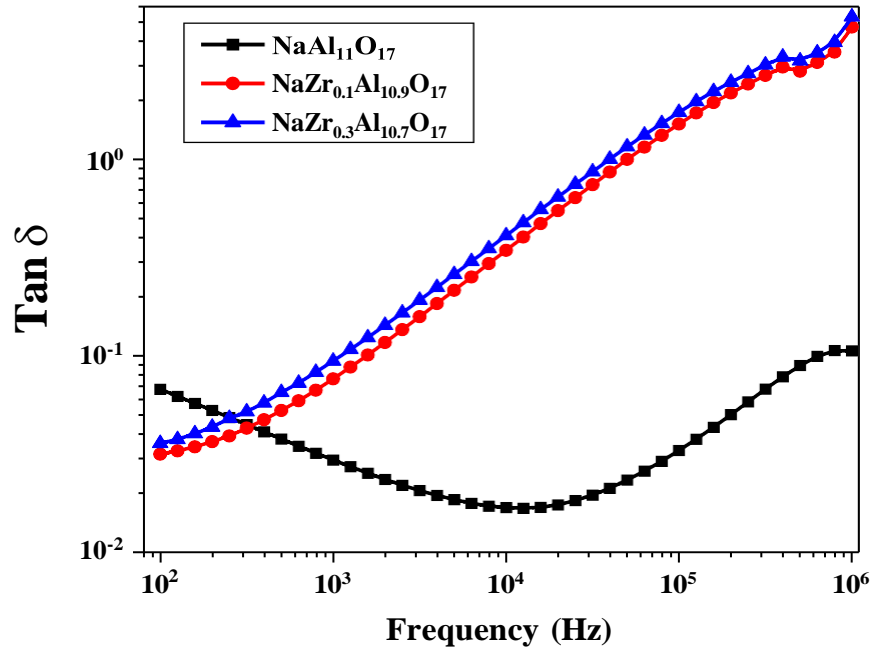


Figure 5.2 Dielectric Tangent Loss with frequency for pure Sodium Beta alumina ($\text{NaAl}_{11}\text{O}_{17}$) with different Zirconyl nitrate doping.

5.3.4 Cole-cole plot of Zirconyl doped beta alumina

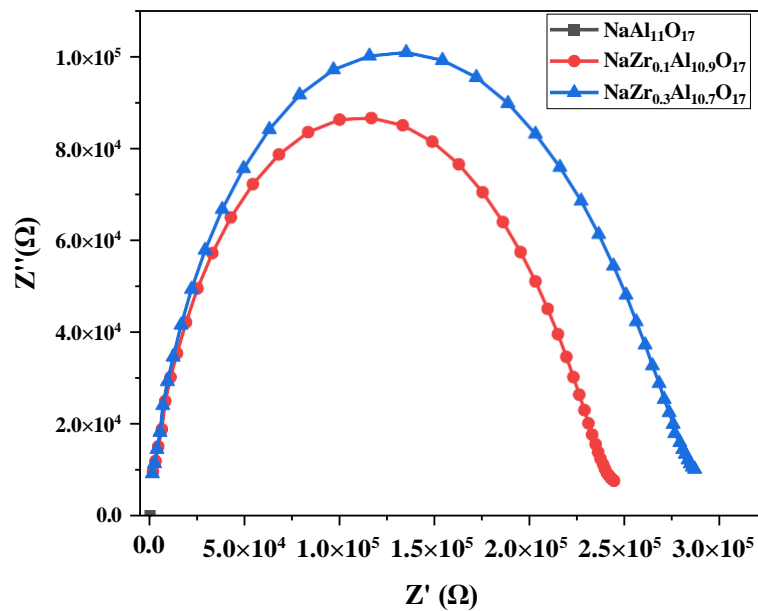


Figure 5.3 Cole-Cole Plot of Sodium beta alumina with different amounts of Zirconyl.

To determine the actual contribution from the grain and grain boundary, Cole-Cole plot of sodium β -alumina and its dopant is shown in Fig.5.3 It is a graphical representation of electrical impedance's imaginary part and the real part. From the graph it is found that in the higher frequency regime, the impedance is of order $10^5 \Omega$ which increases with decrease in a.c frequency. According to the graphical observation, semicircle in eminent frequency region is ascribed to the interfacial resistance between SE and electrode, the portion in the medium frequency area attributed to transfer of charge procedure and inclined line in small frequency area is allocated to solid-state dispersal of zirconyl-ion in the solid electrolyte.

5.3.5 A.C Conductivity of Zirconyl doped sodium beta alumina

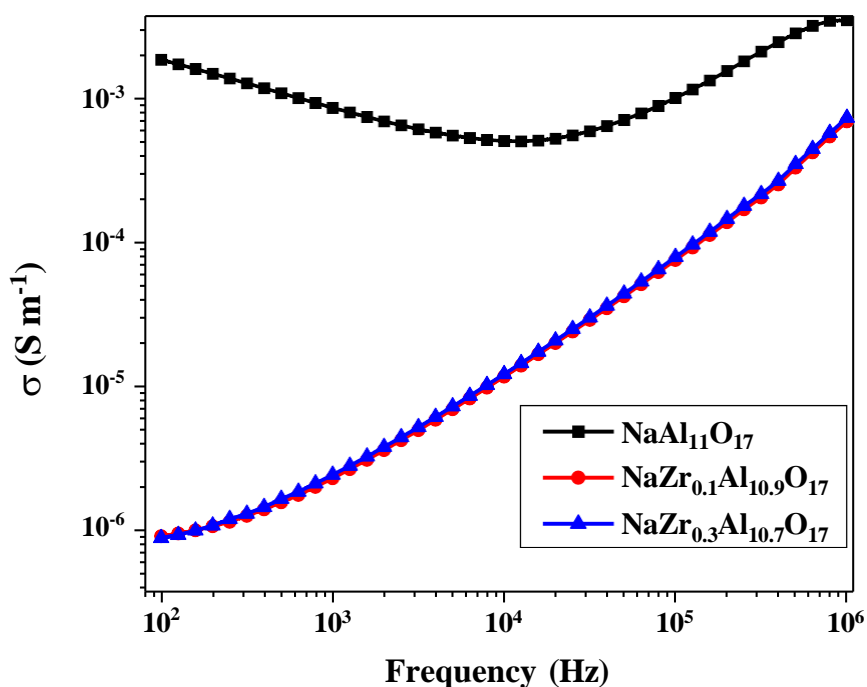


Figure 5.4 Ionic Conductivity of Sodium beta alumina with different amounts of Zirconyl doping.

Fig. 5.4 shows the variation as a function of a.c conductivity of input frequency for as prepared and zirconyl nitrate doped samples of varying concentration. Large conductivity of 10^{-3} S.m^{-1} is observed for as-prepared β -alumina and shows weak frequency dependent a.c conductivity at room temperature. For $x= 0.1$ and 0.3 , a.c conductivity decreases to 10^{-5} S.m^{-1} at 10^4 Hz and is found to increase with increasing frequency. At high frequency of 10^6 Hz , the a.c conductivity is found to be comparable to that of as-prepared sample. At low frequency ($< 1 \text{ KHz}$), the d.c part of the a.c conductivity is found to be negligible, which again confirms no contribution from the charge free carrier at the interface of electrode-sample. With the increasing dopant concentration, the sample becomes denser which has further reduced grain boundary resistance. As a result, ionic conductivity for higher dopant concentration has increased by a small magnitude. Overall, it is found that the Zirconyl dopant has suppressed the ionic conductivity of sodium on account of the coulombic repulsion between Zr^{3+} and Na^+ , as a result the mobility of the Na^+ ion has decreased by significant factor at room temperature.

5.3.6 XRD analysis of Zirconyl doped beta alumina

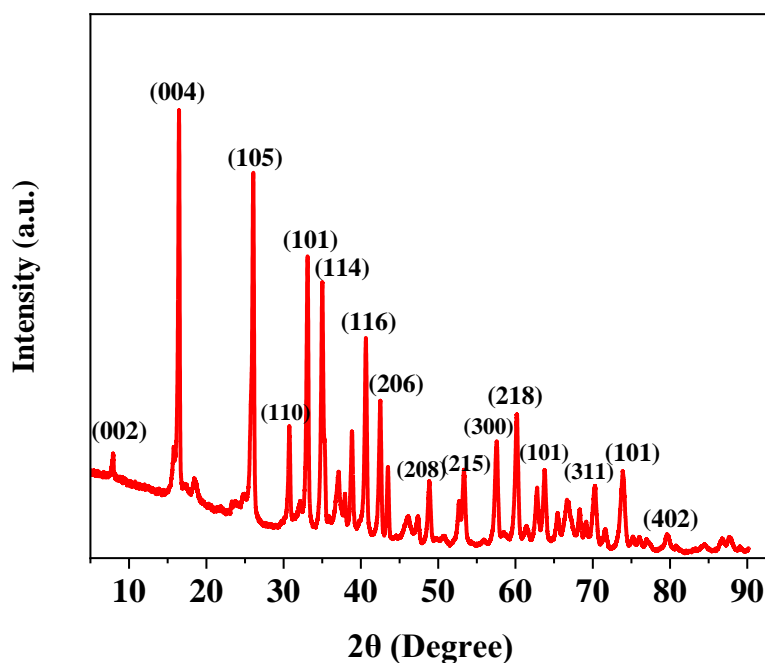


Figure 5.5 XRD pattern of zirconyl doped beta alumina

In *fig 5.5*, XRD pattern for Zirconyl-doped beta alumina demonstrates a polycrystalline structure characterized by several prominent diffraction peaks. These peaks indicate the presence of distinct crystallographic planes within the doped material, highlighting the crystalline nature and phase composition of the sample. The presence of multiple sharp peaks across a range of 2θ values indicates a high degree of crystallinity within the Zirconyl-doped beta alumina. The diversity of hkl values suggests the presence of various crystallographic orientations and potentially multiple phases, including both the beta alumina and zirconyl phases or zirconia-modified phases. The identification of specific planes such as (002), (004), and (110) reflects the structural integration of zirconyl within the beta alumina matrix. The incorporation of zirconyl can lead to lattice distortions or the formation of new phases, evident from the distinct peak patterns observed. The variety in hkl values, particularly the presence of high-index planes like (311), (402), and (215), indicates complex structural modifications due to zirconyl doping. These modifications can influence the material's mechanical, thermal, and electrical properties, making it crucial to understand the phase composition and crystallographic structure. These findings are vital for comprehending the material's properties and optimizing its application in areas such as ion conduction, catalysis, and structural components.

5.3.7 FESEM Analysis

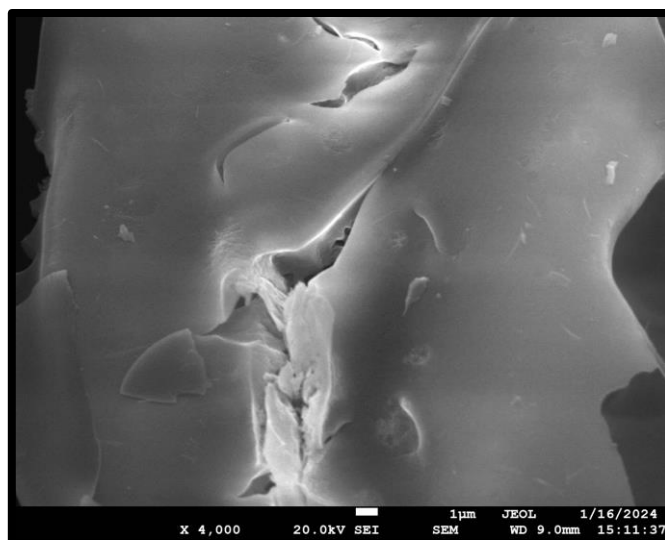


Figure 5.6 FESEM images of zirconyl doped beta alumina

In *fig 5.6*, this study examines the microstructural effects of zirconyl (Zr) doping on sodium beta alumina. Field Emission Scanning Electron Microscopy (FE-SEM) analysis provides insights into the grain morphology, dopant distribution, defect presence, and overall material integrity of the Zr-doped ceramic. The FE-SEM images reveal a distinct refinement in grain size attributed to the incorporation of Zr dopants. The grains are predominantly rounded, with an average diameter of approximately 1.5 μm , compared to larger grains observed in undoped samples. This uniform dispersion is crucial for the dopant's effectiveness in modifying the material's properties, ensuring that every region of the ceramic benefits from the intended enhancements in conductivity and mechanical strength. The doped ceramic shows a notable reduction in porosity and absence of micro-cracks, which are critical for the mechanical integrity and ionic conductivity of the material. Surface examination of the Zr-doped beta alumina exhibits a remarkably smooth finish with few detectable pores, indicative of a high degree of densification. These findings underscore the potential of Zr-doped beta alumina in applications demanding high ionic conductivity and mechanical robustness, such as solid oxide fuel cells and advanced structural ceramics.

5.3.8 Cole-cole plot of zinc doped sodium beta alumina

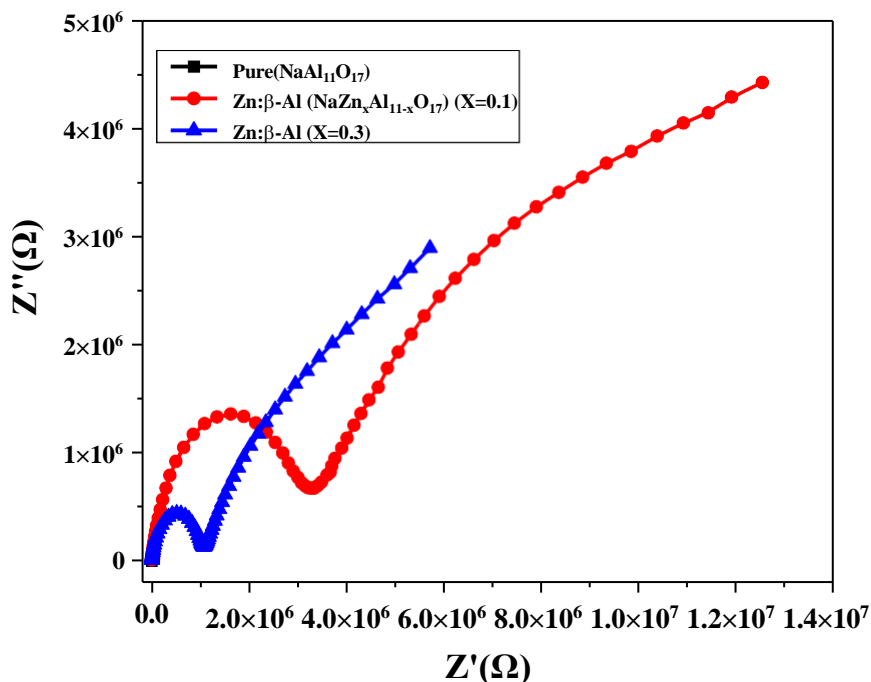


Figure 5.7 Cole-cole plot of sodium beta alumina with different Zinc concentrations.

To determine the actual contribution from the grain and grain boundary, Cole-Cole plot of sodium β -alumina with zinc nitrate dopant is shown in Fig. 5.7 It is a graphical representation of electrical impedance's imaginary part and the real part. From the graph it is found that in the higher frequency regime, the impedance is of order $10^5 \Omega$ which increases with decrease in a.c frequency. According to the graphical observation, semicircle in eminent frequency area is ascribed to the interfacial resistance between SE and electrode, the semicircle in the medium frequency area ascribed to transfer of charge procedure and inclined line in small frequency area is allocated to solid-state dispersal of zinc-ion in the solid electrolyte.

5.3.9 A.C Conductivity of Zin doped sodium beta alumina.

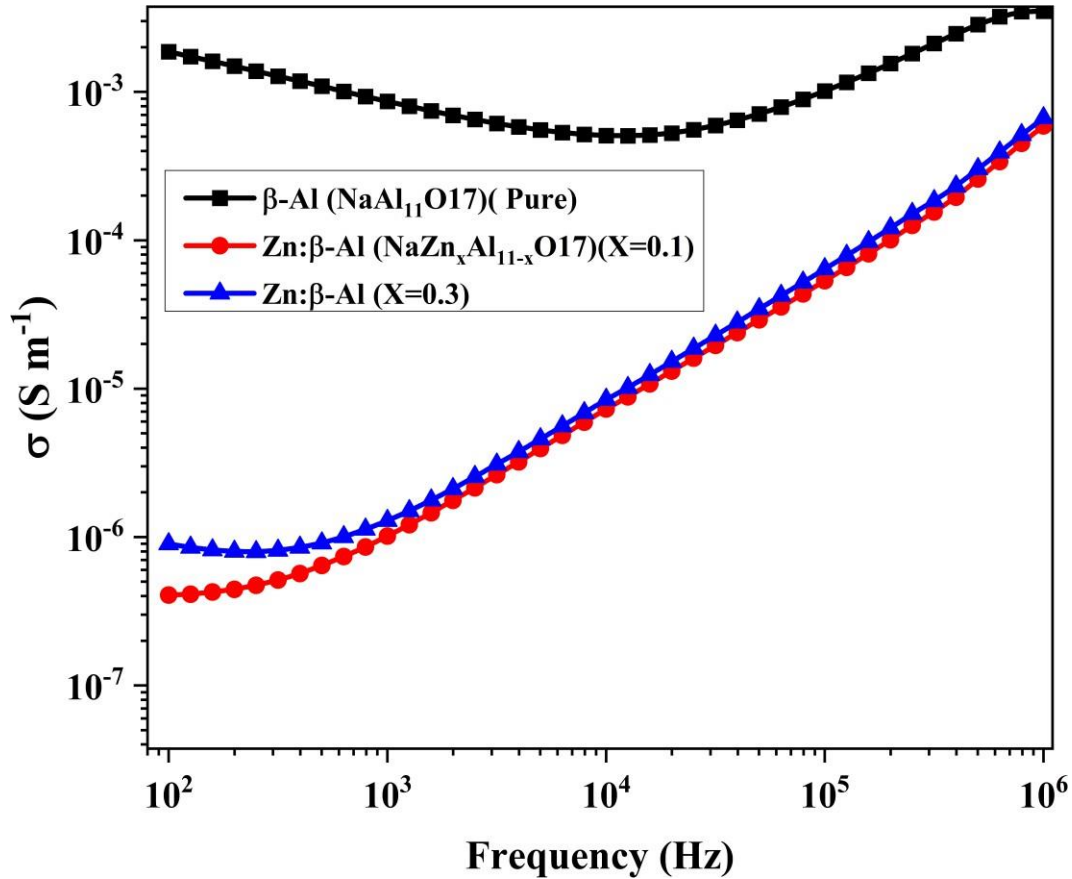


Figure 5.8 Conductivity vs Frequency of sodium beta alumina with zinc dopants.

Fig. 5.8 shows the variation as a function of a.c conductivity of input frequency for as prepared and zinc nitrate doped samples of varying concentration. Large conductivity of 10^{-3} S.m^{-1} is observed for as-prepared β -alumina and shows weak frequency dependent a.c conductivity at room temperature. For $x= 0.1$ and 0.3 , a.c conductivity decreases to 10^{-5} S.m^{-1} at 10^4 Hz and is found to increase with rise in frequency. At the frequency of 10^6 Hz , the a.c conductivity is found to be comparable to that of as-prepared sample. At low frequency ($< 1 \text{ KHz}$), the d.c part of the a.c conductivity is found to be negligible, which again confirms no contribution from the charge free carrier at the interface electrode- sample. With the increasing dopant concentration, the sample becomes denser which has further reduced grain boundary resistance. As a result, ionic conductivity for

higher dopant concentration has increased by a small magnitude. Overall, it is found that the Zinc dopant has suppressed the ionic conductivity of sodium because of the coulombic repulsion between Zn^{3+} and Na^+ , as a result the mobility of the Na^+ ion has decreased by significant factor at room temperature.

5.3.10 XRD analysis of Zinc doped beta alumina

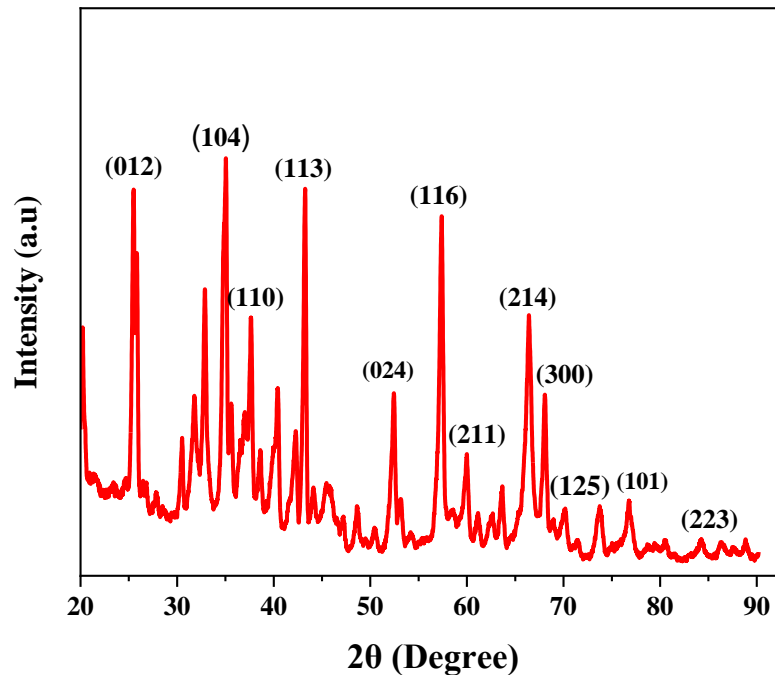


Figure 5.9 XRD pattern of Zinc doped beta alumina

In *fig 5.9*, XRD pattern for Zinc-doped beta alumina reveals the presence of multiple diffraction peaks, indicating a polycrystalline nature with a well-defined crystalline structure. The identification of high-index planes such as (116), (214), (125), and (223) suggests a high degree of crystallinity and complexity in the crystal structure. This complexity might be enhanced by the Zinc doping, which can alter the lattice parameters and potentially introduce new phases or modify existing ones. The appearance of specific peaks, particularly those like (104) and (110), which are commonly associated with the beta alumina structure, confirms the presence of the beta alumina phase within the doped material. The doping of Zinc into the beta alumina matrix may lead to lattice

distortions or expansions, evident from the peak positions and intensities. Shifts in peak positions compared to undoped beta alumina could indicate changes in lattice parameters due to the incorporation of Zinc ions. This detailed structural information is crucial for understanding the material's properties and potential applications, especially in areas where the crystal structure directly influences performance, such as in ionic conduction or catalysis.

5.3.11 FESEM Analysis

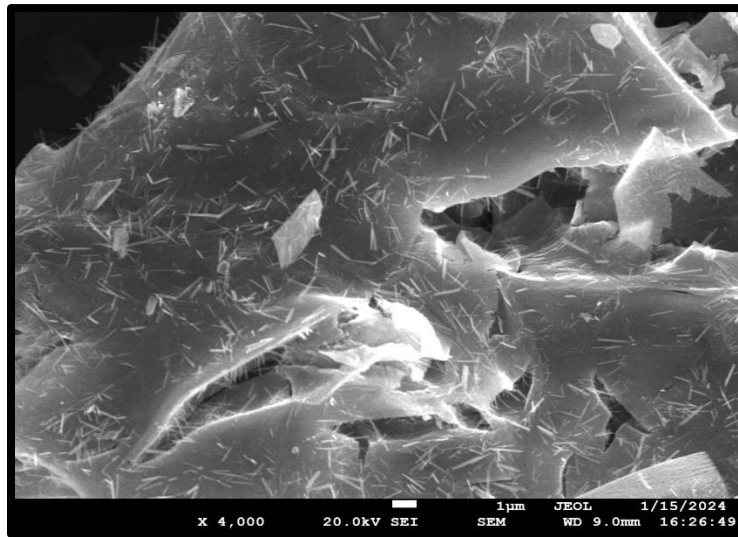


Figure 5.10 FESEM images of zinc doped beta alumina

In *fig 5.10* the FE-SEM micrographs reveal a densely sintered beta alumina matrix with a uniform grain size distribution. The average grain size is observed to be approximately 2-3 μm , indicating a refinement in grain size attributed to the presence of Zn dopants. No significant agglomeration of Zn dopants is observed, suggesting that the doping process effectively achieved a uniform Zn incorporation. This uniform distribution is critical for ensuring consistent electrical and mechanical properties throughout the material. The FE-SEM analysis shows minimal presence of porosity and virtually no detectable cracks within the matrix, pointing towards excellent sintering efficiency and structural integrity of the Zn-doped beta alumina. Secondary phases are not prominently observed, implying that the Zn content ($x=0.1$) is well within the solubility limit in the beta alumina phase or is effectively incorporated into the matrix without forming distinct secondary compounds.

The smooth surface and minimal defect features are indicative of a successful sintering process and appropriate doping levels that enhance the material's microstructural characteristics without introducing significant defects. These observations suggest that Zn doping at this concentration level effectively enhances the sintering and microstructural development of beta alumina, potentially leading to improved electrical and mechanical properties suitable for advanced ceramic applications.

5.4 Conclusion

Successfully synthesized Zirconyl/Zinc doped sodium beta alumina $\text{NaZr}_x\text{Al}_{11-x}\text{O}_{17}$ / $\text{NaZn}_x\text{Al}_{11-x}\text{O}_{17}$ by the sol-gel auto combustion method. The dielectric measurement shows drastic drop in real part of dielectric permittivity from 10^5 for $x=0$ to 10^2 for $x > 0$ at input frequency 10^4 Hz. This drop is mainly attributed to the screening effect by the Zr/Zn atom and the cluster formation which reduces the polarization effect. With the increase in Zr/Zn concentration ($x > 0$), the dielectric loss increases, and the relaxation frequency decreases. Further, Zirconyl/Zinc has suppressed the ionic conductivity to 10^{-5} S m^{-1} around 10^4 Hz in $\text{NaAl}_{11}\text{O}_{17}$ (Sodium β -alumina) which is mainly due to the Zr/Zn occupied vacancies which led to reduced mobility of Na^+ ion. XRD analysis of Zirconyl/Zinc-doped beta alumina reveals a complex, highly crystalline structure, underlined by the integration of zirconyl/zinc into the beta alumina matrix. These findings are vital for comprehending the material's properties and optimizing its application in areas such as ion conduction, catalysis, and structural components. The FE-SEM analysis of Zirconyl/zinc doped beta alumina with a dopant concentration of demonstrates significant microstructural enhancements characterized by uniform grain size, homogeneous dopant distribution, minimal defects, and a smooth surface topography.

Chapter 6

Optimization of electrical and thermal properties in Sodium β -alumina–PVDF composites

Abstract

We synthesize a hybrid nano-composite solid-state electrolyte system comprising of polymer polyvinylidene fluoride (PVDF) and beta alumina $\text{NaAl}_{11}\text{O}_{17}$ with varying PVDF weight percentages to improve the ionic conductivity of the solid electrolyte. XRD, SEM and EDX measurements exhibit correct phase of the system with minimal presence of chlorine as an impurity atom. According to electrochemical impedance spectroscopy (EIS), the composite system shows maximal dielectric permittivity at frequency 1 KHz to be around 10^5 and it drops to 10^3 for $X \geq 0.3$. The rapid fall in permittivity may be due to an increase of conductivity with the increase of PVDF concentration in the composite system. On further increase of PVDF concentration, the ionic conductivity decreases which is due to increase in scattering between Na^+ and PVDF grains. According to the Cole-Cole plot, the main cause of this variation is due to the increase in ionic resistance brought on by the charge transfer process between polymer molecules and beta alumina.

6.1 Introduction

Due to their light weight, low production cost, reliable mechanical qualities, good chemical stabilities, flexible polymers are widely employed in daily life and various industries, including food packaging, membrane separation, agriculture, and medicine [188]. They offer various benefits in heat dissipation systems in addition to being widely utilized as corrosion resistant materials and electrical insulation. The properties of lithium-ion batteries (LIBs), including their high energy density, high efficiency, extended cycle life, and environmental friendliness, make them one of the most promising batteries for next-generation electric vehicles and plug-in hybrid vehicles [189,190]. Higher standards for the energy density and safety performance of LIBs are put forth by these demanding and expanding needs. Yet, because liquid electrolytes are flammable and volatile, conventional lithium-ion batteries frequently have low capacity, poor electrochemical stabilities, and significant safety issues [195].

All-solid-state batteries have gained considerable interest in comparison to conventional liquid batteries because of their prospective benefits, including high weights and volume energy

densities, broad operating temperature ranges, long cycle lives, and superior safety [196-198]. The current mainstream solid electrolytes can be mainly classified into polymer solid electrolytes, sulfide solid electrolytes, and oxide solid electrolytes. Many polymers have so far been studied. Due to its appealing properties, including a high dielectric constant, good electrochemical stability, and good affinity to electrolyte solutions, Polyvinylidene Fluoride (PVDF) has seen a rise in attention for the creation of SPEs [199-201]. When polymer electrolytes are formed, the presence of strong electron-withdrawing fluorine atoms (-C-F) makes it easier for salts to separate into cations and raises the concentration of charge carriers. Many studies have investigated PVdF polymer electrolytes that are Li ion conductive [202-206].

6.2 Experimental Details

6.2.1 Materials and Synthesis Method

We synthesize a hybrid nano-composite solid-state electrolyte system comprising of polymer polyvinylidene fluoride (PVDF) and beta alumina $\text{NaAl}_{11}\text{O}_{17}$ with varying PVDF weight percentages. For the preparation of nanohybrid composite materials are sodium beta alumina and PVDF of Sigma company are used. To make a composite system, by mechanical blending method with PVDF of increasing Concentration (5%, 10%, 20%, 30%) were mixed with the Solid electrolyte Sodium β - Al and was thoroughly mixed until the color of the resultant powder looks uniform. After mixing they were compressed using a 20 Ton KBr pellet press machine at room temperature.

The preparation of hybrid composites $\text{Na}\beta\text{-Al: PVDF}$ via one of the ternary blend preparation methods known as physical blending. Additionally, it is also expected that combining two components with different degradation characteristics would alter the original characteristics of the components. Thus, the composites here are prepared by fine grinding and homogenous mixing of $\text{Na}\beta\text{-Al}$ in the polymer PVDF matrix via mortar and pestle. Additionally, followed by mechanically pressing the samples using the cold-press technique via KBr mechanical press instrument. The $\text{Na}\beta\text{-Al: PVDF}$ nanocomposites are prepared with varying weight percentage of PVDF polymer.

6.2.2 Characterization Techniques

The resulting pallet was then examined by using Field Emission Scanning Electron Microscope (FESEM), Au sputter coater (FE-SEM; JEOL JSM-7610F) to examine the morphology of

samples, EDX, and the dielectric measurement have been performed by Electrochemical Impedance Spectroscopy (EIS) in 100 Hz to 1 MHz (Potentiostat, Galvanostat by NOVA Software).

6.3 Results and Discussions

6.3.1 Dielectric Studies

6.3.1.1 Study of real part of permittivity vs frequency

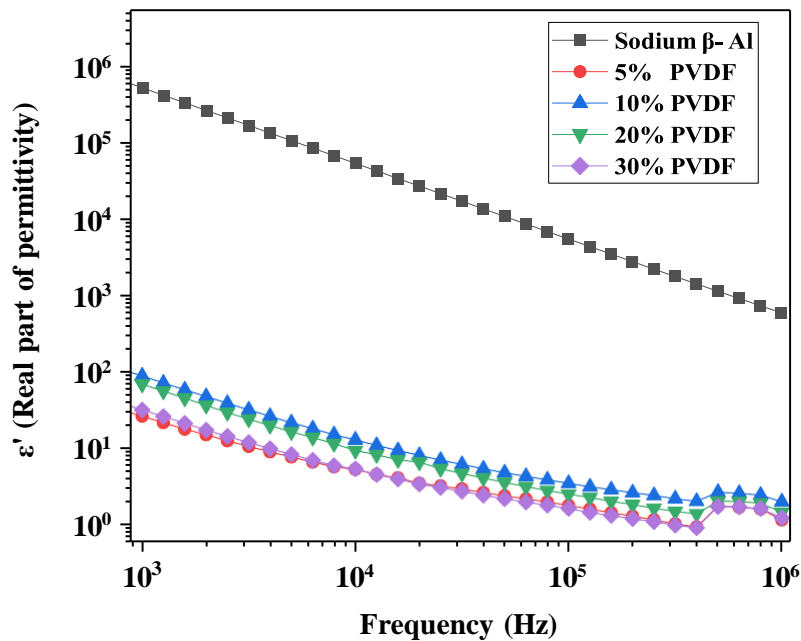


Figure 6.1 Variation of real part of permittivity of Sodium beta alumina ($NaAl_{11}O_{17}$) and PVDF composites.

In fig.6.1 Shows the complex permittivity of dielectric permittivity with frequency of sodium beta alumina solid electrolyte and PVDF with variable percentage. The substantial real component of the dielectric permittivity of 10^6 at 10^3 Hz is present in sodium beta alumina. Al vacancies that were created during the high temperature sintering process are mostly to blame for the occurrence of the significant permittivity. Additionally, the distinct portion of the dielectric permittivity is shown to decline linearly (seen by a black dotted line), supporting the very minimal electrode interfacial impact in our sample. Additionally, the gradual loss of permittivity with increasing frequency is ascribed to the loss of

polarization brought on by the displacement of Na⁺ ions. Interestingly, in hybrid nano-composite of sodium beta alumina and PVDF for percentage 5% & 30% there is subsequent drop in dielectric permittivity by four orders magnitude at 1KHz. Further, the presence of Na ions and its vacancies plays a specific role in determining the dipoles and the alignment of these dipoles gives rise to large permittivity in Sodium beta alumina and movement at the PVDF is added these dipoles are screened out which leads to decrease in permittivity.

6.3.1.2 Dielectric Tangent loss vs frequency

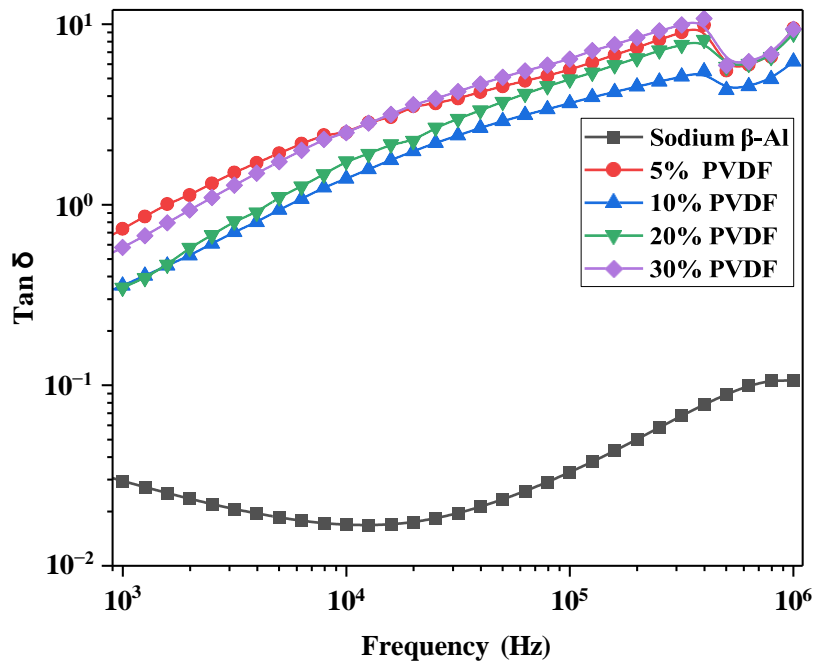


Figure 6.2 Tangent loss of sodium beta alumina and PVDF composites.

In this fig 6.2 dielectric tangent loss of samples shown as frequency function. For sodium beta alumina the loss is found to be almost frequency independent. For as-prepared NaAl₁₁O₁₇ sample, the loss is found to be almost frequency independent whereas for all value of x > 0, (x is PVDF concentration) the peak in the dielectric loss is mostly beyond our frequency range, indicating small relaxation time for the dielectric dipoles. At 1 KHz, dielectric loss in doped samples is 10⁻² which has increased to 10⁻¹ at 10⁴ Hz but remains

higher than as-prepared undoped sample. To shed more-light on the dielectric behavior, the dependence of a.c conductivity on frequency is also investigated.

6.3.1.3 AC conductivity of sodium β -alumina-PVDF composites

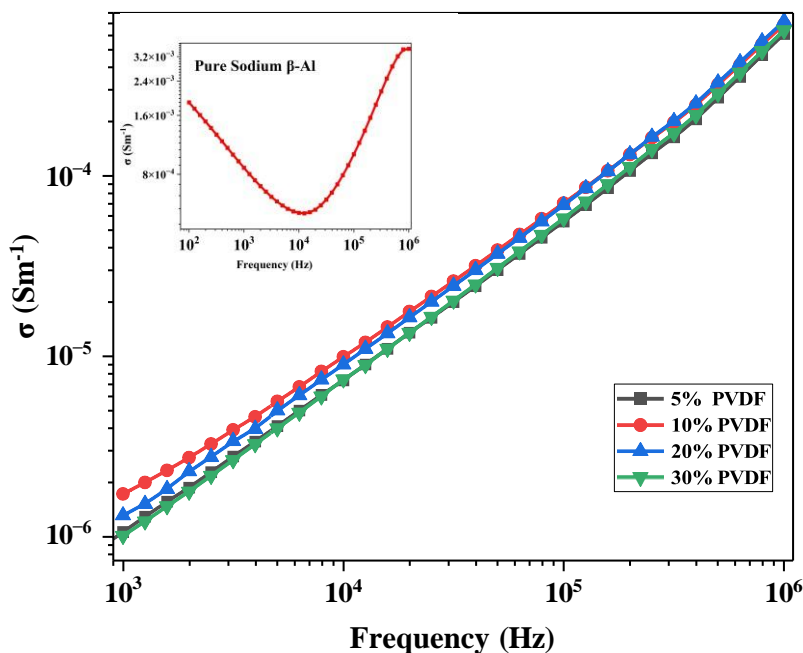


Figure 6.3 Frequency vs Ionic conductivity of PVDF composites. Inset: sodium β -Al Ionic conductivity with same frequency.

In this fig 6.3 shows the fluctuation of (a.c.) conductivity as a function of input frequency for as prepared hybrid nano-composite sodium beta alumina and polyvinylidene fluoride (PVDF) with varying percentage of PVDF to enhance the ionic conductivity. Large conductivity of 10^{-3} S.m^{-1} is observed for β -alumina and shows weak frequency dependent a.c conductivity at room temperature. For 10%, 20% & 30% of PVDF as conductivity decreases with increase in frequency by varying the percentage of PVDF as shown in fig But for 5% there is small decrease in a.c. conductivity at 10^{-6} S m^{-1} at 10^4 Hz and it found to be increase with the increase in frequency. At high frequency 10^6 Hz , the a.c. conductivity is found be comparable. PVDF improves the ionic conductivity of solid electrolytes as PVDF has a high dielectric constant, which enhances its ability to store

electrical energy. This property is beneficial for increasing ionic conductivity in solid electrolytes. Polymer Matrix Modification: The nature of the polymer matrix, when modified with PVDF, affects the electrolyte's morphology and mechanical properties, which in turn influence ionic conductivity. The addition of ionic liquids to PVDF-based electrolytes increases ionic conductivity. These liquids also help reduce polymer crystallinity, facilitating easier ion diffusion. Compatibility with Active Fillers: PVDF is compatible with various active fillers like lithium salts, which are known for their high ionic conductivity. This compatibility enhances the overall conductivity of the electrolyte.

6.3.1.4 Cole-cole plot of sodium β -alumina-PVDF composites

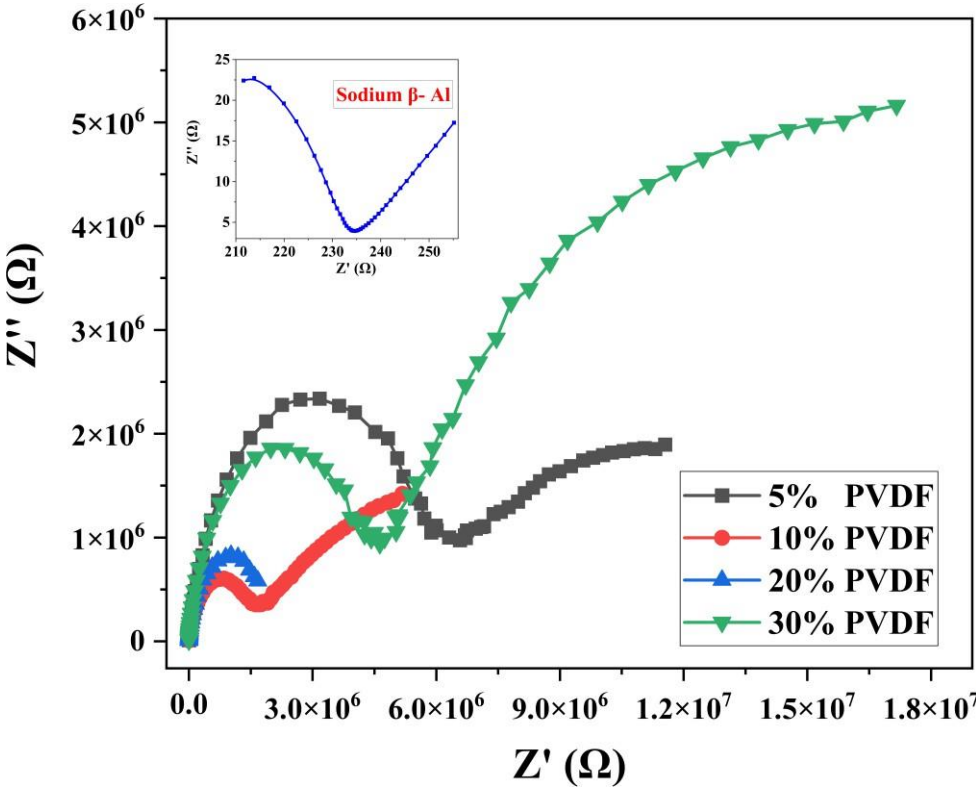


Figure 6.4 Cole-cole plot of PVDF composites and Inset: Cole-cole plot of Sodium beta alumina.

To determine the actual contribution from the grain boundary, cole-cole plot of sodium

beta alumina and PVDF composites are shown in fig 6.4. It is the graphical representation of the real part of permittivity and the imaginary part of complex impedance. From the fig 5.5 in the higher frequency regime, the impedance is of order of 10^5 which increases with the decreases in a.c. frequency. According to the graphical observation, the sloped line in the small frequency area is assigned to solid-state diffusion of polymer ions in solid electrolytes, semicircle in higher frequency region is ascribed to the interfacial resistance between SE and electrode, semicircle in medium frequency region to the charge transfer procedure. The diameter of semicircle increases in 5% and 30% of PVDF composites, polarization is responsible is for such behavior. The first originates from reorientation of the dipoles in PVDF composites. The second is the accumulation of charge carriers at the polymer nanoparticle interfaces. This gives rise to the interfacial polarization effect widely known as the Maxwell-Wagner-Sillars (MWS) polarization. Further two major dielectric processes are observed in this diagram, a low frequency relaxation is observed also observed in this graph and this relaxation produces large dielectric losses at low frequency regime. Arbatti et al., believed that this low frequency relaxation arose from conductive behaviour of composite.

6.3.2 Thermal Analysis

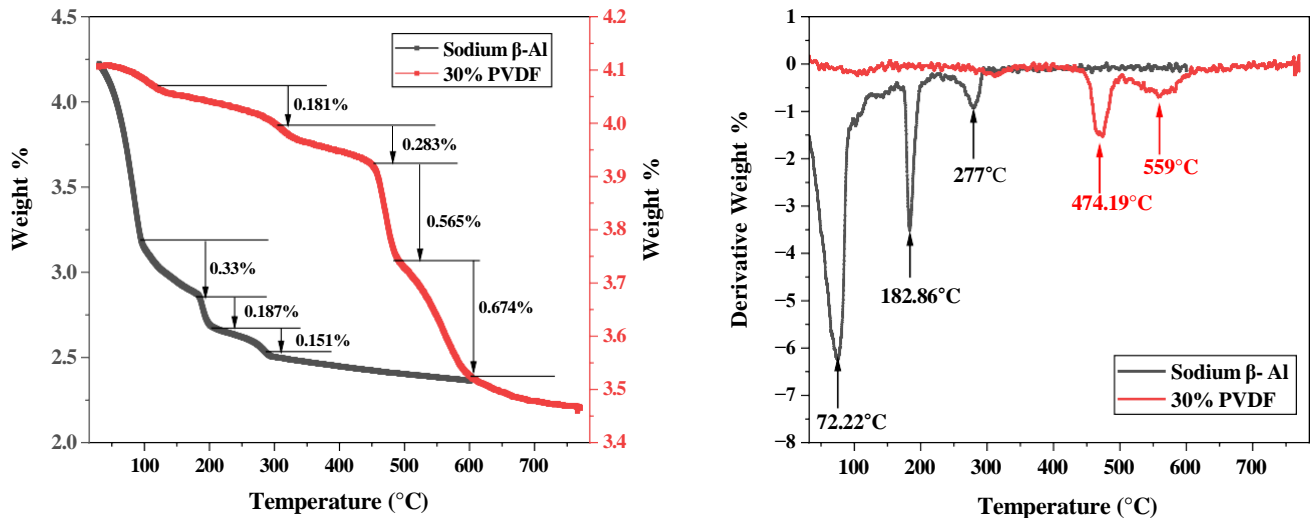


Figure 6.5 (a) TGA Curve of Sodium beta alumina ($\text{NaAl}_{11}\text{O}_{17}$) with PVDF Composite. (b) Derivative weight% of pure sodium beta alumina with PVDF Composite corresponding to the same temperature.

In this fig 6.5 shows the TGA curves of sodium beta alumina and Polyvinylidene Fluoride (PVDF) composite. On quantifying the materials stability, it is found that the weight of beta alumina has reduced by ~46% when heated in the range of temperature 30- 600°C under the air atmosphere. From the derivative TGA curves of beta alumina & PVDF composite sharp peak weight loss is observed at temperature at 72.22, 182.86 & 277°C of beta alumina & PVDF composite at 474.19 & 559°C which is mainly attributed to the evaporation of adsorption of water and the disintegration of unreacted organic solvents respectively. This indicates the PVDF is semicrystalline polymer having remarkable thermal stability, unique piezoelectric and pyroelectric characteristics. Additionally, it has found that adding PVDF concentration thermal stability improves.

6.3.3 Morphological Analysis

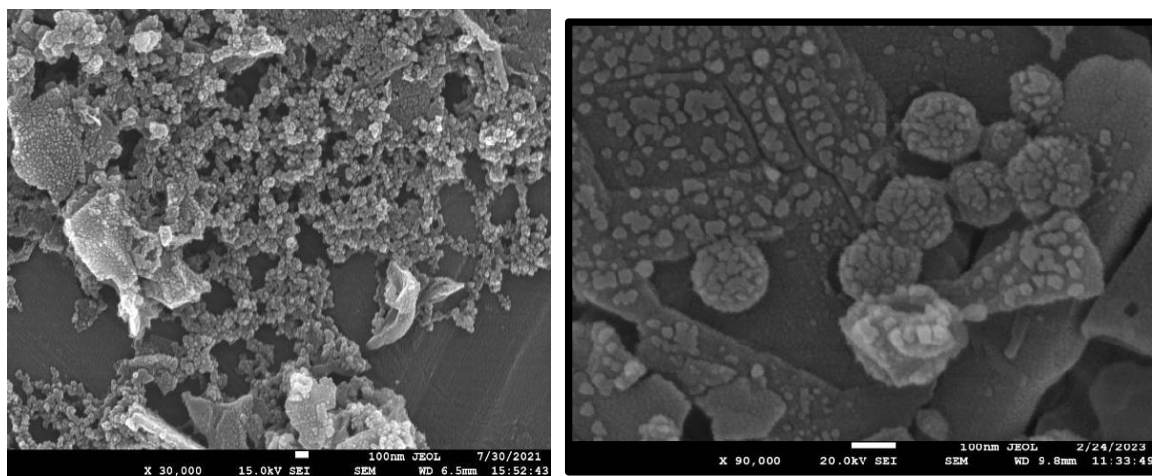


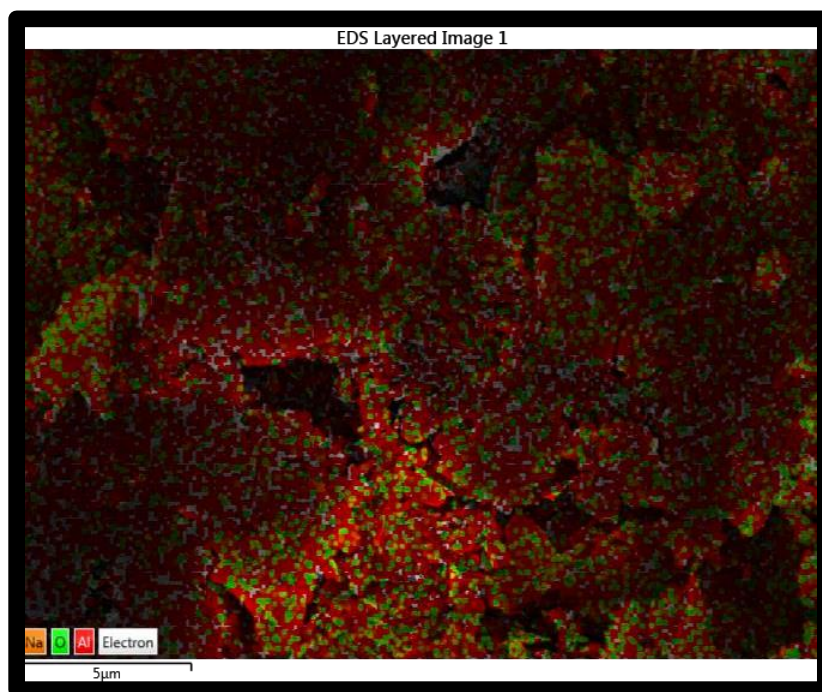
Figure 6.7 SEM images of sodium beta alumina and PVDF composites.

In this fig 6.7 shows the SEM images of as-prepared sodium β -alumina and PVDF composite of varying concentrations. The morphology of as-prepared sample shows thin granular type elongated structure of length around 100 - 200 nm and diameter of 10 - 20

nm. Additionally, Na β -Al exhibits a narrow size and shape distribution that communicates a uniform reduction in stress among the sodium beta alumina particles. However, when PVDF is added in concentration, it becomes apparent that due to the PVDF small particle size, they surround the sodium beta alumina particles, resulting in the formation of large interparticle sodium beta alumina particles.

6.3.4 EDX analysis

To identify the presence of all elements in the prepared nanocomposites, EDX has been carried out. EDX pattern of Sodium β - Al: PVDF composite shown in fig; 6.8 the EDX was examined, which has been carried out for distribution of elements of specimen at the surface. The area scanned in Fig. 5.9 reveals the uniform distribution of elemental components and homogenous composition of chemicals over the entire specimen. The absence of any other elements confirms the purity of our synthesized nanohybrid composite. From this spectrum, it has been observed that the presence of desired elements without any other undesirable elements. This confirms the successful synthesis of the phase pure nanocomposites.



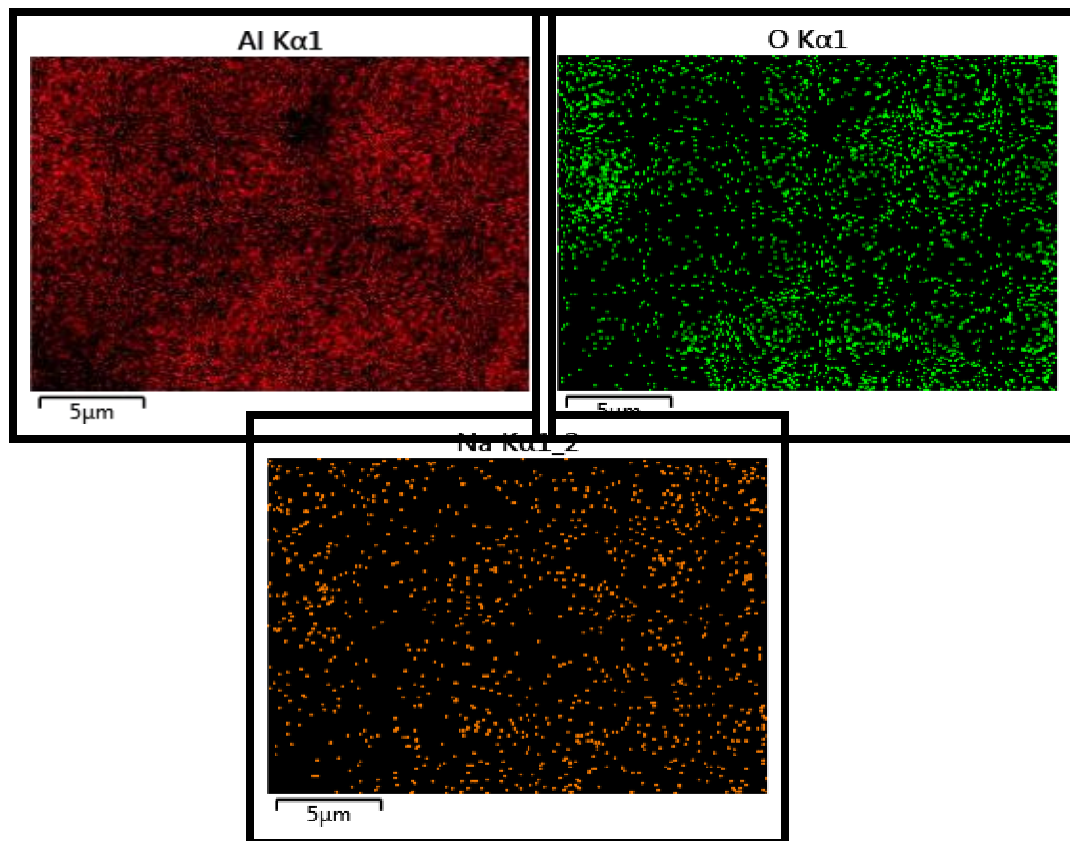


Figure 6.8 EDX spectra of PVDF-Sodium β -Al solid electrolyte

6.3.4 Relation between weight% vs Conductivity

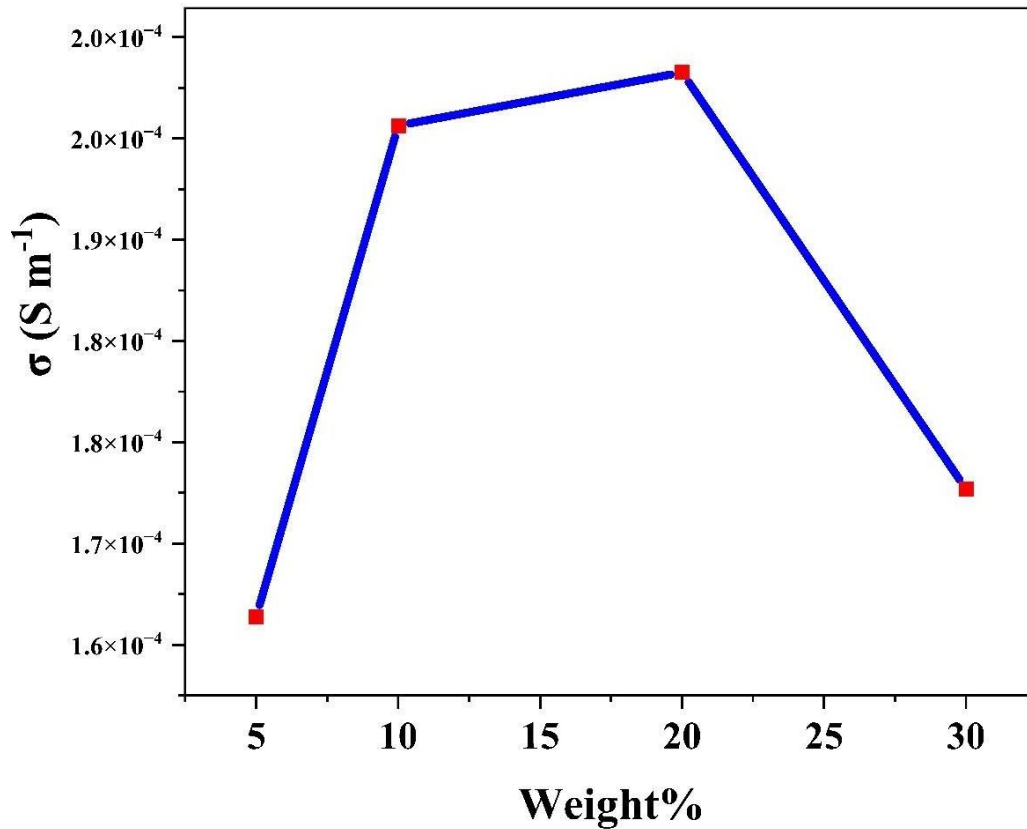


Figure 6.9 Relationship between Conductivity vs Weight % of Na β -Al: PVDF composite

In this fig 6.9, shows the relation between conductivity and weight% of Na β -Al: PVDF nanocomposite. To find the weight% of different PVDF concentration added into composite. From the figure it seems that PVDF with 20% weight has higher conductivity of 2.005×10^{-4} S/m. The electron lone pair is uniformly distributed in the polyvinylidene fluoride due to moderate concentration.

6.3.6 XRD analysis of PVDF: Sodium beta alumina

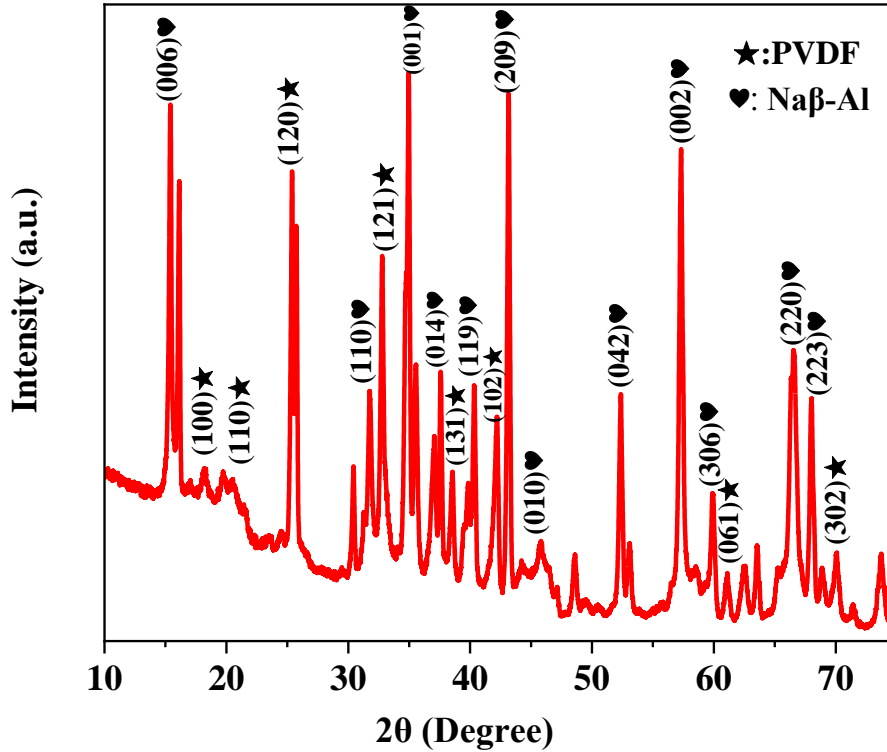


Figure 6.10 XRD pattern of PVDF: sodium beta alumina

In fig 6.10, XRD pattern for PVDF: Sodium beta alumina composite displays distinct peaks, indicating a polycrystalline nature with a complex crystalline phase composition. The array of peaks across the 2θ scale signifies a high degree of crystallinity within the doped material, with a complex interplay of crystallographic planes suggesting the presence of multiple phases or orientations. This complexity is characteristic of materials where doping influences both the host lattice and potentially introduces new phases. The presence of low-index planes such as (001), (002), and (006) alongside high-index planes like (119), (209), and (306) indicates that PVDF doping has a notable effect on the crystal structure of sodium beta alumina. These changes could reflect lattice distortions, expansions, or the formation of new crystalline domains due to the incorporation of PVDF. The variety of hkl values, especially the occurrence of specific

planes such as (113), (114), and (223), suggests significant structural modifications and a high level of structural order. These modifications are likely a result of the interaction between PVDF and the sodium beta alumina matrix, affecting both the microstructure and macroscopic properties of the material. The observed hkl values provide detailed insights into the crystallographic orientations and phase behaviour of the material, indicating that PVDF doping not only modifies the existing lattice structure of sodium beta alumina but may also introduce new phases or crystalline features.

6.4 Conclusion

Successfully synthesized the nanohybrid composites by mechanical blending method. The results obtained imply that on adding the concentration of PVDF improve conductivity of composites. Further, thermal stability is found to be temperature independent in wide range and has improved significantly. The dielectric measurement shows drastic drop in real part of dielectric permittivity from 10^5 for $x=0$ to 10^2 for $x > 0$ at input frequency 10^4 Hz. This drop is mainly attributed to the screening effect and the cluster formation which reduces the polarization effect. With the increase in PVDF concentration the dielectric loss increases. Further, morphology plays a vital role in determining the dielectric properties which leads to large interparticle sodium beta alumina. The XRD analysis of PVDF-doped sodium beta alumina reveals a rich and complex crystalline structure, significantly influenced by the introduction of PVDF.

Chapter 7

Summary and Scope for Future Work

The novelty of the presented work is the choice of solid-state electrolyte. An attempt has been made to synthesis the solid electrolyte sodium β -alumina. This solid electrolyte yields good results as well applications as per literature. But as per our observation it has been found that the change in morphology and thermal stability of solid electrolyte significantly improved upon wide range of temperature, with good structural and dielectric properties.

This research work has attempted to address the problems faced in the fabrication, synthesis, and characterization of solid electrolyte. The properties of solid electrolytes such as structural, thermal, morphological, and dielectric has been studied. The appropriateness of sol-gel auto-combustion method has been confirmed with suitable time and sintering temperature.

By using sol-gel auto-combustion method $\text{NaIn}_x\text{Al}_{11-x}\text{O}_{17}$ has been make-ready successfully. Further the sample is sintered at temperature at 1100°C to study the different properties. From XRD pattern of doped $\text{NaIn}_x\text{Al}_{11-x}\text{O}_{17}$ with $x=0.4$ which were calcinated at 1100°C for 5 hours prior to XRD analysis. The crystalline phase is verified by the XRD pattern of the produced samples, and the intense sharp peaks of the indium doping concentrations demonstrate proportionate and uniform doping in pure alumina. From TGA this indicates that the indium doped β -alumina samples facilitate better thermal stability compared to as-prepared one. The increase in thermal stability is a direct consequence of increase in densification of doped samples as it has previously been confirmed that as-prepared β -alumina inherits aluminum vacancies due to the high temperature calcination process. From FESEM the morphology of as-prepared sample shows thin cylindrical type elongated structure of length around 100 - 200 nm and diameter of 10 - 20 nm. Moreover, the undoped sample shows narrow distribution of its size and shape, which further conveys uniform reduction in stress among the particles during high temperature. Upon indium doping, the particles of the samples tend to disintegrate into smaller thin grains. The effect of Indium doping in our sample was found to slow down the growth of grains which is exactly an opposite behavior observed in TiO_2 doped in sodium β -alumina. DC resistivity measurement confirms large electrical resistivity with the staircase type variation with increasing temperature. The dielectric measurement shows that the as prepared

undoped $\text{NaAl}_{11}\text{O}_{17}$ sample, it exhibits large real part of dielectric permittivity of 10^5 at 1 KHz and low dielectric loss of around 10^{-2} as shown in the inset. The large value of dielectric permittivity is mainly due to presence of Al^{3+} vacancies which were induced during high temperature sintering process. The crystal structure of β -alumina has alternate layers of $[\text{NaO}]$ and spinel like blocks of $[\text{Al}_{11}\text{O}_{16}]$ stacked alternately. The presence of Al^{3+} vacancies break the inversion symmetry due to which strong polarizing field yields large permittivity. The steady decrease in permittivity with increasing frequency is also attributed to the decrease of polarization due to displacement of Na^+ ions. Interestingly, when indium is doped with concentrations $x = 0.1$ and 0.2 , there is subsequent drop-in dielectric permittivity by two orders magnitude at 1 KHz which confirms that indium atom couples strongly with the β -alumina structure and held responsible for the decreases of electrical polarization.

Successfully synthesized Zirconyl/Zinc doped sodium beta alumina $\text{NaZr}_x\text{Al}_{11-x}\text{O}_{17}$ / $\text{NaZn}_x\text{Al}_{11-x}\text{O}_{17}$ by the sol-gel auto combustion method. The dielectric measurement shows drastic drop in real part of dielectric permittivity from 10^5 for $x=0$ to 10^2 for $x > 0$ at input frequency 10^4 Hz. This drop is mainly attributed to the screening effect by the Zr/Zn atom and the cluster formation which reduces the polarization effect. With the increase in Zr/Zn concentration ($x > 0$), the dielectric loss increases, and the relaxation frequency decreases. Further, Zirconyl/Zinc has suppressed the ionic conductivity to 10^{-5} S m^{-1} around 10^4 Hz in $\text{NaAl}_{11}\text{O}_{17}$ (Sodium β -alumina) which is mainly due to the Zr/Zn occupied vacancies which led to reduced mobility of Na^+ ion. XRD analysis of Zirconyl/Zinc-doped beta alumina reveals a complex, highly crystalline structure, underlined by the integration of zirconyl/zinc into the beta alumina matrix. These findings are vital for comprehending the material's properties and optimizing its application in areas such as ion conduction, catalysis, and structural components. The FE-SEM analysis of Zirconyl/zinc doped beta alumina with a dopant concentration demonstrates significant microstructural enhancements characterized by uniform grain size, homogeneous dopant distribution, minimal defects, and a smooth surface topography.

Synthesis of hybrid nano-composite solid-state electrolyte system comprising of polymer polyvinylidene fluoride (PVDF) and beta alumina $\text{NaAl}_{11}\text{O}_{17}$ with varying PVDF weight % to improving ionic conductivity (σ) of SEs is successfully prepared by mechanical blending method. From SEM the morphology of as-prepared sample shows thin granular type elongated structure of length around 100 - 200 nm and diameter of 10 - 20 nm. Additionally, $\text{Na}\beta\text{-Al}$

exhibits narrow distribution of size and shape which communicates the uniform reduction in stress among the sodium beta alumina particles but as soon as the concentration of PVDF is added reveals that due to small size of PVDF particles, it surrounds Sodium beta alumina particles resulting in the formation of large interparticle Sodium beta alumina particles. TGA curves of sodium beta alumina and Polyvinylidene Fluoride (PVDF) composite. This indicates the PVDF is semicrystalline polymer having remarkable thermal stability, unique piezoelectric and pyroelectric characteristics. The dielectric measurement shows drastic drop in real part of dielectric permittivity from 10^5 for $x=0$ to 10^2 for $x > 0$ at input frequency 10^4 Hz. This drop is mainly attributed to the screening effect and the cluster formation which reduces the polarization effect. With the increase in PVDF concentration the dielectric loss increases. Furthermore, the dielectric characteristics that result in large interparticle sodium beta alumina are greatly influenced by morphology. XRD analysis of PVDF-doped sodium beta alumina reveals a rich and complex crystalline structure, significantly influenced by the introduction of PVDF.

Future Work

As the world is growing rapidly and the new technologies and research is going day by day and the demand of new things are more than existing once. As we know, the energy storage conservation is buzzing with sodium ion technology and rightly so. To fulfil the increasing demand for energy storage, the R&D capacities in the battery technology sector are expanding quickly. Researchers exploring practical non-lithium battery alternatives are primarily focused on reducing the strain on global lithium sources.

Decarbonization, the increasing use of electric vehicles, and the increasing integration of renewable energy sources into electrical grids are among the reasons promoting the development of socially and environmentally friendly energy storage technologies. The industrialization of sodium-ion batteries is accelerating due to the global R&D activities. Particularly, the sodium-ion battery market is probably going to profit from R&D to boost operational effectiveness, save costs, and create additional revenue potential. The sodium-ion battery market is anticipated to grow quickly in the next years because of higher spending and targeted R&D investments to simplify the transition from pilot plant-scale production to full commercialization.

Advanced technological capabilities and battery innovation are pivotal to the acceptance and adoption of sodium-ion batteries (SIBs) on a commercial scale. The complicated and varied sodium battery development process will lead to innovation in the battery market. Hybrid batteries, for instance, offer encouraging possibilities to combine the finest qualities of sodium and lithium for improved battery performance. The potential for sodium-ion batteries to establish a significant footing in the battery market is supported by research. The advancement of sodium-ion technology will continue to improve as the world searches more and more for secure and long-lasting energy storage.

Sodium-ion batteries (SIBs) are more cost-effective, energy-efficient, secure, and sustainable than lithium-ion batteries. Now is the time to recharge your SIBs and it is a game changer in the field of batteries.

Bibliography

1. Li, J., Liu, C., Miao, C., Kou, Z., & Xiao, W. (2021). Enhanced ionic conductivity and electrochemical stability of Indium doping $\text{Li}_{1.3}\text{Al}_{0.3}\text{Ti}_{1.7}(\text{PO}_4)_3$ solid electrolytes for all-solid-state lithium-ion batteries. *Ionics*, 7(0123456789).
<https://doi.org/10.1007/s11581-021-04310-8>.
2. Chen, J., Wu, J., Wang, X., Zhou, A., & Yang, Z. (2021). Research progress and application prospect of solid-state electrolytes in commercial lithium-ion power batteries. *Energy Storage Materials* (Vol. 35). Elsevier B.V.
<https://doi.org/10.1016/j.ensm.2020.11.017>.
3. Li, H., Zhang, T., Yang, Z., Shi, Y., Zhuang, Q., & Cui, Y. (2021). Electrochemical Impedance Spectroscopy Study on Using $\text{Li}_{10}\text{GeP}_2\text{S}_{12}$ Electrolyte for All-Solid-State Lithium Batteries. *International Journal of Electrochemical Science*, 16(2), 1–13.
<https://doi.org/10.20964/2021.02.33>.
4. Middlemiss, L. A., Rennie, A. J. R., Sayers, R., & West, A. R. (2020). Characterization of batteries by electrochemical impedance spectroscopy. *Energy Reports*, 6, 232–241.
<https://doi.org/10.1016/j.egy.2020.03.029>.
5. Dai, H., Xu, W., Hu, Z., Chen, Y., Wei, X., Yang, B., ... Wei, W. (2020). Effective Approaches of Improving the Performance of Chalcogenide Solid Electrolytes for All-Solid-State Sodium-Ion Batteries. *Frontiers in Energy Research*, 8. <https://doi.org/10.3389/fenrg.2020.00097>.
6. Tanibata, N., Takimoto, S., Nakano, K., Takeda, H., Nakayama, M., & Sumi, H. (2020). Metastable Chloride Solid Electrolyte with High Formability for Rechargeable All-Solid-State Lithium Metal Batteries. *ACS Materials Letters*, 2(8), 880–886.
<https://doi.org/10.1021/acsmaterialslett.0c00127>.
7. Kim, H. J., Krishna, T. N. V., Zeb, K., Rajangam, V., Muralee Gopi, C. V. V. Sambasivam, S., ... Obaidat, I. M. (2020). *A comprehensive review of li-ion battery materials and their recycling techniques*. *Electronics (Switzerland)* (Vol. 9).
<https://doi.org/10.3390/electronics9071161>.

8. Chandra, A., Chandra, A., & Dhundhel, R. S. (2020). Electrolytes for sodium ion batteries: A short review. *Indian Journal of Pure and Applied Physics*, 58(2), 113–119.
9. Agustina, A. I., Skadell, K., Dirksen, C. L., Schulz, M., & Kusumocahyo, S. P. (2019). Sol-gel method for synthesis of Li⁺-stabilized Na-β"-alumina for solid electrolytes in sodium-based batteries. *AIP Conference Proceedings*, 2175(November). <https://doi.org/10.1063/1.5134634>.
10. Yao, P., Yu, H., Ding, Z., Liu, Y., Lu, J., Lavorgna, M., ... Liu, X. (2019). Review on Polymer-Based Composite Electrolytes for Lithium Batteries. *Frontiers in Chemistry*, 7(August), 1–17. <https://doi.org/10.3389/fchem.2019.00522>.
11. Zhao, W., Yi, J., He, P., & Zhou, H. (2019). Solid - State Electrolytes for Lithium - Ion Batteries: Fundamentals, Challenges and Perspectives. *Electrochemical Energy Reviews*, 2(4), 574–605. <https://doi.org/10.1007/s41918-019-00048-0>.
12. Wang, Y., Song, S., Xu, C., Hu, N., Molenda, J., & Lu, L. (2019). Nano Materials Science Development of solid-state electrolytes for sodium-ion battery – A short review. *Nano Materials Science*, 1(March), 91–100. <https://doi.org/10.1016/j.nanoms.2019.02.007>.
13. Froboese, L., Sichel, J. F. Van Der, Loellhoeffel, T., & Helmers, L. (2019). Effect of Microstructure on the Ionic Conductivity of an All-Solid-State Battery Electrode, *166*(2), 318–328. <https://doi.org/10.1149/2.0601902jes>.
14. Yu, X., Xue, L., Goodenough, J. B., & Manthiram, A. (2019). A High-Performance All- Solid-State Sodium Battery with a Poly (ethylene oxide)-Na₃Zr₂Si₂PO₁₂ Composite Electrolyte. *ACS Materials Letters*, 1(1), 132–138. rapid-communication. <https://doi.org/10.1021/acsmaterialslett.9b00103>.
15. Chen, X., & Vereecken, P. M. (2019). Solid and Solid-Like Composite Electrolyte for Lithium- I o n Batteries: Engineering the Ion Conductivity at Interfaces. *Adv. Mater.Interfaces*, 1800899, 1–31. <https://doi.org/10.1002/admi.201800899>.
16. Famprakis, T., Canepa, P., Dawson, J. A., Islam, M. S., & Masquelier, C. (2019). Fundamentals of inorganic solid-state electrolytes for batteries. *Nature Materials*, 18(12), 1278–1291. <https://doi.org/10.1038/s41563-019-0431-3>.
17. Muhammad Risyad Hasyim and Michael T Lanagan (2018). A new percolation model for composite solid electrolytes and dispersed ionic conductors. *Modelling Simul. Mater. Sci. Eng.*

26 025011. doi 10.1088/1361-651X/aaa26f.

18. Arya, A., & Sharma, A. L. (2018). Structural, electrical properties and dielectric relaxations in Na⁺-ion-conducting solid polymer electrolyte. *Journal of Physics Condensed Matter*, 30(16), 1–57. <https://doi.org/10.1088/1361-648X/aab466>.
19. Skundin, A. M., Kulova, T. L., & Yaroslavtsev, A. B. (2018). Sodium-Ion Batteries (a Review). *Russian Journal of Electrochemistry*, 54(2), 113–152. <https://doi.org/10.1134/S1023193518020076>.
20. Mei, B. A., Munteshari, O., Lau, J., Dunn, B., & Pilon, L. (2018). Physical Interpretations of Nyquist Plots for EDLC Electrodes and Devices. *Journal of Physical Chemistry C*, 122(1), 194–206. <https://doi.org/10.1021/acs.jpcc.7b10582>.
21. Abud Kappel, M. A., Peixoto, F. C., Platt, G. M., Domingos, R. P., & Bastos, I. N. (2017). A study of equivalent electrical circuit fitting to electrochemical impedance using a stochastic method. *Applied Soft Computing Journal*, 50, 183–193. <https://doi.org/10.1016/j.asoc.2016.11.030>.
22. Aziz, S. B. (2015). Study of electrical percolation phenomenon from the dielectric. *Bulletin of Materials Science*. <https://doi.org/10.1007/s12034-015-0978-9>.
23. Saberi, A. A. (2015). Recent advances in percolation theory and its applications. *Physics Reports*. <https://doi.org/10.1016/j.physrep.2015.03.003>.
24. Puthirath, A. B., John, B., Gouri, C., & Jayalekshmi, S. (2015). Lithium doped polyaniline and its composites with LiFePO₄ and LiMn₂O₄-prospective cathode active materials for environment friendly and flexible Li-ion battery applications. *RSC Advances*, 5(85), 69220–69228. <https://doi.org/10.1039/c5ra10706g>.
25. Tang, J., Dysart, A. D., & Pol, V. G. (2015). Advancement in sodium-ion rechargeable batteries. *Current Opinion in Chemical Engineering*, 9, 34–41. <https://doi.org/10.1016/j.coche.2015.08.007>.
26. Mukherjee, R., Lawes, G., & Nadgorny, B. (2014). Enhancement of high dielectric permittivity in CaCu₃Ti₄O₁₂/RuO₂ composites in the vicinity of the percolation threshold. *Applied Physics Letters*, 105(7), 072901. <https://doi.org/10.1063/1.4893009>.
27. Chawla, M., Shekhawat, N., Aggarwal, S., Sharma, A., & Nair, K. G. M. (2014). Cole- cole analysis and electrical conduction mechanism of N⁺ implanted polycarbonate. *Journal of Applied Physics*, 115(18), 1–7. <https://doi.org/10.1063/1.4876123>.

28. Mukherjee, R., Huang, Z. F., & Nadgorny, B. (2014). Multiple percolation tunneling staircase in metal-semiconductor nanoparticle composites. *Applied Physics Letters*, *105*(17). <https://doi.org/10.1063/1.4900777>.
29. Fergus, J. W. (2012). Ion transport in sodium ion conducting solid electrolytes. *Solid State Ionics*, *227*, 102–112. <https://doi.org/10.1016/j.ssi.2012.09.019>.
30. Garagounis, I., Kyriakou, V., Anagnostou, C., Bourganis, V., Papachristou, I., & Stoukides, M. (2011). Solid electrolytes: Applications in heterogeneous catalysis and chemical cogeneration. *Industrial and Engineering Chemistry Research*, *50*(2), 431– 472. <https://doi.org/10.1021/ie1001058>.
31. Lu, X., Xia, G., Lemmon, J. P., & Yang, Z. (2010). Advanced materials for sodium-beta alumina batteries: Status, challenges and perspectives. *Journal of Power Sources*, *195*(9), 2431–2442. <https://doi.org/10.1016/j.jpowsour.2009.11.120>.
32. Uvarov, N. F. (2008). Composite solid electrolytes: Recent advances and design strategies. *Journal of Solid-State Electrochemistry*, *15*(2), 367–389. <https://doi.org/10.1007/s10008-008-0739-4>.
33. Agrawal, R. C., & Pandey, G. P. (2008). Solid polymer electrolytes: Materials designing and all-solid-state battery applications: An overview. *Journal of Physics D: Applied Physics*, *41*(22). <https://doi.org/10.1088/0022-3727/41/22/223001>.
34. Kumar, P. P., & Yashonath, S. (2006). Ionic conduction in the solid state, *journal of chemical science*. *118*(1), 135–154.
35. Soares, B. G., Leyva, M. E., Barra, G. M. O., & Khastgir, D. (2006). Dielectric behavior of polyaniline synthesized by different techniques. *European Polymer Journal*, *42*(3), 676–686. <https://doi.org/10.1016/j.eurpolymj.2005.08.013>.
36. Fonseca, F. C., & Muccillo, R. (2004). Impedance spectroscopy analysis of percolation in (yttria-stabilized zirconia)-yttria ceramic composites. *Solid State Ionics*, *166*(1–2), 157– 165. <https://doi.org/10.1016/j.ssi.2003.10.002>.
37. Tongwen, X., Weihua, Y., & Binglin, H. (2001). Ionic conductivity threshold in sulfonated poly (phenylene oxide) matrices : a combination of three-phase model and percolation theory, *56*, 5343–5350.
38. Kumar, B., Rodrigues, S. J., & Scanlon, L. G. (2001). Ionic Conductivity of Polymer- Ceramic Composites, *4*, 1191–1195. <https://doi.org/10.1149/1.1403729>.
39. Gromov, O. G., Kunshina, G. B., Kuz'min, A. P., & Kalinnikov, V. T. (1996). Ionic

- conductivity of solid electrolytes based on $\text{Li}_{1.3}\text{Al}_{10.3}\text{Ti}_{1.7}(\text{PO}_4)_3$. *Russian Journal of Applied Chemistry*, 69(3), 385–388.
40. Islam, S., Lakshmi, G. B. V. S., Siddiqui, A., Husain, M., & Zulfequar, M. (2013). Synthesis and Electrochemical Properties of Graphene / Graphene / V_2O_5 Composites. *International Journal of Polymer Science*, 2013, 1–7.
41. Wang, C., & Hong, J. (2007). Ionic/electronic conducting characteristics of LiFePO_4 cathode materials. *Electrochemical and Solid-State Letters*, 10(3), 65–69. <https://doi.org/10.1149/1.2409768>.
42. Yamada Pittini, Y., Daneshvari, D., Pittini, R., Vaucher, S., Rohr, L., Leparoux, S., & Leuenberger, H. (2008). Cole-Cole plot analysis of dielectric behavior of monoalkyl ethers of polyethylene glycol (C_nEm). *European Polymer Journal*, 44(4), 1191–1199. <https://doi.org/10.1016/j.eurpolymj.2008.01.016>.
43. Guin, M., & Tietz, F. (2015). Survey of the transport properties of sodium superionic conductor materials for use in sodium batteries. *Journal of Power Sources*, 273, 1056–1064. <https://doi.org/10.1016/j.jpowsour.2014.09.137>.
44. Kim, J. K., Lim, Y. J., Kim, H., Cho, G. B., & Kim, Y. (2015). A hybrid solid electrolyte for flexible solid-state sodium batteries. *Energy and Environmental Science*, 8(12), 3589–3596. <https://doi.org/10.1039/c5ee01941a>.
45. Tel'Nova, G. B., & Solntsev, K. A. (2015). Structure and ionic conductivity of a beta- alumina-based solid electrolyte prepared from sodium polyaluminate nanopowders. *Inorganic Materials*, 51(3), 257–266. <https://doi.org/10.1134/S0020168515030176>.
46. Yu, X., & Manthiram, A. (2019). Sodium-Sulfur Batteries with a Polymer-Coated NASICON-type Sodium-Ion Solid Electrolyte. *Matter*, 1(2), 439–451. <https://doi.org/10.1016/j.matt.2019.03.008>.
47. Alexander Herega. (2015). Some Applications of the Percolation Theory: Review of the Century Beginning. *Journal of Materials Science and Engineering A*, 5(12), 409–414. <https://doi.org/10.17265/2161-6213/2015.11-12.004>.
48. Cao, C., Li, Z., Wang, X., Zhao, X., & Han, W. (2014). Recent advances in inorganic solid electrolytes for lithium batteries, 2(June), 1–10. <https://doi.org/10.3389/fenrg.2014.00025>.
49. Ponrouch, A., Monti, D., Boschini, A., Steen, B., Johansson, P., & Palacín, M. R. (2015). Non-

- aqueous electrolytes for sodium-ion batteries. *Journal of Materials Chemistry A*, 3(1), 22–42. <https://doi.org/10.1039/c4ta04428b>.
50. Bruce, P. G., & Abrahams, I. (1991). A defect cluster model for ion migration in solid electrolytes. *Journal of Solid-State Chemistry*, 95(1), 74–82. [https://doi.org/10.1016/0022-4596\(91\)90377-T](https://doi.org/10.1016/0022-4596(91)90377-T).
51. Nitta, N., Wu, F., Lee, J. T., & Yushin, G. (2015). Li-ion battery materials: Present and future. *Materials Today*, 18(5), 252–264. <https://doi.org/10.1016/j.mattod.2014.10.040>.
52. Sun, X. G., Zhang, Z., Guan, H. Y., Bridges, C. A., Fang, Y., Hu, Y. S., ... Dai, S. (2017). A sodium-aluminum hybrid battery. *Journal of Materials Chemistry A*, 5(14), 6589–6596. <https://doi.org/10.1039/C7TA00191F>.
53. Wang, L. P., Yu, L., Srinivasan, M., Xu, Z. J., & Wang, X. (2015). Recent developments in electrode materials for sodium-ion batteries. *Journal of Materials Chemistry A*, 3(18), 9353–9378. <https://doi.org/10.1039/c4ta06467d>.
54. Ellis, B. L., & Nazar, L. F. (2012). Sodium and sodium-ion energy storage batteries. *Current Opinion in Solid State and Materials Science*, 16(4), 168–177. <https://doi.org/10.1016/j.cossms.2012.04.002>.
55. Che, H., Chen, S., Xie, Y., Wang, H., Amine, K., Liao, X. Z., & Ma, Z. F. (2017). Electrolyte design strategies and research progress for room-temperature sodium-ion batteries. *Energy and Environmental Science*, 10(5), 1075–1101. <https://doi.org/10.1039/c7ee00524e>.
56. Zhang, R., Tutusaus, O., Mohtadi, R., & Ling, C. (2018). Magnesium-sodium hybrid battery with high voltage, capacity and cyclability. *Frontiers in Chemistry*, 6(DEC), 1–10. <https://doi.org/10.3389/fchem.2018.00611>.
57. Palomares, V., Serras, P., Villaluenga, I., Hueso, K. B., Carretero-González, J., & Rojo, T. (2012). Na-ion batteries, recent advances and present challenges to become low cost energy storage systems. *Energy and Environmental Science*, 5(3), 5884–5901. <https://doi.org/10.1039/c2ee02781j>.
58. Wu, E. A., Banerjee, S., Tang, H., Richardson, P. M., Doux, J. M., Qi, J., ... Ong, S. P. (2021). A stable cathode-solid electrolyte composite for high-voltage, long-cycle-life solid-state sodium-ion batteries. *Nature Communications*, 12(1), 1–11. <https://doi.org/10.1038/s41467-021-21488-7>.
59. Balberg, I., Azulay, D., Toker, D., & Millo, O. (2004). Percolation and Tunneling in

- Composite Materials. *International Journal of Modern Physics B*, 18(15), 2091–2121. <https://doi.org/10.1142/S0217979204025336>.
60. Cao, R., Peng, D., Xu, H., Jiang, S., Luo, Z., Ao, H., & Liu, P. (2016). Synthesis and luminescence properties of NaAl₁₁O₁₇:Mn²⁺ green phosphor for white LEDs. *Journal of Luminescence*, 178, 388–391. <https://doi.org/10.1016/j.jlumin.2016.06.028>.
61. Danzi, F., Valente, M., Terlicka, S., & Braga, M. H. (2022). Sodium and potassium ion rich ferroelectric solid electrolytes for traditional and electrode-less structural batteries. *APL Materials*, 10(3), 0–15. <https://doi.org/10.1063/5.0080054>.
62. Yabuuchi, N., Kubota, K., Dahbi, M., & Komaba, S. (2014). Research development on sodium-ion batteries. *Chemical Reviews*, 114(23), 11636–11682. <https://doi.org/10.1021/cr500192f>.
63. Hwang, J. Y., Myung, S. T., & Sun, Y. K. (2017). Sodium-ion batteries: Present and future. *Chemical Society Reviews*, 46(12), 3529–3614. <https://doi.org/10.1039/c6cs00776g>.
64. Liu, Z., Chen, J., Wang, X., Wang, Y., Wang, D., & Mao, Z. (2020). Synthesis and characterization of high ionic-conductive sodium beta-alumina solid electrolyte derived from boehmite. *Journal of Materials Science: Materials in Electronics*, 31(20), 17670–17678. <https://doi.org/10.1007/s10854-020-04321-7>.
65. Owens, B. B. (2000). Solid state electrolytes: Overview of materials and applications during the last third of the Twentieth Century. *Journal of Power Sources*, 90(1), 2–8. [https://doi.org/10.1016/S0378-7753\(00\)00436-5](https://doi.org/10.1016/S0378-7753(00)00436-5).
66. Ambrosetti, G., Balberg, I., & Grimaldi, C. (2010). Percolation-to-hopping crossover in conductor-insulator composites. *Physical Review B - Condensed Matter and Materials Physics*, 82(13), 1–7. <https://doi.org/10.1103/PhysRevB.82.134201>.
67. Huggins, R. A. (2002). Simple method to determine electronic conductivity and ionic components of the conductors in mixed a review. *Ionics*, 8(3–4), 300–313. <https://doi.org/10.1007/BF02376083>.
68. Anwane, S. W. (2014). Solid Electrolytes: Principles and Applications. *Advanced Energy Materials*, 9781118686, 259–294. <https://doi.org/10.1002/9781118904923.ch6>.
69. Garagounis, I., Kyriakou, V., Anagnostou, C., Bourganis, V., Papachristou, I., & Stoukides, M. (2011). Solid electrolytes: Applications in heterogeneous catalysis and chemical

cogeneration. *Industrial and Engineering Chemistry Research*, 50(2), 431– 472. <https://doi.org/10.1021/ie1001058>.

70. Ojha, S. K., Purkait, P., Chatterjee, B., & Chakravorti, S. (2019). Application of Cole- Cole model to transformer oil-paper insulation considering distributed dielectric relaxation. *High Voltage*, 4(1), 72–79. <https://doi.org/10.1049/hve.2018.5079.74>

71. Kanwade, A., Gupta, S., Kankane, A., & Tiwari, K. (2022). RSC Advances Transition metal oxides as a cathode for indispensable Na-ion batteries, 23284–23310. <https://doi.org/10.1039/d2ra03601k>.

72. Uddin, M. J., & Cho, S. J. (2018). Reassessing the bulk ionic conductivity of solid-state electrolytes. *Sustainable Energy and Fuels*, 2(7), 1458–1462. <https://doi.org/10.1039/c8se00139a>.

73. Rajendran, S., Mahendran, O., & Kannan, R. (2002). Ionic conductivity studies in composite solid polymer electrolytes based on methyl methacrylate. *Journal of Physics and Chemistry of Solids*, 63(2), 303–307. [https://doi.org/10.1016/S0022-3697\(01\)00144-5](https://doi.org/10.1016/S0022-3697(01)00144-5).

74. Lu, Y., Li, L., Zhang, Q., Niu, Z., & Chen, J. (2018). Electrolyte and Interface Engineering for Solid-State Sodium Batteries. *Joule*, 2(9), 1747–1770. <https://doi.org/10.1016/j.joule.2018.07.028>.

75. Lu, X., Xia, G., Lemmon, J. P., & Yang, Z. (2010). Advanced materials for sodium-beta alumina batteries: Status, challenges, and perspectives. *Journal of Power Sources*, 195(9), 2431–2442. <https://doi.org/10.1016/j.jpowsour.2009.11.120>.

76. Zhang, Q., Liang, F., Yao, Y., Ma, W., Yang, B., & Dai, Y. (2019). Sodium-Based Solid-State Electrolyte and Its Applications in Energy. *Progress in Chemistry*, 31(1), 210– 222. <https://doi.org/10.7536/PC180434>.

77. Li, Z., Liu, P., Zhu, K., Zhang, Z., Si, Y., Wang, Y., & Jiao, L. (2021). Solid-State Electrolytes for Sodium Metal Batteries. *Energy and Fuels*, 35(11), 9063–9079. <https://doi.org/10.1021/acs.energyfuels.1c00347>.

78. Srivastava, N., & Tiwari, T. (2009). New trends in polymer electrolytes: A review. *E-Polymers*, (146), 1–17. <https://doi.org/10.1515/epoly.2009.9.1.1738>.

79. Wei, Z., Ren, Y., Wang, M., He, J., Huo, W., & Tang, H. (2020). Improving the Conductivity of Solid Polymer Electrolyte by Grain Reforming. *Nanoscale Research Letters*, 15(1). <https://doi.org/10.1186/s11671-020-03355-4>.

80. Ma, Q., & Tietz, F. (2020). Solid-State Electrolyte Materials for Sodium Batteries: Towards Practical Applications. *ChemElectroChem*, 7(13), 2693–2713. <https://doi.org/10.1002/celec.202000164>.
81. Gebert, F., Knott, J., Gorkin, R., Chou, S. L., & Dou, S. X. (2021). Polymer electrolytes for sodium-ion batteries. *Energy Storage Materials*, 36, 10–30. <https://doi.org/10.1016/j.ensm.2020.11.030>.
82. Dai, H., Xu, W., Hu, Z., Chen, Y., Gu, J., Xie, F., ... Zhang, G. (2021). Novel Solid-State Sodium-Ion Battery with Wide Band Gap NaTi₂(PO₄)₃ Nanocrystal Electrolyte. *ACS Omega*, 6(17), 11537–11544. <https://doi.org/10.1021/acsomega.1c00664>.
83. Lu, W., Wang, Z., & Zhong, S. (2021). Sodium-ion battery technology: Advanced anodes, cathodes and electrolytes. *Journal of Physics: Conference Series*, 2109(1). <https://doi.org/10.1088/1742-6596/2109/1/012004>.
84. Evans, J., Vincent, C. A., & Bruce, P. G. (1987). Electrochemical measurement of transference numbers in polymer electrolytes. *Polymer*, 28(13), 2324–2328. [https://doi.org/10.1016/0032-3861\(87\)90394-6](https://doi.org/10.1016/0032-3861(87)90394-6).
85. Goodenough, J. B., & Singh, P. (2015). Review—Solid Electrolytes in Rechargeable Electrochemical Cells. *Journal of The Electrochemical Society*, 162(14), A2387–A2392. <https://doi.org/10.1149/2.0021514jes>.
86. Heavens, S. N. (1984). Structural transformation during sintering and annealing of beta alumina. *Journal of Materials Science*, 19(7), 2223–2232. <https://doi.org/10.1007/BF01058099>.
87. Zhu, C., & Xue, J. (2012). Structure and properties relationships of beta-Al₂O₃ electrolyte materials. *Journal of Alloys and Compounds*, 517, 182–185. <https://doi.org/10.1016/j.jallcom.2011.12.080>.
88. Zhu, C., Hong, Y., & Huang, P. (2016). Synthesis and characterization of NiO doped beta-Al₂O₃ solid electrolyte. *Journal of Alloys and Compounds*, 688, 746–751. <https://doi.org/10.1016/j.jallcom.2016.07.264>.
89. Chen, G., Lu, J., Li, L., Chen, L., & Jiang, X. (2016). Microstructure control and properties of β"-Al₂O₃ solid electrolyte. *Journal of Alloys and Compounds*. <https://doi.org/10.1016/j.jallcom.2016.03.009>.
90. Chayambuka, K., Mulder, G., Danilov, D. L., & Notten, P. H. L. (2020). From Li-Ion

Batteries toward Na-Ion Chemistries: Challenges and Opportunities. *Advanced Energy Materials*, 10(38), 1–11. <https://doi.org/10.1002/aenm.202001310>.

91. Deng, Y., Eames, C., Fleutot, B., David, R., Chotard, J. N., Suard, E., ... Islam, M. S. (2017). Enhancing the Lithium Ion Conductivity in Lithium Superionic Conductor (LISICON) Solid Electrolytes through a Mixed Polyanion Effect. *ACS Applied Materials and Interfaces*, 9(8), 7050–7058. <https://doi.org/10.1021/acsami.6b14402>.

92. Li, H., Fan, H., Wang, B., Wang, C., Zhang, M., Chen, G., ... Zhang, J. (2020). Mechanical and electrical properties of lithium stabilized sodium beta alumina solid electrolyte shaping by non-aqueous gelcasting. *Journal of the European Ceramic Society*, 40(8), 3072–3079. <https://doi.org/10.1016/j.jeurceramsoc.2020.02.037>.

93. Heinz, M. V. F., Bay, M. C., Vogt, U. F., & Battaglia, C. (2021). Grain size effects on activation energy and conductivity: Na- β "-alumina ceramics and ion conductors with highly resistive grain boundary phases. *Acta Materialia*, 213, 116940. <https://doi.org/10.1016/j.actamat.2021.116940>.

Janek, J., & Zeier, W. G. (2016). A solid future for battery development. *Nature Energy*, 1(9), 1–4. <https://doi.org/10.1038/nenergy.2016.141>.

94. Shan, S. J., Yang, L. P., Liu, X. M., Wei, X. L., Yang, H., & Shen, X. D. (2013). Preparation and characterization of TiO₂ doped and MgO stabilized Na- β "-Al₂O₃ electrolyte via a citrate sol-gel method. *Journal of Alloys and Compounds*, 563, 176–179. <https://doi.org/10.1016/j.jallcom.2013.02.092>.

95. Cao, D., Sun, X., Li, Q., Natan, A., Xiang, P., & Zhu, H. (2020). Lithium Dendrite in All-Solid-State Batteries: Growth Mechanisms, Suppression Strategies, and Characterizations. *Matter*, 3(1), 57–94. <https://doi.org/10.1016/j.matt.2020.03.015>.

96. Xi, G., Xiao, M., Wang, S., Han, D., Li, Y., & Meng, Y. (2021). Polymer-Based Solid Electrolytes: Material Selection, Design, and Application. *Advanced Functional Materials*, 31(9), 1–28. <https://doi.org/10.1002/adfm.202007598>.

97. Judez, X., Zhang, H., Li, C., Eshetu, G. G., González-Marcos, J. A., Armand, M., & Rodríguez-Martínez, L. M. (2018). Review—Solid Electrolytes for Safe and High Energy Density Lithium-Sulfur Batteries: Promises and Challenges. *Journal of The Electrochemical Society*, 165(1), A6008–A6016. <https://doi.org/10.1149/2.0041801jes>.

98. Slater, M. D., Kim, D., Lee, E., & Johnson, C. S. (2013). Sodium-ion batteries. *Advanced*

Functional Materials, 23(8), 947–958. <https://doi.org/10.1002/adfm.201200691>.

99. Jetybayeva, A., Uzakbaiuly, B., Mukanova, A., Myung, S. T., & Bakenov, Z. (2021). Recent advancements in solid electrolytes integrated into all-solid-state 2D and 3D lithium-ion microbatteries. *Journal of Materials Chemistry A*, 9(27), 15140–15178. <https://doi.org/10.1039/d1ta02652f>.

100. Jian, S., Cao, Y., Feng, W., Yin, G., Zhao, Y., Lai, Y., Zhang, T., Ling, X., Wu, H., Bi, H., & Dong, Y. (2022). Recent progress in solid polymer electrolytes with various dimensional fillers: a review. *Materials Today Sustainability*, 20, 100224. <https://doi.org/10.1016/j.mtsust.2022.100224>.

101. Meng, N., Zhu, X., & Lian, F. (2022). Particles in composite polymer electrolyte for solid-state lithium batteries: A review. *Particuology*, 60, 14–36. <https://doi.org/10.1016/j.partic.2021.04.002>.

102. Li, L., Deng, Y., & Chen, G. (2020). Status and prospect of garnet/polymer solid composite electrolytes for all-solid-state lithium batteries. *Journal of Energy Chemistry*, 50, 154–177. <https://doi.org/10.1016/j.jechem.2020.03.017>.

103. Manthiram, A., Yu, X., & Wang, S. (2017). Lithium battery chemistries enabled by solid-state electrolytes. *Nature Reviews Materials*, 2(4), 1–16. <https://doi.org/10.1038/natrevmats.2016.103>.

104. Osada, I., De Vries, H., Scrosati, B., & Passerini, S. (2016). Ionic-Liquid-Based Polymer Electrolytes for Battery Applications. *Angewandte Chemie - International Edition*, 55(2), 500–513. <https://doi.org/10.1002/anie.201504971>.

105. Tang, S., Guo, W., & Fu, Y. (2021). Advances in Composite Polymer Electrolytes for Lithium Batteries and Beyond. *Advanced Energy Materials*, 11(2), 1–29. <https://doi.org/10.1002/aenm.202000802>.

106. Wang, W., & Alexandridis, P. (2016). Composite polymer electrolytes: Nanoparticles affect structure and properties. *Polymers*, 8(11). <https://doi.org/10.3390/polym8110387>.

107. Lim, H. D., Park, J. H., Shin, H. J., Jeong, J., Kim, J. T., Nam, K. W., ... Chung, K. Y. (2020). A review of challenges and issues concerning interfaces for all-solid-state batteries. *Energy Storage Materials*, 25, 224–250. <https://doi.org/10.1016/j.ensm.2019.10.011>.

108. Duchêne, L., Remhof, A., Hagemann, H., & Battaglia, C. (2020). Status and prospects of hydroborate electrolytes for all-solid-state batteries. *Energy Storage Materials*, 25(August),

782–794. <https://doi.org/10.1016/j.ensm.2019.08.032>.

109. Koerver, R., Aygün, I., Leichtweiß, T., Dietrich, C., Zhang, W., Binder, J. O., ... Janek, J. (2017). Capacity Fade in Solid-State Batteries: Interphase Formation and Chemomechanical Processes in Nickel-Rich Layered Oxide Cathodes and Lithium Thiophosphate Solid Electrolytes. *Chemistry of Materials*, 29(13), 5574–5582. <https://doi.org/10.1021/acs.chemmater.7b00931>.

110. Asano, T., Sakai, A., Ouchi, S., Sakaida, M., Miyazaki, A., & Hasegawa, S. (2018). Solid Halide Electrolytes with High Lithium-Ion Conductivity for Application in 4 V Class Bulk-Type All-Solid-State Batteries. *Advanced Materials*, 30(44), 1–7. <https://doi.org/10.1002/adma.201803075>.

111. Li, X., Liang, J., Kim, J. T., Fu, J., Duan, H., Chen, N., Li, R., Zhao, S., Wang, J., Huang, H., Sun X(2022). Highly Stable Halide-Electrolyte-Based All-Solid-State Li–Se Batteries. *Advanced Materials*, 34, 2200856. <https://doi.org/10.1002/adma.202200856>.

112. Viallet, V., & Fleutot, B. (2018). All-Solid-State Battery Technology Using Solid Sulfide Electrolytes. *Inorganic Massive Batteries*, 47–96. <https://doi.org/10.1002/9781119007050.ch3>.

113. Li, P., Hu, N., Wang, J., Wang, S., & Deng, W. (2022). Recent Progress and Perspective: Na Ion Batteries Used at Low Temperatures. *Nanomaterials*, 12(19). <https://doi.org/10.3390/nano12193529>.

114. Song, J., Xiao, B., Lin, Y., Xu, K., & Li, X. (2018). Interphases in Sodium-Ion Batteries. *Advanced Energy Materials*, 8(17), 1–24. <https://doi.org/10.1002/aenm.201703082>.

115. Liu, T., Wang, B., Gu, X., Wang, L., Ling, M., Liu, G., ... Zhang, S. (2016). All-climate sodium ion batteries based on the NASICON electrode materials. *Nano Energy*, 30, 756–761. <https://doi.org/10.1016/j.nanoen.2016.09.024>.

116. Serra Moreno, J., Maresca, G., Panero, S., Scrosati, B., & Appetecchi, G. B. (2014). Sodium-conducting ionic liquid-based electrolytes. *Electrochemistry Communications*, 43, 1–4. <https://doi.org/10.1016/j.elecom.2014.02.010>.

117. Xie, D., Zhang, M., Wu, Y., Xiang, L., & Tang, Y. (2020). A Flexible Dual-Ion Battery Based on Sodium-Ion Quasi-Solid-State Electrolyte with Long Cycling Life. *Advanced Functional Materials*, 30(5), 1–7. <https://doi.org/10.1002/adfm.201906770>.

118. Zhu, Y., He, X., & Mo, Y. (2016). First principles study on electrochemical and chemical

stability of solid electrolyte-electrode interfaces in all-solid-state Li-ion batteries. *Journal of Materials Chemistry A*, 4(9), 3253–3266. <https://doi.org/10.1039/c5ta08574h>.

119. Hayashi, A., Masuzawa, N., Yubuchi, S., Tsuji, F., Hotehama, C., Sakuda, A., & Tatsumisago, M. (2019). A sodium-ion sulfide solid electrolyte with unprecedented conductivity at room temperature. *Nature Communications*, 10(1). <https://doi.org/10.1038/s41467-019-13178-2>.

120. Wang, S., Bai, Q., Nolan, A. M., Liu, Y., Gong, S., Sun, Q., & Mo, Y. (2019). Lithium Chlorides and Bromides as Promising Solid-State Chemistries for Fast Ion Conductors with Good Electrochemical Stability. *Angewandte Chemie - International Edition*, 58(24), 8039–8043. <https://doi.org/10.1002/anie.201901938>.

121. Ong, S. P., Mo, Y., Richards, W. D., Miara, L., Lee, H. S., & Ceder, G. (2013). Phase stability, electrochemical stability and ionic conductivity of the $\text{Li}_{10\pm 1}\text{MP}_2\text{X}_{12}$ (M = Ge, Si, Sn, Al or P, and X = O, S or Se) family of superionic conductors. *Energy and Environmental Science*, 6(1), 148–156. <https://doi.org/10.1039/c2ee23355j>.

122. Ramazanov, M. A., Maharramov, A. M., Shirinova, H. A., & Palma, L. Di. (2020). Structure and electrophysical properties of polyvinylidene fluoride (PVDF)/magnetite nanocomposites. *Journal of Thermoplastic Composite Materials*, 33(1), 138–149. <https://doi.org/10.1177/0892705718796542>.

123. Wu, Y., Li, Y., Wang, Y., Liu, Q., Chen, Q., & Chen, M. (2022). Advances and prospects of PVDF based polymer electrolytes. *Journal of Energy Chemistry*, 64(August), 62–84. <https://doi.org/10.1016/j.jechem.2021.04.007>.

124. Li, Boyu & Su, Qingmei & Yu, Lintao & Wang, Dong & Ding, Shukai & Zhang, Miao & Du, Gaohui & Xu, Bingshe. (2019). $\text{Li}_{0.35}\text{La}_{0.55}\text{TiO}_3$ Nanofibers Enhanced Poly(vinylidene fluoride)-Based Composite Polymer Electrolytes for All-Solid-State Batteries. *ACS Applied Materials & Interfaces*. 2019. 10.1021/acsami.9b14824.

125. Kozdra, S., Wójcik, A., Możdżonek, M., Florczak, Ł., Opaliński, I., & Michałowski, P. P. (2022). Poly (vinylidene fluoride) solid polymer electrolyte structure revealed by secondary ion mass spectrometry. *Polymer*, 259(July), 1–5. <https://doi.org/10.1016/j.polymer.2022.125364>.

126. Dissanayake, M. A. K. L., Jayathilaka, P. A. R. D., & Bokalawala, R. S. P. (2003). Effect of concentration and grain size of alumina filler on the ionic conductivity enhancement of the (PEO)₉ LiC₃SO₃ :Al₂O₃ composite polymer electrolyte, 121, 409–414.

[https://doi.org/10.1016/S0378-7753\(03\)00262-3](https://doi.org/10.1016/S0378-7753(03)00262-3).

128. Polu, A. R., & Rhee, H. W. (2017). Ionic liquid doped PEO-based solid polymer electrolytes for lithium-ion polymer batteries. *International Journal of Hydrogen Energy*, 42(10), 7212–7219. <https://doi.org/10.1016/j.ijhydene.2016.04.160>.

129. Camacho-Forero, L. E., & Balbuena, P. B. (2018). Exploring interfacial stability of solid-state electrolytes at the lithium-metal anode surface. *Journal of Power Sources*, 396(May), 782–790. <https://doi.org/10.1016/j.jpowsour.2018.06.092>.

130. Amin, O., & Mukherjee, R. (2019). The Effect Of Metallic Inclusion On The Capacitance Of Fe₃O₄ As Dielectric Matrix, *Journal of Emerging Technologies and Innovative Research (JETIR)*, 6(1), 744–751.

131. Liu Xiangdong, Panguluri Raghava P., Mukherjee Rupam, Mishra Debabrata, Pokhrel Shiva, Shoemaker Daniel P., Huang Zhi-Feng, Nadgorny Boris (2022). Nanoparticle geometrical effects on percolation, packing density, and magnetoresistive properties in ferromagnet-superconductor-insulator nanocomposites. *APS Physical Review B*, 106(22), 224417. [10.1103/PhysRevB.106.224417](https://doi.org/10.1103/PhysRevB.106.224417).

132. Verma, P., Maire, P., & Novák, P. (2010). A review of the features and analyses of the solid electrolyte interphase in Li-ion batteries. *Electrochimica Acta*, 55(22), 6332–6341. <https://doi.org/10.1016/j.electacta.2010.05.072>.

133. Wang, W. M. (2012). Study on all solid-state composite polymer electrolyte. *Advanced Materials Research*, 571, 13–16. <https://doi.org/10.4028/www.scientific.net/AMR.571.13>.

134. Xu K. (2004). Nonaqueous liquid electrolytes for lithium-based rechargeable batteries. *Chem. Rev.* 104, 4303–4417. [10.1021/cr030203g](https://doi.org/10.1021/cr030203g).

135. Serra, J. P., Fidalgo-Marijuan, A., Barbosa, J. C., Correia, D. M., Gonçalves, R., Porro, J. M., ... Costa, C. M. (2022). Lithium-Ion Battery Solid Electrolytes Based on Poly(vinylidene Fluoride)-Metal Thiocyanate Ionic Liquid Blends. *ACS Applied Polymer Materials*, 4(8), 5909–5919. <https://doi.org/10.1021/acsapm.2c00789>.

136. Aravindan, V., Karthikaselvi, G., Vickraman, P., & Naganandhini, S. P. (2009). Polyvinylidene fluoride-based novel polymer electrolytes for magnesium-rechargeable batteries with Mg(CF₃SO₃)₂. *Journal of Applied Polymer Science*, 112(5), 3024–3029. [doi:10.1002/app.29877](https://doi.org/10.1002/app.29877).

137. Barbosa, J. C., Dias, J. P., Lanceros-Méndez, S., & Costa, C. M. (2018). Recent advances

- in poly(Vinylidene fluoride) and its copolymers for lithium-ion battery separators. *Membranes*, 8(3). <https://doi.org/10.3390/membranes8030045>.
138. Miguel, C., & Fernandes, V. (2020). *Electroactive poly (vinylidene fluoride) -based materials : recent progress , challenges , and opportunities. Fascinating Fluoropolymers and Their Applications*. Elsevier Inc. <https://doi.org/10.1016/B978-0-12-821873-0/00001-1>.
139. Bae, J. H., & Chang, S. H. (2019). PVDF-based ferroelectric polymers and dielectric elastomers for sensor and actuator applications: A review. *Functional Composites and Structures*, 1(1). <https://doi.org/10.1088/2631-6331/ab0f48>.
140. Kotobuki, M., Lu, L., Savilov, S. V., & Aldoshin, S. M. (2017). Poly(vinylidene fluoride)-Based Al Ion Conductive Solid Polymer Electrolyte for Al Battery. *Journal of The Electrochemical Society*, 164(14), A3868–A3875. <https://doi.org/10.1149/2.1601714jes>.
141. Park, M., Zhang, X., Chung, M., Less, G. B., & Sastry, A. M. (2010). A review of conduction phenomena in Li-ion batteries. *Journal of Power Sources*, 195(24), 7904–7929. <https://doi.org/10.1016/j.jpowsour.2010.06.060>.
142. Kimura, K., & Tominaga, Y. (2018). Understanding Electrochemical Stability and Lithium Ion-Dominant Transport in Concentrated Poly(ethylene carbonate) Electrolyte. *ChemElectroChem*, 5(24), 4008–4014. <https://doi.org/10.1002/celec.201801105>.
143. Barbosa, J. C., Gonçalves, R., Costa, C. M., & Lanceros-Méndez, S. (2022). Toward Sustainable Solid Polymer Electrolytes for Lithium-Ion Batteries. *ACS Omega*, 7(17), 14457–14464. <https://doi.org/10.1021/acsomega.2c01926>.
144. Jiayao Lu, Ying Li, Wenlong Huang (2022). Study on structure and electrical properties of PVDF/Li₃/8Sr₇/16Zr₁/4Ta₃/4O₃ composite solid polymer electrolytes for quasi-solid-state Li battery. *Materials Research Bulletin*, 153,111880. <https://doi.org/10.1016/j.materresbull.2022.111880>.
145. Ponam, & Singh, P. (2021). Improved mechanical and electrochemical properties of pvdf/peo/licl₄ based solid polymer electrolyte by using TiO₂ and MgO nanoparticles. *Journal of Engineering Research (Kuwait)*, 2021, 1–16. <https://doi.org/10.36909/jer.ICETET.14993>.
146. Kumar, S., Singh, P.K., Agarwal, D., Singh Dhapola, P., Sharma, T., Savilov, S.V., Arkhipova, E.A., Singh, M.K. and Singh, A. (2022). Structure, Dielectric, and Electrochemical Studies on Poly (Vinylidene Fluoride-Co-Hexafluoropropylene)/Ionic Liquid 1-Ethyl-3-Methylimidazolium Tricyanomethanide-Based Polymer Electrolytes. *Phys. Status Solidi A*,

219: 2100711. <https://doi.org/10.1002/pssa.202100711>.

147. Wang, F., Li, L., Yang, X., You, J., Xu, Y., Wang, H., ... Gao, G. (2018). Influence of additives in a PVDF-based solid polymer electrolyte on conductivity and Li-ion battery performance. *Sustainable Energy and Fuels*, 2(2), 492–498.

<https://doi.org/10.1039/c7se00441a>.

148. Gao, Q., Wang, Y., Li, J., Sheng, K., & Liu, C. (2020). An Enhanced Percolation Method for Automatic Detection of Cracks in Concrete Bridges. *Advances in Civil Engineering*, 2020.

<https://doi.org/10.1155/2020/8896176>.

149. Artime, O., & De Domenico, M. (2021). Percolation on feature-enriched interconnected systems. *Nature Communications*, 12(1). <https://doi.org/10.1038/s41467-021-22721-z>.

150. Bagnoli, F., Bellini, E., Massaro, E., & Rechtman, R. (2019). Percolation and internet science. *Future Internet*, 11(2), 1–26. <https://doi.org/10.3390/fi11020035>.

151. Roy, S. (2021). From Nucleation to Percolation: The Effect of System Size when Disorder and Stress Localization Compete. *Frontiers in Physics*, 9(November), 1–11. <https://doi.org/10.3389/fphy.2021.752086>.

152. Sakuda, A., Hayashi, A., & Tatsumisago, M. (2013). Sulfide solid electrolyte with favorable mechanical property for all-solid-state lithium battery. *Scientific Reports*, 3, 2–6. <https://doi.org/10.1038/srep02261>.

153. Zhao, Q., Stalin, S., Zhao, C. Z., & Archer, L. A. (2020). Designing solid-state electrolytes for safe, energy-dense batteries. *Nature Reviews Materials*, 5(3), 229–252. <https://doi.org/10.1038/s41578-019-0165-5>.

154. Wang, X., He, K., Li, S., Zhang, J., & Lu, Y. (2022). Realizing high-performance all-solid-state batteries with sulfide solid electrolyte and silicon anode: A review. *Nano Research*, 1–25. <https://doi.org/10.1007/s12274-022-4526-9>.

155. Zhang, Q., Kong, Y. Q., Gao, K. X., Wen, Y. J., Zhang, Q., Fang, H. Y., ... Du, Y. P. (2022). Research progress on space charge layer effect in lithium-ion solid-state battery. *Science China Technological Sciences*, 65(10), 2246–2258. <https://doi.org/10.1007/s11431-021-2027-3>.

156. Wang, C., Liang, J., Zhao, Y., Zheng, M., Li, X., & Sun, X. (2021). All-solid-state lithium batteries enabled by sulfide electrolytes: From fundamental research to practical engineering design. *Energy and Environmental Science*, 14(5), 2577–2619.

<https://doi.org/10.1039/d1ee00551k>.

157. Li, Z., Yu, R., Weng, S., Zhang, Q., Wang, X., & Guo, X. (2023). Tailoring polymer electrolyte ionic conductivity for production of low- temperature operating quasi-all-solid-state lithium metal batteries. *Nature Communications*, *14*(1), 1–12. <https://doi.org/10.1038/s41467-023-35857-x>.

158. Bachman, J. C., Muy, S., Grimaud, A., Chang, H. H., Pour, N., Lux, S. F., ... Shao-Horn, Y. (2016). Inorganic Solid-State Electrolytes for Lithium Batteries: Mechanisms and Properties Governing Ion Conduction. *Chemical Reviews*, *116*(1), 140–162. <https://doi.org/10.1021/acs.chemrev.5b00563>.

159. Staunton, E., Andreev, Y. G., & Bruce, P. G. (2005). Structure and conductivity of the crystalline polymer electrolyte β -PEO6: LiAsF₆. *Journal of the American Chemical Society*, *127*(35), 12176–12177. <https://doi.org/10.1021/ja053249v>.

160. Henderson, W. A., & Passerini, S. (2003). Ionic conductivity in crystalline-amorphous polymer electrolytes - P(EO)6:LiX phases. *Electrochemistry Communications*, *5*(7), 575–578. [https://doi.org/10.1016/S1388-2481\(03\)00131-0](https://doi.org/10.1016/S1388-2481(03)00131-0).

161. Ohta, N., Takada, K., Zhang, L., Ma, R., Osada, M., & Sasaki, T. (2006). Enhancement of the high-rate capability of solid-state lithium batteries by nanoscale interfacial modification. *Advanced Materials*, *18*(17), 2226–2229. <https://doi.org/10.1002/adma.200502604>.

162. Gao, Y., Yan, Z., Gray, J. L., He, X., Wang, D., Chen, T., ... Wang, D. (2019). Polymer–inorganic solid–electrolyte interphase for stable lithium metal batteries under lean electrolyte conditions. *Nature Materials*, *18*(4), 384–389. <https://doi.org/10.1038/s41563-019-0305-8>.

163. Karabelli, D., Singh, S., Kiemel, S., Koller, J., Konarov, A., Stubhan, F., ... Birke, K. P. (2020). Sodium-Based Batteries: In Search of the Best Compromise Between Sustainability and Maximization of Electric Performance. *Frontiers in Energy Research*, *8*(December), 1–16. <https://doi.org/10.3389/fenrg.2020.605129>.

164. Ming, J., Guo, J., Xia, C., Wang, W., & Alshareef, H. N. (2019). *Zinc-ion batteries: Materials, mechanisms, and applications. Materials Science and Engineering: R: Reports*, *135*, 58–84. doi:10.1016/j.mser.2018.10.002.

165. Mossali, E., Picone, N., Gentilini, L., Rodríguez, O., Pérez, J. M., & Colledani, M. (2020). Lithium-ion batteries towards circular economy: A literature review of opportunities and issues of recycling treatments. *Journal of Environmental Management*, *264*.

<https://doi.org/10.1016/j.jenvman.2020.110500>.

166. Nayak, P. K., Yang, L., Brehm, W., & Adelhelm, P. (2018). From Lithium-Ion to Sodium-Ion Batteries: Advantages, Challenges, and Surprises. *Angewandte Chemie - International Edition*, *57*(1), 102–120. <https://doi.org/10.1002/anie.201703772>.

167. Ortiz-Vitoriano, N., Drewett, N. E., Gonzalo, E., & Rojo, T. (2017). High performance manganese-based layered oxide cathodes: Overcoming the challenges of sodium ion batteries. *Energy and Environmental Science*, *10*(5), 1051–1074. <https://doi.org/10.1039/c7ee00566k>.

168. Qi, X., Liu, L., Song, N., Gao, F., Yang, K., Lu, Y., ... Chen, L. (2017). Design and Comparative Study of O3/P2 Hybrid Structures for Room Temperature Sodium-Ion Batteries. *ACS Applied Materials and Interfaces*, *9*(46), 40215–40223. <https://doi.org/10.1021/acsami.7b11282>.

169. Sun, X., Hao, H., Hartmann, P., Liu, Z., & Zhao, F. (2019). Supply risks of lithium-ion battery materials: An entire supply chain estimation. *Materials Today Energy*, *14*, 100347. <https://doi.org/10.1016/j.mtener.2019.100347>.

170. Zhu, X., Lin, T., Manning, E., Zhang, Y., Yu, M., Zuo, B., & Wang, L. (2018). Recent advances on Fe- and Mn-based cathode materials for lithium and sodium ion batteries. *Journal of Nanoparticle Research*, *20*(6). <https://doi.org/10.1007/s11051-018-4235-1>.

171. Li, J., Ma, C., Chi, M., Liang, C., & Dudney, N. J. (2015). Solid electrolyte: The key for high-voltage lithium batteries. *Advanced Energy Materials*, *5*(4), 1–6. <https://doi.org/10.1002/aenm.201401408>.

172. Nurohmah, A. R., Nisa, S. S., Stulasti, K. N. R., Yudha, C. S., Suci, W. G., Aliwarga, K., ... Purwanto, A. (2022). Sodium-ion battery from sea salt: a review. *Materials for Renewable and Sustainable Energy*, *11*(1), 71–89. <https://doi.org/10.1007/s40243-022-00208-1>.

173. Chen, A., Qu, C., Shi, Y., & Shi, F. (2020). Manufacturing Strategies for Solid Electrolyte in Batteries. *Frontiers in Energy Research*, *8*. <https://doi.org/10.3389/fenrg.2020.571440>.

174. Shan, Y., Li, Y., & Pang, H. (2020). Applications of Tin Sulfide-Based Materials in Lithium-Ion Batteries and Sodium-Ion Batteries. *Advanced Functional Materials*, *30*(23), 1–31. <https://doi.org/10.1002/adfm.202001298>.

175. Yuan, M., & Liu, K. (2020). Rational design on separators and liquid electrolytes for safer lithium-ion batteries. *Journal of Energy Chemistry*, *43*, 58–70. <https://doi.org/10.1016/j.jechem.2019.08.008>.

176. Zhang, H., Li, C., Piszcz, M., Coya, E., Rojo, T., Rodriguez-Martinez, L. M., ... Zhou, Z. (2017). Single lithium-ion conducting solid polymer electrolytes: Advances and perspectives. *Chemical Society Reviews*, *46*(3), 797–815. <https://doi.org/10.1039/c6cs00491a>.
177. Zhang, Q., Cao, D., Ma, Y., Natan, A., Aurora, P., & Zhu, H. (2019). Sulfide-Based Solid-State Electrolytes: Synthesis, Stability, and Potential for All-Solid-State Batteries. *Advanced Materials*, *31*(44), 1–42. <https://doi.org/10.1002/adma.201901131>.
178. Zhang, X., Liu, T., Zhang, S., Huang, X., Xu, B., Lin, Y., ... Shen, Y. (2017). Synergistic coupling between $\text{Li}_{6.75}\text{La}_3\text{Zr}_{175}\text{Ta}_{0.25}\text{O}_{12}$ and poly(vinylidene fluoride) induces high ionic conductivity, mechanical strength, and thermal stability of solid composite electrolytes. *Journal of the American Chemical Society*, *139*(39), 13779–13785. <https://doi.org/10.1021/jacs.7b06364>.
179. Zhou, Q., Zhang, J., & Cui, G. (2018). Rigid–Flexible Coupling Polymer Electrolytes toward High-Energy Lithium Batteries. *Macromolecular Materials and Engineering*, *303*(11), 1–14. <https://doi.org/10.1002/mame.201800337>.
180. Yuan, M., & Liu, K. (2020). Rational design on separators and liquid electrolytes for safer lithium-ion batteries. *Journal of Energy Chemistry*, *43*, 58–70. <https://doi.org/10.1016/j.jechem.2019.08.008>.
181. Zhao, Y., Wang, L., Zhou, Y., Liang, Z., Tavajohi, N., Li, B., & Li, T. (2021). Solid Polymer Electrolytes with High Conductivity and Transference Number of Li Ions for Li-Based Rechargeable Batteries. *Advanced Science*, *8*(7), 1–22. <https://doi.org/10.1002/advs.202003675>.
182. Johari, S. N., Afini M., Tajuddin, N. A., Hanibah, H., & Deraman, S. K. (2021). A Review: Ionic Conductivity of Solid Polymer Electrolyte Based Polyethylene Oxide. *International Journal of Electrochemical Science*, *16*, 1–15. <https://doi.org/10.20964/2021.10.53>.
183. Polu AR, Singh PK, Siva kumar P, et al (2023) . Development of solid polymer electrolytes based on poly (ethylene oxide) complexed with 2-trifluoromethyl-4, 5-dicyanoimidazole lithium salt and 1-ethyl-3-methylimidazolium bis(trifluoromethylsulfonyl)imide ionic liquid for Li-ion batteries. *High Performance Polymers*.*35*(1):4-9. doi:10.1177/09540083221113035.
184. Zhou Weidong, Huang Qiu, Xie Xiaoxin, Chen Kejun, Li Wei, Qiu Jieshan (2022). Research progress of polymer electrolyte for solid state lithium batteries. *Energy Storage*

- Science and Technology*,11(6): 1788-1805. doi: 10.19799/j.cnki.2095-4239.2022.0168.
185. Sun, B., Mindemark, J., Edström, K., & Brandell, D. (2014). Polycarbonate-based Solid Polymer Electrolytes for Li-ion Batteries. *Solid State Ionics*, 262, 738-742. doi:10.1016/J.SSI.2013.08.014.
186. Foran, G.Y., Verdier, N., Lepage, D., Prébé, A., Ayme-perrot, D., & Dollé, M. (2021). Thermal and Electrochemical Properties of Solid Polymer Electrolytes Prepared via Lithium Salt-Catalyzed Epoxide Ring Opening Polymerization. *Applied Sciences*, 11, 1561. doi:10.3390/APP11041561.
187. Guo, Q., Han, Y., Wang, H., Xiong, S., Liu, S., Zheng, C., & Xie, K. (2018). Preparation and characterization of nanocomposite ionic liquid-based gel polymer electrolyte for safe applications in solid-state lithium battery. *Solid State Ionics*. doi:10.1016/J.SSI.2018.03.032.
188. Yuan, H., Luan, J., Yang, Z., Zhang, J., Wu, Y., Lu, Z., & Liu, H. (2020). Single Lithium-Ion Conducting Solid Polymer Electrolyte with Superior Electrochemical Stability and Interfacial Compatibility for Solid-State Lithium Metal Batteries. *ACS Applied Materials & Interfaces*, 12(6), 7249–7256. <https://doi.org/10.1021/acsami.9b20436>.
189. Chi-Yang Tsai, Ying-Ling Liu, (2022). Building up ion-conduction pathways in solid polymer electrolytes through surface and pore functionalization of PVDF porous membranes with ionic conductors. *Journal of Membrane Science*,651,120456, <https://doi.org/10.1016/j.memsci.2022.120456>.
190. Zhongran Yao, Kongjun Zhu, Xia Li, Jie Zhang, Jiatao Chen, Jing Wang, Kang Yan, Jinsong Liu, (2022).3D poly(vinylidene fluoride–hexafluoropropylene) nanofiber-reinforced PEO-based composite polymer electrolyte for high-voltage lithium metal batteries. *Electrochimica Acta*, 404,139769, <https://doi.org/10.1016/j.electacta.2021.139769>.
191. K.A. Vishnumurthy, K.H. Girish. (2021). A comprehensive review of battery technology for E-mobility, *Journal of the Indian Chemical Society*,98,10,100173,<https://doi.org/10.1016/j.jics.2021.100173>.
192. Méry, A., Rousselot, S., Lepage, D., & Dollé, M. (2021). A Critical Review for an Accurate Electrochemical Stability Composite Electrolytes. *Materials*, 14(14), 3840. doi:10.3390/ma14143840.
193. Wang, Z., Liu, J., Wang, M., Shen, X., Qian, T., & Yan, C. (2020). Toward safer solid-state lithium metal batteries: a review. *Nanoscale Advances*, 2(5), 1828–1836.

<https://doi.org/10.1039/d0na00174k>.

194. Zou, J., & Ben, T. (2022). Recent Advances in Porous Polymers for Solid-State Rechargeable Lithium Batteries. *Polymers*, *14*(22), 4804.

<https://doi.org/10.3390/polym14224804>.

195. Ji, X., Zhang, Y., Cao, M., Gu, Q., Wang, H., Yu, J., ... Zhou, X. (2022). Advanced inorganic/polymer hybrid electrolytes for all-solid-state lithium batteries. *Journal of Advanced Ceramics*, *11*(6), 835–861. <https://doi.org/10.1007/s40145-022-0580-8>.

196. H, Wu, N. (2022). Ionic conductivity and ion transport mechanisms of solid-state lithium-ion battery electrolytes: a review. *Energy Sci Eng*.10: 1643- 1671. doi:10.1002/ese3.1163.

197. Yang, H, Wu, N. (2022). Ionic conductivity and ion transport mechanisms of solid-state lithium-ion battery electrolytes: a review. *Energy Sci Eng*.10: 1643- 1671.

198. Kim, A., Woo, S., Kang, M., Park, H., & Kang, B. (2020). Research Progresses of Garnet-Type Solid Electrolytes for Developing All-Solid-State Li Batteries. *Frontiers in Chemistry*, *8*. doi:10.3389/fchem.2020.00468.

199. Chung, H., & Kang, B. (2017). Mechanical and Thermal Failure Induced by Contact between a Li_{1.5}Al_{0.5}Ge_{1.5}(PO₄)₃ Solid Electrolyte and Li Metal in an All Solid-State Li Cell. *Chemistry of Materials*, *29*(20), 8611–8619. doi:10.1021/acs.chemmater.7b02301.

200. Lora, M., Lim, J. S., & McHugh, M. A. (1999). Comparison of the solubility of PVF and PVDF in supercritical CH₂F₂ and CO₂ and in CO₂ with acetone, dimethyl ether, and ethanol. *Journal of Physical Chemistry B*, *103*(14), 2818–2822. <https://doi.org/10.1021/jp9844462>.

201. Fei, H., Liu, Y., Wei, C., Zhang, Y., Feng, J., Chen, C., & Yu, H. (2020). Poly(propylene carbonate)-based polymer electrolyte with an organic cathode for stable all-solid-state sodium batteries. *Wuli Huaxue Xuebao/ Acta Physico - Chimica Sinica*, *36*(5), 1–6. <https://doi.org/10.3866/PKU.WHXB201905015>.

202. Zeng, G., Liu, Y., Gu, C., Zhang, K., An, Y., Wei, C., ... Ni, J. (2020). A nonflammable fluorinated carbonate electrolyte for sodium-ion batteries. *Wuli Huaxue Xuebao/ Acta Physico - Chimica Sinica*, *36*(5), 3–7. <https://doi.org/10.3866/PKU.WHXB201905006>.

203. Fertig, M. P., Skadell, K., Schulz, M., Dirksen, C., Adelhelm, P., & Stelter, M. (2022). From High- to Low-Temperature: The Revival of Sodium-Beta Alumina for Sodium Solid-State Batteries. *Batteries and Supercaps*, *5*(1), 1–26. <https://doi.org/10.1002/batt.202100131>.

204. Tiwari, V., & Srivastava, G. (2014). Effect of thermal processing conditions on the structure and dielectric properties of PVDF films. *Journal of Polymer Research*, 21(11), 0–8. <https://doi.org/10.1007/s10965-014-0587-0>.
205. Xia, W., & Zhang, Z. (2018). PVDF-based dielectric polymers and their applications in electronic materials. *IET Nanodielectrics*, 1(1), 17–31. <https://doi.org/10.1049/iet-nde.2018.0001>.
206. Liu, W., Zhang, X. K., Wu, F., & Xiang, Y. (2017). A study on PVDF-HFP gel polymer electrolyte for lithium-ion batteries. *IOP Conference Series: Materials Science and Engineering*, 213(1). <https://doi.org/10.1088/1757-899X/213/1/012036>.
207. Li, Jun; Zhu, Kongjun; Wang, Jing; Yan, Kang; Liu, Jinsong; Yao, Zhongran; Xu, Yuan (2020). *Optimisation of conductivity of PEO/PVDF-based solid polymer electrolytes in all-solid-state Li-ion batteries. Materials Technology*, (), 1–8. doi:10.1080/10667857.2020.1827873.

List of Publications

1. **Amin, O.**, Sinha, S., Maji, P.S. *et al.* Effect of indium doping on thermal stability and dielectric property in sodium beta alumina solid electrolyte. *J Solid State Electrochemistry* (2023). <https://doi.org/10.1007/s10008-023-05523-9>.
2. Malik, A. Q., Mir, T. ul G., **Amin, O.**, Sathish, M., & Kumar, D. (2022). Synthesis, characterization, photocatalytic effect of CuS-ZnO nanocomposite on photodegradation of Congo red and phenol pollutant. *Inorganic Chemistry Communications*. <https://doi.org/10.1016/j.inoche.2022.109797>.
3. Sharma, B., Sharma, R., Kour, S., Sharma, M. D., **Amin, O.**, Maity, A. R., & Mukherjee, R. (2021). Fractional exponents of electrical and thermal conductivity of vanadium intercalated layered 2H-NbS₂ bulk crystal. *Indian Journal of Physics*, 4–8. <https://doi.org/10.1007/s12648-021-02045-w>.
4. **Amin, O.**, & Mukherjee, R. (2019). The Effect Of Metallic Inclusion On The Capacitance Of Fe₃O₄ As Dielectric Matrix. *Journal of Emerging Technologies and Innovative Research*, 6(1), 744–751.
5. Simrandeep Kour, **O. Amin**, B. Sharma, M. Kalyan, N. Kumari, R. Sharma, and R. Mukherjee. "Frequency dependent conductivity in vanadium intercalated MnPSe₃ bulk single crystal." *Journal of Emerging Technologies and Innovative Research* 6 (2019): 738-43.

Oral and Poster Presentation

1. **Owais Amin**, presented a paper titled Structural and Dielectric Properties of indium doped beta alumina at the International Conference on Recent Advances in Functional Materials (RAFM-2022) , 14-16 March 2022 conference led by Department of Physics, IQAC and Star College Scheme (GoI), ARSD College University of Delhi. (Oral Presentation).
2. **Owais Amin**, presented a paper titled Synthesis and optimization of ionic conductivity in PVDF- sodium β -alumina hybrid nanocomposite system at the International Conference on Advanced Functional Materials & Devices (AFMD-2023) 13-15 March 2023 conference organized by Department of Physics, IQAC

and Star College Scheme (GoI), ARSD College University of Delhi. (Oral Presentation).

Awards

- ❖ **Best Oral Presentation** Award, (Owais Amin, Lovely Professional University, India), on paper titled Synthesis and optimization of ionic conductivity in PVDF-sodium β -alumina hybrid nanocomposite system, at the International Conference on Advanced Functional Materials & Devices (AFMD-2023), 13-15 March 2023 conference organized by IQAC & Department of Physics, ARSD College University of Delhi.



Effect of indium doping on thermal stability and dielectric property in sodium beta alumina solid electrolyte

Owais Amin¹ · Subhojyoti Sinha³ · Partha Sona Maji² · Rupam Mukherjee¹

Received: 18 March 2023 / Revised: 18 April 2023 / Accepted: 26 April 2023
 © The Author(s), under exclusive licence to Springer-Verlag GmbH Germany, part of Springer Nature 2023

Abstract

We report the effect of indium doping on thermal stability and ionic conductivity of beta alumina $\text{NaIn}_x\text{Al}_{1-x}\text{O}_{17}$ solid electrolyte which is synthesized by sol–gel auto combustion method on varying dopant concentration as $x=0, 0.1, 0.2, 0.3,$ and 0.4 . X-ray diffraction (XRD) pattern and microstructure are investigated on the doped samples calcined at $1100\text{ }^\circ\text{C}$ for 5 h. XRD confirms the change in unit cell volume on increasing the dopant concentration. Field emission scanning microscope (FESEM) reveals the conversion of cylindrical morphology to small spherical particles at dopant concentration $x \geq 0.5$. Thermal stability is found to improve drastically over a broad temperature range even at small dopant concentrations in β -alumina as found from thermo-gravimetric analysis (TGA). Electrochemical impedance spectroscopy (EIS) shows a considerable reduction in frequency-dependent dielectric permittivity for doped beta alumina. At frequency 1 kHz, the permittivity of around $\sim 10^5$ in as-prepared shows non-monotonous dependence and decreases to 10^3 for $x \geq 0.1$. This steep variation is mainly attributed to the change in morphology caused by steric effect and formation of random clusters which reduces the net polarization.

Keywords Dielectric · Morphology · Ionic conductivity · Doping · Impedance

Introduction

Smart materials play an important role in the development of renewable energy sources such as solar energy, wind energy, and hydrothermal energy. Rechargeable batteries are one such renewable resource that can store chemical energy and convert it into electrical energy with high efficiency [1, 2]. To date, the lithium-ion battery (LIB) has dominated the market of portable electronic devices due to its high energy densities, long life cycle, and high output voltage [3]. Simultaneously, LIB has certain advantages over other chemistries as lithium has the lowest reduction potential among all elements which enable cells with high operational voltage and high energy density [4, 5].

However, the high cost, high flammability, leakage of liquid electrolyte, and shortage of lithium resources have undoubtedly hindered the application of LIB in large-scale energy storage [6]. Solid-state sodium-ion battery (SIB) on the other hand is another class of batteries which uses solid electrolyte rather than liquid organic electrolyte in LIBs [7]. SIB is recently found to be a good alternative of LIB because sodium is abundant, low cost, minimum leakage, greater thermal stability, and does not support any dendrite formation [8]. Despite all the advantages in solid-state batteries, the ionic conductivity in sodium-ion battery is still found to be much lower as compared to lithium-ion battery, thus restricting their use in commercial application. Moreover, as the sodium (Na) atom being larger in size with respect to lithium atom, the volumetric energy density in SIB remains low and makes it less competent against LIB [9–11]. Solid-state SIB batteries are usually classified based on type of solid electrolytes as for example inorganic ceramic electrolytes (LATP), organic polymer electrolyte (PVA), and polymer ceramic composite electrolytes (PEO/LGPs). β -alumina ($\text{NaAl}_3\text{O}_{17}$) which comes in two distinct phases, hexagonal symmetry, and rhombohedral symmetry (β'' -alumina), is an oxide based inorganic ceramic electrolyte that exhibits high ionic conductivity $\sim 1\text{ S cm}^{-1}$ especially in the rhombohedral phase at 573 K [12–15]. It is an anisotropic layered material with alternating layers of

✉ Rupam Mukherjee
rupam.23644@lpu.co.in

¹ School of Chemical Engineering and Physical Sciences, Lovely Professional University, Phagwara, Punjab 144411, India

² Department of Physics, Amity School of Applied Sciences, Amity University, Rajarhat Newton, Kolkata 700135, India

³ Department of Physics and Nanotechnology, Faculty of Engineering and Technology, SRM Institute of Science and Technology, Kattankulathur, Tamil Nadu 603203, India



Contents lists available at ScienceDirect

Inorganic Chemistry Communications

journal homepage: www.elsevier.com/locate/inoche

Short communication

Synthesis, characterization, photocatalytic effect of CuS-ZnO nanocomposite on photodegradation of Congo red and phenol pollutant

Azad Qayoom Malik^{a,*}, Tahir ul Gani Mir^b, Owais Amin^a, Manda Sathish^c, Deepak Kumar^{a,*}^a School of Chemical Engineering and Physical Sciences, Lovely Professional University, Phagwara, Punjab-144411, India^b School of Bioengineering and Biosciences, Lovely Professional University, Phagwara, Punjab-144411, India^c Centro de Investigación de Estudios Avanzados del Maule (CIEAM), Vicerrectoría de Investigación y Postgrado, Universidad Católica del Maule, Talca-3460000, Chile

ARTICLE INFO

Keywords:

Quantum dots
Nanocomposite
Nanoparticles
Dyes
Organic pollutants

ABSTRACT

The CuS/ZnO nanocomposite was prepared by using a simple mechanical method. CuS/ZnO nanocomposite synthesized were analysed with XRD and SEM. The average particle size of CuS/ZnO was found to be 30–35 nm. The electrochemical study of nanocomposite was done by using electrochemical impedance and Cyclic voltammetry analysis. CuS nanoparticles mechanically combined with ZnO nanoparticles served as an electron absorber in the nanocomposite, assisting in the enhancement of ZnO photocatalysis. CuS served as an electron collector in the nanocomposite, which aided in the enhancement of ZnO photocatalysis. Experiment performed under visible light source also showed that CuS could aid ZnO in the degradation of Congo red and Phenol. From the UV analysis it was found that CuS/ZnO nanocomposite exhibits better photochemical stability. All of these results suggested that prepared sample could be useful in practical applications.

1. Introduction

Dye wastewater from industrial effluents is a serious threat to aquatic ecosystem due to high content of organic pollutants, high alkalinity, high chemical abundance and high chromaticity [1]. The large percentage of dyes are synthetic, including cationic, anionic and non-ionic dyes. They are classified based on their chemical composition as azo, Nitro, Nitroso, anthraquinone, indigoid dyes. The discharge of dyes effluents into natural water poses a significant environmental threat due to their elemental composition including toxic components such as heavy metal ions and aromatic compounds. Dyes are the most prevalent pollutant model for evaluating the degradation efficiency of photocatalyst. Many organic dyes, such as azo dyes (methyl orange, rhodamine, congo red, acid orange), thiazine, and cationic dyes (methylene blue), have been examined in light-assisted photodegradation. Congo red (sodium 3,3'-(1E,1E)-biphenyl-4,4'-diylbis(diazene-2,1-diyl) bis(4-aminonaphthalene-1-sulfonate)) introduced in 1884 is one of the most prominent benzidine secondary diazo dyes. Benzidine is a poisonous metabolite of Congo red that causes cancer in humans. Congo red toxic by-products are strongly pigmented, have a low biological oxygen demand (BOD) and a high chemical oxygen demand (COD), and include a high concentration of dissolved solids. Congo red degradation involves

not only basic organic reactions (addition, elimination, and substitution), but also complex organic reactions because of its intricate molecular structure and large number of functional groups. As a result, degrading Congo red is quite difficult. Similarly, phenol, which is widely used as a raw material in a various sector, is one of the most prevalent contaminants found in industrial wastewater and is mentioned in the refractory wastewater category. Due to its toxicity, carcinogenic and mutagenesis potentials, it is one of the most important pollutant in the aquatic environment [2]. As a result, Congo red and phenol, two key refractory organics, were chosen as a target contaminant in this study. Several techniques for removing Congo red and phenol from wastewater have been investigated, including adsorption [3] electrochemistry [4], and biological processes [5]. The photocatalytic degradation has recently got a lot of interest due to its efficient catalytic degradation of organic pollutants into carbon dioxide, water and other tiny inorganic molecules without causing secondary pollution. Various nanomaterials such as TiO₂/montmorillonite and Au-TiO₂, have been developed to degrade organic pollutants [6]. However, many of the photocatalysts developed were stimulated by UV energy, which was less beneficial in modern application.

* Corresponding authors.

E-mail addresses: kaiserhpu@gmail.com (A.Q. Malik), smanda@ucm.cl (M. Sathish), deepak.sharma99967@gmail.com (D. Kumar).<https://doi.org/10.1016/j.inoche.2022.109797>

Received 31 March 2022; Received in revised form 28 June 2022; Accepted 17 July 2022

Available online 19 July 2022

1387-7003/© 2022 Elsevier B.V. All rights reserved.

The Effect Of Metallic Inclusion On The Capacitance Of Fe₃O₄ As Dielectric Matrix

O. Amin, R. Mukherjee

Department of Physics, School of Chemical Engineering and Physical Science, Lovely Professional University, Phagwara, Punjab

Abstract


We observe a large drop in capacitance when small volume fraction of copper as metallic fillers is embedded into Fe₃O₄ dielectric matrix system. On further inclusion, a jump in capacitance is observed above percolation threshold which is not in accord with the conventional percolation phenomenon. To understand the nature of this dielectric response we have also measured the dc conductivity of our composite system Fe₃O₄:Cu at room temperature corresponding to different range of metallic volume fraction. A power law behavior near threshold yields a non-universal value of critical exponent which is mainly attributed to tunneling effect in disordered system.

Keywords: Capacitance, critical exponents, dielectric, percolation, conductivity.

1. Introduction

The composite systems have recently gained a huge attention in developing multi- functional sensors, energy storage devices, biocompatible polymers and various semiconductor based composite devices [1–5]. Geometrical phase transition is one of the interesting phenomena in composite systems where interconnectivity of one component in presence of other leads to a rich physical phenomenon called percolation. It is a common phenomenon in a composite system (metal-insulator) where connectivity among small finite metallic clusters leads to formation of one infinite cluster that spans the entire system. This also results in a power law behavior of many electrical and geometrical parameters at threshold. As for example, near the percolation threshold the resistance (R) of a composite system follows as $R \sim |\Phi - \Phi_c|^{-t}$, where Φ is a volume fraction and t is the critical exponent[6]. The behavior of classical random disordered system near percolation threshold has been an interesting subject for many scientific investigators since long period of time. In particular large enhancement of dielectric permittivity and dc conductivity by 3-5 orders of magnitude higher is observed at percolation threshold in various metal-dielectric and metal-insulator composite systems [7,8]. This has opened up a new opportunity for the development of

Fractional exponents of electrical and thermal conductivity of vanadium intercalated layered 2H-NbS₂ bulk crystal

B Sharma¹, R Sharma¹, S Kour¹, M D Sharma¹, O Amin¹, A R Maity² and R Mukherjee^{1*} 

¹Department of Physics, School of Chemical Engineering and Physical Science, Lovely Professional University, Phagwara, Punjab 144001, India

²Amity Institute of Biotechnology, Amity University, Newtown, Kolkata 700135, India

Received: 11 April 2020 / Accepted: 18 February 2021

Abstract: Intercalation of transition metal dichalcogenides (TMDs) by *3d* or *4d* transition metal elements are of considerable interest as the intercalated atoms can finely tune the physical and chemical properties of host TMDs. On addition, these intercalation complexes show interesting magnetic property and displays anomalous transport behavior at the magnetic ordering temperature. Here, we have synthesized and measured transport properties of single crystal vanadium intercalated Niobium Di-sulphide. At 300 K, electrical resistivity and thermal conductivity of V_{0.3}NbS₂ is found to be $\sim 10^{-6}$ Ω m and 36 W m⁻¹ K⁻¹ respectively. Unlike phonon scattering, the spin scattering is found to affect both electrical and phonon conduction at low temperature. The electrical resistivity at temperature $T < 45$ K follows $T^{3/2}$ behavior, whereas the electronic part of thermal conductivity shows exponent of 0.8. Using steady-state method, the temperature dependent lattice part of thermal conductivity shows exponents of 0.5 and -0.5 at $T < 45$ K and $T > 45$ K respectively. Moreover, the peak of the total thermal conductivity also overlaps with the magnetic transition temperature, indicating the participation of spin dependent phonon dynamics below 45 K.

Keywords: Transport; Intercalation; Single crystal; Spin scattering; Lattice

1. Introduction

The layered transitional metal dichalcogenides (TMDC) have drawn a immense interest since the discovery of graphene [1–3]. Unlike graphene, the presence of band gap in Van der Waals layered materials have provided more opportunities for the development of scientific and technological applications [4, 5]. Moreover, *3d* intercalated layered metal chalcogenides have particularly gained a significant reputation for its rich flavor of physics. This ranges from helimagnetism to skyrmions; ferromagnetic to anti ferromagnetic and superconductor to charge density wave, thus depending on the family of intercalated atoms within the host [6–9]. Presence of Van der Waals gap among the inter layers have given an additional freedom to tailor the physical, thermal and magnetic properties depending on the needs of application [10–12]. The gap in between the atomic layers facilitates the process of intercalation of dopants while still maintaining the thermal and

structural stability of host material [13]. Over the past decade, 2D layered materials have proved to be the building blocks for constructing various electrical, optoelectronic, energy conversion and storage-based devices [14, 15]. Thermal and electrical properties in these thin devices needs a comprehensive understanding as the heat dissipation and device performance are coupled together.

Till date many theoretical estimations of transport properties of TMDCs have been reported but experimental results on these small bulk crystals have still remains surprisingly limited [16]. Experimental study of thermal transport of few layers of graphene, MoS₂, SnSe, h-BN, black phosphorous (BP) and Bi₂Te₃ have been investigated intensely over the past few years [17–19]. Several sensitive techniques like opto-thermal Raman characterization, suspended micro-bridge method to measure thermal conductivity of these layered materials [20]. Laser-power dependent Raman characterization on mono layer MoS₂ have yield 34.5 ± 4 W m⁻¹ K⁻¹ at room temperature [21]. Similarly in the case of bilayer graphene, WS₂ and WSe₂, thermal conductivity is measured using micro-bridge method and time domain thermoreflectance, respectively

*Corresponding author, E-mail: rupam.iitg83@gmail.com

Frequency Dependent Conductivity In Vanadium Intercalated MnPSe₃ Bulk Single Crystal

S. Kaur, O. Amin, B. Sharma, M. Kalyan, N. Kumari, R. Sharma, R. Mukherjee

Department of Physics, School of Chemical Engineering and Physical Science, Lovely Professional University, Phagwara, Punjab, India

Abstract

We observe large dielectric constant of 10^3 at 380 K in low frequency regime which decreases to 40 at 10^6 Hz for MnPSe₃ single crystal. We have also synthesized vanadium intercalated MnPSe₃ with varying concentration x which is represented as V_xMnPSe₃. Suppression of the dielectric constant is found for low vanadium concentration ($0 < x < 0.05$) at low frequency whereas it shows increasing nature above this $x = 0.05$. Moreover we have also measured frequency dependent polarization conductivity of the same intercalated system which shows hopping type behavior of mobile charge carriers contributed by vanadium.

Keywords: Single crystal, intercalation, dielectric, polarization, hopping.

1. Introduction

Discovery of graphene has also initiated a race which has focused on developing other types of new generation semiconductors with multifunctional properties [1–3]. Layered metal thiophosphates with chemical formula MPX₃ where M is a metal and X is a chalcogen have emerged as a novel group of semiconductors having access to fine tunable band gap [4,5]. MnPSe₃ is one of the promising Van der Waal magnetic material with rich physics and many undiscovered physical phenomenon's. The major advantage of this material is the ability to host various transitional metal atoms such as Mn, Fe, Co at the M (Transitional metal) site which corresponds to diverse physical and chemical properties [6–8]. Moreover the Chalcogenide of MnPSe₃ can be replaced by other atoms in the same group like Sulphur while keeping the same crystal structure. On the other hand, carrier doping and transitional metal



Department of Physics, Internal Quality Assurance Cell (IQAC) & Star College Scheme (GoI)

ATMA RAM SANATAN DHARMA COLLEGE

(University of Delhi)

Accredited Grade 'A' By NAAC

All India 12th Rank in NIRF (Ministry of Education, Govt. of India)



Certificate No: ARSD/RAFM-22/OP/134

Certificate of Participation

This is to certify that **Mr. Owais Amin**, Department of Physics, LOVELY PROFESSIONAL UNIVERSITY has presented his/her research work as a **Oral Presentation (OT-92)** on topic entitled **Structural and Di electrical Properties of indium doped beta-alumina** at online **International Conference on Recent Advances in Functional Materials (RAFM-2022)** organized by Department of Physics, IQAC and Star College Scheme (GoI), ARSD College University of Delhi from 14-16th March 2022.

(Dr. MANISH KUMAR)
Convener

(Dr. VINITA TULI)
Coordinator, IQAC

(Prof. GYANTOSH KUMAR JHA)
Principal



ATMA RAM SANATAN DHARMA COLLEGE

(University of Delhi)

Accredited Grade 'A' By NAAC
All India 7th Rank in NIRF (MHRD)



Certificate No: AFMD-2023/OP/058

*2nd International Conference on
"Advanced Functional Materials & Devices" (AFMD-2023)*

**Organized by
IQAC & Department of Physics, ARSD College**

This is to certify that Prof./Dr./Mr./Ms. OWAIS AMIN from LOVELY PROFESSIONAL UNIVERSITY, PHAGWARA PUNJAB has presented his/her research work as **Oral Presentation** in *2nd International Conference on "Advanced Functional Materials and Devices" (AFMD-2023)* organised by IQAC & Department of Physics, ARSD College, University of Delhi during 13-15th March 2023 via online mode.

(DR. SHANKAR SUBRAMANIAN)
CONVENER

(DR. VINITA TULI)
CONFERENCE CHAIR

(PROF. GYANTOSH KUMAR JHA)
PRINCIPAL



ATMA RAM SANATAN DHARMA COLLEGE

(University of Delhi)

Accredited Grade 'A' By NAAC
All India 7th Rank in NIRF (MHRD)



Certificate No: AFMD-2023/BOP/012

*2nd International Conference on
"Advanced Functional Materials & Devices" (AFMD-2023)*

**Organized by
IQAC & Department of Physics, ARSD College**

This is to certify that Prof./Dr./Mr./Ms. OWAIS AMIN from LOVELY PROFESSIONAL UNIVERSITY, PHAGWARA PUNJAB has presented his/her research work as **Oral Presentation** and received **Best Oral Presentation** in *2nd International Conference on "Advanced Functional Materials and Devices" (AFMD-2023)* organised by IQAC & Department of Physics, ARSD College, University of Delhi during 13-15th March 2023 via online mode.

(DR. SHANKAR SUBRAMANIAN)
CONVENER

(DR. VINITA TULI)
CONFERENCE CHAIR

(PROF. GYANTOSH KUMAR JHA)
PRINCIPAL